AD

USAAVLABS TECHNICAL REPORT 67-38

A METHOD FOR PREDICTING THE AERODYNAMIC LOADS AND DYNAMIC RESPONSE OF THE ROTOR BLADES OF A TANDEM-ROTOR HELICOPTER

By

John C. Balcerak

June 1967

U. S. ARMY AVIATION MATERIEL LABORATORIES
FORT EUSTIS, VIRGINIA

CONTRACT DA 44-177-AMC-207(T)
CORNELL AERONAUTICAL LABORATORY, INC.
BUFFALO, NEW YORK

DEPARTMENT OF THE ARMY
U. S. ARMY AVIATION MATERIEL LABORATORIES
FORT EUSTIS, VIRGINIA 23604

This report has been reviewed by the U. S. Army Aviation Materiel Laboratories and is considered to be technically sound. The report is published for the exchange of information and the stimulation of ideas.

Task 1F125901A14604
Contract DA 44-177-AMC-207(T)
USAAVLABS Technical Report 67-38
June 1967

A METHOD FOR PREDICTING THE AERODYNAMIC LOADS AND DYNAMIC RESPONSE OF THE ROTOR BLADES OF A TANDEM-ROTOR HELICOPTER

by

John C. Balcerak

Prepared by
Cornell Aeronautical Laboratory, Inc.
Buffalo, New York

U. S. ARMY AVIATION MATERIEL LABORATORIES
FORT EUSTIS, VIRGINIA

SUMMARY

In recent efforts, refined methods have been developed for predicting the aerodynamic loads and dynamic response of the blades of a single-rotor helicopter. The method described herein adopts similar procedures and applies them to the tandem-rotor helicopter.

The blades of each rotor are represented by segmented lifting lines located at the quarterchord positions of the blades, and the vortex strength is assumed to be constant over each segment of the blade at each of an arbitrary number of azimuth positions. The wake is represented by a mesh of shed and trailing vortex filaments up to an arbitrary finite distance behind each blade, and beyond this point the wake is represented by a segmented, tip-trailing vortex or by segmented, tip- and root-trailing vortices.

The aerodynamic loadings and the flapwise structural bending moments were computed for a CH 47A tandem-rotor helicopter for advance ratios of 0.08, 0.14 and 0.24. Comparisons of these results with measured results for individual test points are presented as radial distributions of the first three harmonic components and as time histories which include eleven harmonics. The measured data were generally presented in the form of typical results from a statistical sampling of measured data from similar test conditions.

FOREWORD

The work described in this report was performed at Cornell Aeronautical Laboratory, Inc. (CAL), Buffalo, New York, for the U. S. Army Aviation Materiel Laboratories (USAAVLABS), Fort Eustis, Virginia. The work is an extension of work accomplished at CAL over a period of years beginning in 1960 under Contract DA 44-177-TC-698.

Mr. John C. Balcerak was project engineer and author of this report. The author is particularly indebted to Mr. Raymond A. Piziali for his contributions in this effort. The assistance of Mr. Richard P. White, Jr., and Mr. Frank A. DuWaldt is also appreciated. Mr. John Yeates administered the project for USAAVLABS.

LIST OF ILLUSTRATIONS

BLANK PAGE

LIST OF TABLES

LIST OF SYMBOLS

ADV	fractional part of an azimuthal increment which the wake is advanced toward the blade producing it (nondimensional)
a_{n_s}, b_{n_s}	Fourier coefficients of the blade response in the s^{th} flapwise bending mode (ft)
$\bar{A}_{n_s}$, $\bar{B}_{n_s}$	Fourier coefficients of the generalized air load in the s^{th} flapwise bending mode (lb)
BA	azimuth position number of a blade with respect to an individual rotor
b	blade semichord (ft)
C_{l_α}	sectional airfoil lift-curve slope (nondimensional)
$f_s(r)$	normalized blade mode shape in the s^{th} flapwise bending mode
G_s	generalized air load in the s^{th} flapwise bending mode (lb)
g	structural damping coefficient (nondimensional)
h	plunging velocity of a blade section (positive upward) (ft/sec)
KB	azimuth position number of a blade with respect to both rotors
$\mathcal{L}$	lift per unit span of unstalled blade section (lb/ft)
$\bar{\mathcal{L}}$	lift per unit span of stalled blade section (lb/ft)
Δl	cross-flow drag force of blade section (lb/ft)
M_s	generalized mass in the s^{th} mode (lb-sec^2/ft)
m	pitching moment per unit span of blade section about the midchord (ft-lb/ft)
$\bar{m}$	pitching moment per unit span of stalled blade section about the midchord (ft-lb/ft)

$\bar{m}_s(r)$	bending moment distribution in the s^{th} mode (in. -lb/ft)
NA	number of azimuth positions in one rotor disk used in the computation
ND	number of flapwise bending degrees of freedom used in the computation
NR	number of radial segments used in the computation
$NW(1), NW(2)$	number of revolutions of wake used in the computation for the aft and forward rotors, respectively
$NRA2$	total number of collocation points in the rotor disks; $NRA2 = NR \cdot NA \cdot 2$
NSV	the azimuth position number of the last shed vortex wake element in the mesh wake
p_{ij}	position of the endpoints of the wake elements
q_s	generalized tip deflection in the s^{th} normal mode (ft)
R	blade radius (ft)
r	radius to a blade section (ft)
t	time (sec)
Δt	increment of time corresponding to an azimuthal increment; $\Delta t = \Delta\psi/\Omega$ (sec)
V_f	rotor translational velocity (ft/sec)
V_1	tangential component of total local velocity at a blade section (ft/sec)
V_2	normal component of total local velocity at a blade section (ft/sec)
V_T	total local velocity at a blade section (ft/sec)
$\bar{w}(r, \psi, 1)$, $\bar{w}(r, \psi, 2)$	specified induced part of the z -component of the wake transport velocity for the aft and forward rotors, respectively (ft/sec)
α_e	effective angle of attack of blade section relative to V_T (radians)

α_g	geometric angle of attack of blade section relative to the shaft plane (radians)
α_T	tip-path-plane angle relative to V_f (radians)
α_m	stall angle for airfoil section (radians)
Γ	total bound vorticity of blade section (ft^2/sec)
μ	advance ratio: $\mu = \frac{V_f \cos \alpha_T}{\Omega R}$ (nondimensional)
ρ	air density ($lb\text{-}sec^2/ft^4$)
$\sigma_x, \sigma_y, \sigma_z$	x, y and z-components of the induced velocity coefficients of the Γ-equations, respectively (ft^{-1})
$\phi(r)$	plunging displacement of the blade relative to the shaft plane (ft)
ψ	azimuth angle (radians)
$\Delta\psi$	incremental azimuth angle; $\Delta\psi = \frac{2\pi}{NA}$ (radians)
Ω	blade rotational speed (radians/sec)
ω_s	natural frequency of the blade in the s^{th} mode (radians/sec)
n	subscript denoting harmonic order
k	subscript denoting collocation points in the disk
s	subscript denoting the blade mode number

INTRODUCTION

The U. S. Army Aviation Materiel Laboratories (USAAVLABS) has been directing a unified experimental and theoretical research effort which has as its objective the improvement of the state of the art used in the design and development of V/STOL aircraft. For the past several years, Cornell Aeronautical Laboratory, Inc., has been participating in this effort with due emphasis directed toward the problem of predicting the aerodynamic loads and dynamic response experienced by rotor blades.

The problem of predicting the nonuniform inflow distribution resulting from the wake of rotor blades has been heretofore concentrated on single-rotor systems. In the earliest efforts (Reference 1), the blade was represented by a segmented lifting line, wake configurations were specified, and the prediction of the blade response was circumvented by assuming that the blade response was also specified. In later efforts (Reference 2), the aerodynamic representations of the blades were improved by satisfying the chordwise aerodynamic boundary conditions at the midpoints of the blade segments, the representations of the wake were improved to allow distortions, and the blade flapping and flapwise bending motions were predicted. The results of these efforts with regard to the development of procedures for predicting the aerodynamic loads and dynamic response of the blades of a single-rotor helicopter and the generally favorable comparisons shown between measured and computed results encouraged the undertaking of the program for tandem overlapped rotors. The method presented herein is an adaptation of the methods described in References 1 and 2. The blade is represented by a segmented lifting line as in Reference 1, but the representation of the wake and the prediction of the blade flapping and flapwise bending motions is similar to that which is described in Reference 2. No effort was made to improvise wake distortions which could be peculiar to tandem-rotor helicopters.

In conjunction with the effort described herein, a program was also initiated to measure the aerodynamic loads and dynamic response of a tandem-rotor helicopter (References 3, 4 and 5) which provided the requisite experimental data for comparison with the computed results.

The results of these efforts have demonstrated the feasibility of the computational approach to the problem of predicting the aerodynamic loads and dynamic response of the blades of a tandem-rotor helicopter and should encourage further effort in additional aspects of the problems peculiar to tandem-rotor systems.

ASSUMPTIONS

The primary objective in this effort was to develop a method for predicting the aerodynamic loads and the dynamic response of the blades of a tandem-rotor system for a prescribed wake configuration. The basis of this method lies in the efforts described in References 1 and 2, in which procedures were developed for predicting the aerodynamic loads and dynamic response of the blades of a single-rotor system. The results of these efforts were encouraging enough to undertake the present work, and it was felt that, as far as practicable, the computational model for each rotor and wake configuration should be that which had been assumed for the single-rotor system. The induced velocities on the blades were allowed to be influenced by the vortices of the wakes from the blades of both rotors. In both the single- and tandem-rotor applications, it is assumed that a wake configuration can be prescribed which adequately represents that generated by the actual rotor blades. However, less confidence can be held in this assumption for the tandem-rotor wake than for the single-rotor wake since the wakes of the two rotors intermesh.

The tandem-rotor system is assumed to be in steady-state translational flight. In addition, it is assumed that:

1. The wake configuration for each rotor is prescribed.

2. The spanwise slopes of the blade and the angles of attack of each blade section below stall are small.

3. The inplane components of the induced velocities at the tip path plane are small and can be neglected.

4. The slope of the lift curve below stall is constant across each blade section.

5. The circulation is limited to a maximum prescribed value when the angle of attack at a blade section is stalled.

6. Above stall, the normal force of a blade section is approximated by the sum of the limited value of the circulatory force and a cross-flow drag force.

7. The effects due to Mach number and Reynolds number influence only the slope of the lift curve.

8. The interference effects of the rotor hubs, fuselage, wake interaction, etc., are negligible.

9. The dynamic response of the blades is computed for the flapwise degrees of freedom only. The dynamic response for the pitch, torsion, and inplane degrees of freedom, and the associated mass, elastic, and geometric coupling between all degrees of freedom are neglected.

10. The rotor control settings are assumed to be known, and the total resultant forces and moments computed for the rotors are required to balance the fuselage forces and moment.

11. The effects of viscous dissipation in the wake are neglected.

COMPUTATIONAL MODEL

The theoretical basis for the representation of the wake which is briefly described below has been fully discussed in Reference 2.

Each blade of each rotor is represented by a segmented lifting line (bound vortex) located along the steady deflected position of the quarterchord. The number of spanwise segments, NR, and the length of each segment are arbitrary. The vortex strength is assumed to be constant over each blade segment at each of NA equally spaced azimuth positions. Thus, there are NRA ($NR \times NA$) points in the disk of each rotor where the strengths of the bound vortices and, hence, the air loads are computed.

The wake is represented by a mesh of shed and trailing vortex filaments up to an arbitrary finite distance (to a maximum of one revolution of wake) behind each blade, and beyond this point the wake is represented by a segmented tip-trailing vortex or by segmented root- and tip-trailing vortices. The trailing vortices in the mesh wake are assumed to emanate from the quarterchord of the blade such that the first set of filaments behind the blade connects the endpoints of the bound and shed vortex filaments. Beyond the truncation point of the mesh wake, the radial positions of the root- and tip-trailing vortices are arbitrary. The wake can be advanced (in time) toward the blade producing it up to a time increment which corresponds to one azimuthal segment. Thus, the lengths of the trailing vortices in the first segment of wake behind the blade are correspondingly shortened in comparison to the remaining segment of wake. The wake advance was incorporated into the wake representation on the basis of the results of efforts made to improve the prediction of the lift and pitching-moment transfer functions for a two-dimensional oscillating airfoil at zero mean angle of attack for the pitching and plunging cases which are described in detail in Reference 2. Simplified wake configurations are shown in Figure 1, where the wake has been advanced approximately 0.7 of an azimuthal segment.

The strength, $d\Gamma/d\psi$, of each shed element is equal to the change in strength of the bound vortex segment between successive azimuth positions. In the mesh wake, the strength, $d\Gamma/d\psi$, of each trailing element is equal to the difference in strength between adjacent bound vortex segments. Beyond the truncation point of the mesh wake, the strengths of the root- and tip-trailing vortex elements are equal to the maximum value of the radial distribution of the bound vortex segments in the azimuth position from which the elements were shed. The effects of viscous dissipation are neglected.

Each endpoint of each wake vortex segment is given an individual transport velocity when it is deposited in the wake. The wake transport velocity is represented by the first four terms of a Fourier series expansion in azimuth at each radial position in the disk. It is assumed that the endpoints of the wake elements maintain their initial transport velocities throughout the wake. The transport velocities of the endpoints of the root- and tip-trailing vortices in the rolled-up wake are those of the endpoints of the furthest inboard and outboard wake elements, respectively, of the azimuthal position from which the elements were deposited in the wake.

The wake representation described herein is similar to that described in Reference 2. In the cited work, the endpoints of the wake elements can be constrained to move with a common velocity after a specified interval of time. If, however, the time interval is such that it encompasses the entire wake under consideration, the wake representation used in this report becomes identical with that of Reference 2.

The positions of the blade and wake elements of both rotors are described in a single frame of reference. It is a nonrotating right-hand Cartesian coordinate system with its origin at the hub of the rear rotor and is oriented such that the x-y plane is parallel to the tip path plane as shown in Figure 2. The positive x-axis is downstream. Since the coordinate system translates with the rotor system at the velocity V_f, the transport velocities of the wake elements in the x and z directions are, respectively,

$$V_x = V_f \cos \alpha_T$$

$$V_z = V_f \sin \alpha_T + \bar{w}(r, \psi) \qquad (1)$$

where $\bar{w}(r, \psi)$ is a distribution over the rotor disk of the induced part of the z-component of the wake transport velocity.

The endpoints of the wake elements in the wake behind a blade are labeled as $p_{i,j}$, where i is related to the azimuthal position of the endpoints and j is related to the radial position. In the mesh wake representation, $i = 1$ refers to the endpoints of the wake elements on the quarterchord of the blade, while in the rolled-up wake representation, $i = 1$ refers to the azimuthal location of the endpoints of the first trailing vortex segments. In both the mesh and rolled-up wake representations, $j = 1$ refers to the furthest inboard radial segment. Figure 3 illustrates the notation.

The expressions for the Cartesian coordinates of the endpoints of the wake elements, p_{ij}, in the mesh wake of the rear rotor are $(2 \le i \le NAM)$

$$x = (V_f \cos \alpha_T)\left(\frac{\Delta\psi}{\Omega}\right)(i - 1.0 - ADV) + r_j \cos(BA - i + ADV)\Delta\psi$$

$$y = -r_j \sin(BA - i - ADV)\Delta\psi$$

$$z = -\left[V_f \sin \alpha_T - \bar{w}(r_j, \psi)\right]\left(\frac{\Delta\psi}{\Omega}\right)(i - 1.0 - ADV) + \phi_{oc}(r_j) \qquad (2)$$

where $\phi_{oc}(r_j)$ are the steady deflections of the endpoints of the blade segments.

The expressions for the Cartesian coordinates of the endpoints of the wake elements, p_{ij}, in the rolled-up wake of the rear rotor are $(i \ge 1)$

$$x = (V_f \cos \alpha_T)\frac{\Delta\psi}{\Omega}(i - 2.0 - ADV + NSV) + (r + \Delta r)_j \cos(BA - i + 2.0 - NSV)$$

$$y = -(r - \Delta r)_j \sin(BA - i + 2.0 - NSV)$$

$$z = -\left[V_f \sin \alpha_T - \bar{w}(r, \psi)\right]\frac{\Delta\psi}{\Omega}(i - 2.0 - ADV + NSV) + \phi_{oc}(r_j) \qquad (3)$$

where $(r + \Delta r)_j$ is the radial coordinate to the tip or root vortex representing the rolled-up wake.

The coordinates of the forward rotor are initially obtained from the above expressions by using the proper values of α_T, $\bar{w}$ and ϕ_{oc} and then transformed into the coordinate system of the rear rotor as follows:

$$x = x_2 \cos \Delta\alpha_T + z_2 \sin \Delta\alpha_T + x_D$$

$$y = -y_2$$

$$z = -x_2 \sin \Delta\alpha_T + z_2 \cos \Delta\alpha_T + z_D \qquad (4)$$

where x_2, y_2 , and z_2 are the coordinates in the forward rotor system, $\Delta\alpha_r = \alpha_r - \alpha_{r_2}$, and x_0, z_0 are the coordinates of the origin of the forward rotor system with respect to the rear rotor system. (See Figure 2.)

The air loads are computed at the midpoints of the lifting-line segments. These points of the disks are labeled as P_k, with the subscript k referring to the position in the disks. The notation for both rotors is illustrated in Figure 4.

The lift per unit span for a blade section at any point P_k is given by

$$l_k = \rho V_k \Gamma_k \tag{5}$$

where

$$\Gamma_k = a_k b_k |V_k| \left(\alpha_g - \frac{\dot{h}}{V_1} + \frac{b}{2} \frac{\dot{\alpha}_g}{V_1} + \frac{w}{V_1} \right)_k \tag{6}$$

The quantity in parentheses represents the instantaneous effective angle of attack at the three-quarterchord of the blade section. α_g is the instantaneous geometric angle of attack with respect to the tip path plane, $\dot{h}$ is the effective plunging velocity with respect to the tip path plane, and w is the velocity component normal to the tip path plane induced by the vorticity in the wake of all blades. The bound vortex strength for each radial segment is assumed to be periodic, and the wake vorticity depends on the radial and azimuthal change of the bound vorticity. Hence, each of the strengths of the vortex elements in the wake can be expressed in terms of the *NRA2* strengths of the bound vortices. Figure 5 illustrates the relation between the strengths of the wake vortices and the bound vortices for a simple wake configuration. If the relative orientations of the blade segments and the wake elements are known, the induced velocity on a blade segment at a point k in the disk can be expressed in terms of the strengths of the wake vortices (thus, in terms of the *NRA2* strengths of the bound vortices) from the Biot-Savart law as

$$w_k = \sum_{j=1}^{NRA2} C_{k_j} \Gamma_j \tag{7}$$

where C_{k_j} is the sum of the Biot-Savart coefficients for all wake elements whose strengths depend on Γ_j . It should be noted that, in the single frame of reference, the velocity components induced by the vorticity in the wake are computed normal to the tip path plane of the rear rotor. Hence, the velocity components normal to the tip path

plane of the forward rotor are

$$w_x = w_{2x} \cos \Delta\alpha_T - w_{2z} \sin \Delta\alpha_T$$

$$w_z = w_{2x} \sin \Delta\alpha_T + w_{2z} \cos \Delta\alpha_T \qquad (8)$$

where w_{2x} and w_{2z} are the induced velocity coefficients of the forward rotor computed normal to the tip path plane of the rear rotor.

Substituting Equation 7 into Equation 6, we have

$$\Gamma_k = \frac{|V_k|}{V_k}\left(I_k + a_k b_k \sum_{j=1}^{NRA2} C_{kj}\,\Gamma_j\right) \qquad (9)$$

where

$$I_k = \left(V_1 \alpha_g - \dot{h} + \frac{b}{2}\dot{\alpha}_g\right)_k a_k b_k \,. \qquad (10)$$

The Γ_k in Equation 9 represents the bound vortex strength at a point k which denotes each blade segment at each azimuth position. The set of $NRA2$ simultaneous equations is solved iteratively by the Gauss-Seidel method to obtain the solutions for the Γ_k. The constant term, I_k, of Equation 9 depends only on the blade response and flight condition and is referred to as the quasi-steady part of the bound vorticity, while the second term of Equation 9 represents the induced part of Γ_k.

In the computational model, only the flapping and flapwise bending degrees of freedom are considered in the calculation of the blade dynamic response. The pitching and torsional displacements are specified. Hence, the total plunging displacement and plunging velocity due to blade flapping with respect to the rotor shaft plane are, respectively,

$$\phi_{KB}(r) = \sum_{S=1}^{ND} f_S(r)\, q_{KB_S} \qquad (11)$$

$$\dot{\phi}_{KB}(r) = \sum_{S=1}^{ND} f_S(r)\, \dot{q}_{KB_S} \qquad (12)$$

where ND is the number of modes, $f_S(r)$ is the normalized bending mode shape, and q_{KB_S} is the tip deflection in the S^{th} mode at azimuth station KB.

The $\dot{h}$ term in Equation 6 is the effective plunging velocity. In addition to the plunging velocity due to blade flapping described in Equation 12, it includes the component of rotor translational velocity

normal to each spanwise segment of the blades. Thus,

$$\dot{h} = V_f \sin \alpha_s + V_f \cos \alpha_s \cos \psi \sum_{s=1}^{ND} f_s'(r) q_{KBs} + \sum_{s=1}^{ND} f_s(r) \dot{q}_{KBs} \quad . \tag{13}$$

During the iterative solution of the set of simultaneous Γ equations, the values of Γ_k are restricted in magnitude to a value, Γ_{m_k}, defined by

$$\Gamma_{m_k} = a_k b_k V_{I_k} \sin \alpha_m$$

where α_m is a specified stall angle for the airfoil section. This restriction prohibits unrealistic values of vorticity from being shed into the wake from sections which are above their stalling angle of attack. The section is defined to be stalled when $\Gamma_k / \Gamma_{m_k} > 1.0$.

When $\Gamma_k / \Gamma_{m_k} < 1.0$, the lift per unit span is computed from Equation 5 and the moment per unit span about the midchord is given by

$$m_k = \frac{1}{2} \rho b_k |V_k| \Gamma_k \quad . \tag{14}$$

Hence, the signs of the lift and moment remain consistent with the signs of Γ and the local velocity, V_{I_k}, even in the region of reversed flow. Above stall, the lift per unit span is given by

$$\bar{\mathcal{L}} = \rho V_{I_k} \Gamma_{m_k} + \Delta \ell_k \tag{15}$$

where

$$\Delta \ell_k = 2 \rho b_k V_{T_k}^2 \left| \sin \alpha_{e_k} \right| \sin \alpha_{e_k} \tag{16}$$

and the moment per unit span about the midchord is, simply,

$$\bar{m}_k = \frac{1}{2} b_k \rho V_{I_k} \Gamma_{m_k} \quad . \tag{17}$$

Thus, above stall, the lift is computed as the sum of the maximum circulatory lift at stall and a cross-flow drag force, $\Delta \ell$. The corresponding pitching moment about the midchord is simply the moment due to the lift acting at the quarterchord. The velocity, V_T, is the total

resultant velocity acting normal to the spanwise axis of the local blade segment and is given by

$$V_T^2 = V_1^2 + V_2^2 . \tag{18}$$

The velocities V_1 and V_2 are the two orthogonal components of V_T in a plane normal to the local spanwise axis. The velocity V_1 lies on the intersection of this plane with a plane normal to the shaft. Thus,

$$V_1 = (V_f \cos \alpha_s) \sin \psi + \Omega r \tag{19}$$

$$V_2 = w - V_f \sin \alpha_s - (V_f \cos \alpha_s) \frac{\partial \phi}{\partial r} \cos \psi - \dot{\phi} \tag{20}$$

where ϕ is the blade displacement given by Equation 11.

The effective angle of attack, α_e, is the local angle between the line of zero lift for the airfoil and the direction of V_T. It is given by

$$\alpha_e = \alpha_g + \delta \tag{21}$$

where

$$\delta = \tan^{-1}(V_2/V_1)$$

COMPUTATIONAL PROCEDURE

An iterative procedure is used to compute the aerodynamic loads and to solve the equations of motion of the blades so as to obtain consistent air loads and blade response. The solution includes all the aerodynamic coupling between the flapping degrees of freedom considered. The dynamic response in the torsional degrees of freedom is specified.

The computational procedure also requires the wake configuration to be specified; that is, the relative orientation of the blade segments and the wake vortex elements is assumed to be known. This relative orientation is determined from the rotor translational velocity, shaft angle, wake transport velocities, and a reasonable approximation to the steady-state displacement of the blade relative to the shaft and the first harmonic cosine flapping angle. Since the steady-state displacement and first harmonic cosine flapping angle are also predicted by the analyses, it is evident that these quantities should be in reasonable agreement with the assumed values.

Following the computation of the blade and wake coordinates, a summation of the Biot-Savart coefficients is performed to obtain the matrix of induced velocity coefficient, C_{k_j} . These coefficients correspond to the induced velocities normal to the tip path planes and are computed at the steady-state deflected positions of the blades. Since the spanwise slopes of the deflected blades are small, the induced velocities are assumed to act in the direction of V_2 (Equation 20). The bound vortex (Γ) equations are computed from the matrix of the induced velocity coefficients.

The Γ equations are solved iteratively by the Gauss-Seidel method, and the lift and pitching moment are subsequently computed. A generalized air load, defined as the integral of the product of the air load and the mode shape, is then computed for each degree of freedom and at each azimuth position. The forcing function for each mode at each harmonic is obtained from the harmonic analysis of the generalized air loads. The equations of motion of the blade for each mode are then solved for the response at each harmonic. If the total blade response for each degree of freedom at each azimuth position does not repeat to within prescribed limits, the I's of the Γ equations are recomputed and the computational process is repeated until the total blade response converges or the limit on the number of iterations is reached. Additional computations, as required, are consequently performed for the normal output, and these are listed in the succeeding section.

As discussed in Reference 2, the generalized air load is not the forcing function as conventionally defined, and the scheme of subtracting the quasi-steady damping from each side of the equations of motion to improve the convergence of the iterative solution was applied without alteration to the present problem and worked with equal success. The details of the solution as they appear in Reference 2 are repeated below for convenience.

If q_s is the generalized coordinate in the s^{th} flapwise bending mode, the equation of motion expressing the balance of all generalized forces in this coordinate at an azimuth position, Ωt, is

$$M_s \ddot{q}_s + M_s \omega_s^2 (1 + j g_s) q_s = G_s \tag{22}$$

where G_s is the generalized air load, g_s is the structural damping coefficient, ω_s is the natural frequency, and M_s is the generalized mass defined by

$$M_s = \int_0^R m(r) f_s^2(r) dr. \tag{23}$$

The quasi-steady damping terms of the generalized air load can be approximated by

$$D_s = -\rho \Omega C_{\ell_\alpha} \dot{q}_s \int_0^R b(r) r f_s^2(r) dr. \tag{24}$$

The generalized coordinate and the generalized air load can be expressed in Fourier series as

$$q_s = a_{0_s} + \sum_{n=1}^{\infty} \left(a_{n_s} \cos n\Omega t + b_{n_s} \sin n\Omega t \right) \tag{25}$$

and

$$G_s = \bar{A}_{0_s} + \sum_{n=1}^{N/2} \left(\bar{A}_{n_s} \cos n\Omega t + \bar{B}_{n_s} \sin n\Omega t \right) \tag{26}$$

respectively.

By substituting the expressions for q_s and G_s in Equations 22 and 24, subtracting Equation 24 from each side of Equation 22 and equating

coefficients of like terms in the result, we obtain

$$M_s = \omega_s^2 a_{o_s}^i = \bar{A}_{o_s}^{(i-1)}$$

and

$$M_s(\omega_s^2 - n^2\Omega^2) a_{n_s}^i + (M_s \omega_s^2 g_s + C_s n\Omega) b_{n_s}^i =$$

$$\bar{A}_{n_s}^{(i-1)} + (C_s n\Omega) b_{n_s}^{(i-1)}$$

$$-(M_s \omega_s^2 g_s + C_s n\Omega) a_{n_s}^i + M_s(\omega_s^2 - n^2\Omega^2) b_{n_s}^i =$$

$$\bar{B}_{n_s}^{(i-1)} + (C_s n\Omega) a_{n_s}^{(i-1)}$$

$$n = 1, 2, 3, \cdots \qquad (27)$$

where the superscript i indicates the iteration number and

$$C_s = \rho\Omega C_{l_\alpha} \int_0 b(r) r f_s^2(r)\, dr, \qquad (28)$$

the coefficient of the quasi-steady damping term. Thus, a pair of linear simultaneous equations for the cosine and sine components of the response has to be solved for each degree of freedom at each harmonic of the rotational speed.

When the total response, q_s, for each degree of freedom at each azimuth position has converged to within prescribed limits, the radial distributions of the cosine and sine harmonic components of the structural flapwise bending moments are computed from the harmonics of the blade response and the moment distributions in each flapwise bending mode. Thus

$$\bar{M}_o(r) = \sum_{s=1}^{ND} a_{o_s} \bar{m}_s(r)$$

$$\bar{M}_{n_a}(r) = \sum_{s=1}^{ND} a_{n_s} \bar{m}_s(r)$$

$$\bar{M}_{n_b}(r) = \sum_{s=1}^{ND} b_{n_s} \bar{m}_s(r) \qquad (29)$$

where $\bar{m}_s(r)$ are the bending moment distributions in each flapwise bending mode, s.

COMPUTER PROGRAM

The computer program is written in FORTRAN IV for the IBM 7044. Physically, due to core storage limitations, the program is separated into four parts which can be run sequentially. Each part is also divided into several subroutines for convenience in programming, checkout, and program modification. The principal functions of each part are listed below.

Part I

1. Reads the necessary input for Parts I and II.

2. Computes the blade and wake coordinates.

Two tape drives are required in Part I. One tape drive is used to transfer variables and the blade and wake coordinates to Part II, while the second is used for temporary storage of data. The data are later transferred in proper sequence to the first tape.

Part II

1. Computes the matrices of the induced velocity coefficients.

Three tape drives are used in Part II. The first is, evidently, the input from Part I. The second is used to transfer variables and the matrix of the z-component of the induced velocity coefficients to Part III, and the third is used to transfer the matrices of the x- and y-components of the induced velocity coefficients to Part IV.

Part III

1. Reads additional input for Parts III and IV.

2. Computes the initial trial values of the bound circulation.

3. Computes the initial trial values of the generalized coordinates.

Three tape drives are also required in Part III. The first is, of course, the input from Part II. The second transfers the modified matrix of the z-component of the induced velocity coefficients to Part IV while the third transfers all other data from Part III to Part IV.

Part IV

1. Solves the bound circulation equations.

2. Solves the equations of motion.

3. Computes the induced velocities in the x, y, and z directions.

4. Computes the blade structural bending moments.

5. Harmonically analyzes the normal output.

Three tape drives are used in Part IV. As noted above, there are two input tapes from Part III and one from Part II. When the blade response converges to within the prescribed limits, the tape which contains the modified z-components of the induced velocity coefficients is destroyed and the quantities to be harmonically analyzed are then transferred onto this tape.

A plotting routine, which may also be run sequentially with the foregoing program, generates a tape from which the time histories of the blade structural bending moments and the aerodynamic lift and pitching moments can be plotted for each radial station.

The following list summarizes the normal printed output of the program:

1. All input data.

2. Initial trial values of the bound vorticity.

3. Initial trial values of the generalized coordinates.

4. Blade response in the generalized coordinates.

5. Lift distribution.

6. Aerodynamic moment distribution.

7. Bound vortex strength distribution.

8. Maximum bound vortex strength at each azimuth position and its radial position.

9. Effective angle-of-attack distribution.

10. Maximum allowable values of the bound vortices at and above stall.

11. Quasi-steady distribution of the bound vortex strengths.

12. Fourier coefficients of the generalized coordinates.

13. Structural bending moment distribution.

14. x-, y-, and z-components of the induced velocity distribution.

The following quantities are also harmonically analyzed, and the Fourier coefficients for $(NA-1)/2$ harmonics are printed out:

Aerodynamic lift

Aerodynamic moment

Bound vortex strengths

Effective angle of attack

Quasi-steady bound vortex strengths

x-, y-, and z-components of induced velocity

In addition, there are many optional data which may be printed out as, for example, the blade and wake coordinates and the induced velocity coefficients. The selection of the optional print-out is accomplished by control words which are part of the input.

The running time of the program is dependent on too many factors which make it impractical, at present, to estimate the running time accurately for a particular configuration. Table I in Appendix I, however, contains some of the pertinent data from the configurations which were run in the present program from which a reasonable estimate of the running time can be made.

A simplified chart showing the major steps used in the iterative procedure for solving the equations of motion is shown in Figure 6; more detailed flow diagrams, showing the program logic for each part of the program, are given in Appendix II.

COMPUTED RESULTS AND COMPARISON WITH MEASURED RESULTS FOR THE CH 47A TANDEM-ROTOR HELICOPTER

With the exception of the vibration modes and frequencies, all requisite input data for the computer program were determined from the data reported in References 3, 4 and 5. For the computer program, the mass and stiffness distributions of Reference 3 were used to calculate the uncoupled rotating flapwise modes and frequencies which were used as inputs. As shown in Table I, the frequencies so computed were in close agreement with the computed coupled rotating flapwise bending-torsion frequencies listed in Reference 3. A comparison of the measured and computed frequencies for the nonrotating case presented in Reference 5 showed that only the frequencies of the second flapwise bending mode were in good agreement, while the measured frequencies of the third and fourth flapwise bending modes were approximately 10 percent higher than the computed values. Dynamic response data were not presented for the first flapwise bending mode, so an evaluation of the accuracy to which it is predicted could not be made.

TABLE I. COMPARISON OF UNCOUPLED FLAPWISE BENDING AND COUPLED FLAPWISE BENDING-TORSION CALCULATED FREQUENCIES

MODE	FREQUENCY (cpm)			
	Ω = 202 rpm		Ω = 230 rpm	
	UNCOUPLED	COUPLED	UNCOUPLED	COUPLED
FLAPPING	204	207	233	237
1st FLAPWISE BENDING	520	522	583	585
2nd FLAPWISE BENDING	984	987	1077	1080
1st TORSION	*	1188	*	1200
3rd FLAPWISE BENDING	1656	1665	1776	1785
4th FLAPWISE BENDING	2605	2595	2737	2727
*NOT COMPUTED				

Computations to determine the aerodynamic loads and dynamic response were made for 24 azimuth positions (for each rotor), and the blades were segmented into 10 spanwise stations as shown in Figure 7. Eight of the midpoints of these segments coincided with the radial stations at which measured data were obtained. Also, in all cases, three azimuthal segments of wake behind each blade were represented by a grid wake, and the remainder of the wake was represented by a tip vortex positioned at 90 percent of the blade radius. The number of revolutions of wake used for each rotor in the representation varied with advance ratio such that the wake terminated at approximately one to one and one-half rotor diameters from either rotor.

The computed momentum-induced velocity was used for the induced part of the z-component of the wake transport velocity for each rotor. The disk loading in each case was determined from the total measured lift per blade for each rotor.

The first four uncoupled flapwise bending modes and the flapping mode were used to describe the blade motions and, hence, to compute the blade bending moments. Because of excessive scatter in the measured collective pitch data, the collective and cyclic pitch coefficients used as inputs to the computer program were those based on trim calculations reported in Reference 4 which were included in revisions to Reference 3.

In Reference 5, it was indicated that considerable torsional motions were experienced by the blades and that these motions were significantly different for the blades of the forward rotor as compared to those of the aft rotor, and both were significantly affected by the gross weight. The torsional moment data, which were included in Reference 5 as typical for a flight test with a high gross weight, were not comparable with the torsional moment data presented in Reference 3 for the particular flight test cases with high gross weights which were analyzed herein. Consequently, the torsional motions were reluctantly neglected in the computations.

Comparisons of measured and computed data are shown both as time histories at specified radial stations and as radial distributions for the zeroth and the first three harmonic cosine and sine components. Comparisons of the measured and computed data for higher harmonics were made, but there were no significant differences from the conclusions reached on the basis of the data presented for the lower harmonics. Therefore, these results are not included in this report. The steady components of the lifts and the bending moments have been subtracted from the time histories.

Comparisons of measured data, as listed in Reference 3 and 4, and computed data have been made for the three flight conditions listed below.

TABLE II. FLIGHT CONDITIONS FOR CASES INVESTIGATED

FLIGHT NUMBER	DATA POINT NUMBER	RUN GROSS WEIGHT (lb)	TRUE AIRSPEED (knots)	μ	Ω (rpm)
394	32	32,700	28	0.08	202
395	61	25,500	54	0.14	229
394	46	33,200	101	0.24	231

Comparison of Measured and Computed Air Loads

Table III below lists the pertinent parameters which were used to establish the wake configurations for the three flight test cases investigated. The tip-path-plane angles, α_T, were based on the fuselage attitude and the first-harmonic cosine flapping angles from the trim calculations reported in Reference 4 and on the built-in tilt of each rotor.

TABLE III. WAKE PARAMETERS FOR CASES INVESTIGATED

μ	V_f fps	α_T (degrees)		$\bar{w}(r,\psi)$ (fps)		NUMBER OF REVOLUTIONS OF WAKE	
		AFT	FWD	AFT	FWD	AFT	FWD
0.08	47.3	-2.91	2.74	-33.4	-30.3	6	9
0.14	91.2	-1.72	3.91	-16.9	-15.8	3	5
0.24	170.6	-0.24	5.02	-9.5	-8.4	2	3

The measured and computed radial distributions of the steady and first three harmonic components of the lift per unit span are shown in Figures 8, 16 and 24 for the aft rotor for advance ratios of 0.08, 0.14 and 0.24, respectively, and in each succeeding figure for the forward rotor.

As shown in Figures 8 and 16, the comparison of the measured and computed steady component of the lift distribution for the aft rotor at μ = 0.08 and 0.14, respectively, is quite good up to about the 85-percent blade radius. Outboard of this blade station, a sharp drop in the lift is shown experimentally which is not predicted theoretically. This characteristic is also shown at μ = 0.24 in Figure 24, but somewhat poorer correlation was obtained between the computed and experimental values of the lift at the 75-percent and 85-percent blade radius stations. The tip loss, which is evident in the experimental data, is somewhat exaggerated in comparison to that which is typically exhibited by the blades of a helicopter and thus leads to poor correlation between the measured and computed results on the outboard sections of the blades of the aft rotor.

As illustrated in Figures 9, 17 and 25, the comparison of the measured and computed steady component of the lift distributions for the forward rotor is much poorer, particularly outboard of about the

55-percent blade radius. The experimental data show that the radial distributions for the forward rotor do not exhibit the typical peaks on the outboard section of the blade which are shown by the blades of the aft rotor and, generally, by the blades of a single-rotor helicopter. It is believed that this phenomenon was the result of mutual interference effects between the rotors which were not predicted by the assumed fixed-wake model. The computed radial distributions of the induced velocity show a greater upwash on the inboard sections of the blades of the forward rotor than on the blades of the aft rotor. The effective angles of attack exhibited a corresponding relationship but not to the extent which apparently existed in the measured data.

In Reference 5, torsional moment data are presented for one flight test case from which the total live twist is estimated to be approximately 0.6 degree. The torsional moment data for the flight test cases which were analyzed in this investigation (presented in Reference 3) were scant,but indications are that these torsional moments were much larger than those presented in Reference 5. It is believed that the estimated 0.6 degree of live twist could have been conservative for some of the flight test cases which were analyzed. Further, the computed effective angle of attack shows a sharp drop outboard of the 90-percent blade radius so that the effect of live twist on the radial air load distributions would be most pronounced on this section of the blade.

The total lift per blade for the computed data was determined by numerical integration of the steady component of the lift; comparisons of these data, the run gross weight of the ship, and the sum of the total measured lift per blade are tabulated below.

TABLE IV. COMPARISON OF MEASURED AND COMPUTED LIFT

μ	RUN GROSS WEIGHT (lb)	SUM OF MEASURED LIFT PER ROTOR (lb)		INTEGRATED COMPUTED LIFT PER UNIT SPAN (lb)	
		AFT ROTOR	FWD ROTOR	AFT ROTOR	FWD ROTOR
0.08	32,700	17,900	15,600	21,300	20,600
0.14	25,500	12,100	11,400	15,000	15,000
0.24	33,200	17,400	15,500	18,200	17,600

It is obvious that the correlation between the integrated computed lift and the run gross weight becomes poorer with decreasing advance ratio. The measured lift compares reasonably well with the run gross weight at $\mu = 0.08$ and $\mu = 0.24$ but is somewhat low at $\mu = 0.14$. The net lift on the fuselage was estimated to be approximately 300 pounds for the cases investigated and, thus, appears to be negligible in comparison to the run gross weight for the purpose of these analyses.

The prediction of the total lift of the blades of the aft rotor was surprisingly poor, since the interference effects of the forward rotor were expected to be small and the comparison of the measured and computed total lift was expected to be as favorable as that reported in Reference 2 for single-rotor helicopters. Since the total lift is quite dependent on the collective pitch and live twist angles of the rotor, it is felt that these data should be reviewed to determine if further adjustments are justified. In Reference 6, the blade loads and dynamic response of the blades of a single-rotor helicopter were computed using the trim constraints as variables. The results of the calculations show only a small difference between the computed collective pitch angle from the measured value and good correlation in the steady lift distribution. In Reference 2, it was also found that good correlation between the measured and computed steady lift distribution was obtained when the measured trim constraints were used as input. It is felt that the lack of accurate trim and live twist data contributed primarily to the poor correlation between the measured and computed results which was shown herein.

The computed air loads at $\mu = 0.08$ for the forward rotor are greatly influenced by the tip vortex from the blades of the aft rotor which yields the sharp peak in the steady air load shown in Figure 9. The pronounced influence of this tip vortex is also reflected in the measured data and re-emphasizes the importance of the effects of the wake in computing the loading characteristics of tandem-rotor systems as well as those of a single rotor.

The radial distributions of the harmonic components of the air loads do not generally compare favorably with the measured results. The first-harmonic components of the computed air load show fair qualitative comparison with the measured data except at $\mu = 0.08$ for the sine component of the aft rotor blade and the cosine component of the forward rotor blade.

The measured data for this case were obtained at a sideslip angle of approximately -9.0 degrees (nose right), and the effect of sideslip on the air loads was found to be significant for certain flight configurations as reported in Reference 5. Since it is assumed that the sideslip angles are zero in the computational procedure, this effect could not be shown in the computed results. The abrupt change in the radial distribution of the first harmonic cosine component of the forward

rotor at μ = 0.08 results from the proximity of the tip vortex from the wake of a blade in the aft rotor to a blade on the forward rotor. This interference effect does not occur at the higher advance ratios since the wake of the aft rotor has a lower value of the momentum induced velocity and is also swept back faster with the increase in advance ratio. A contributing factor to this interference effect is the increasingly opposing orientation of the tip-path planes of the rotors as advance ratio decreases.

The comparison of the measured and computed lift for the higher harmonics is generally neither better nor worse than that shown for the first harmonics. Somewhat better qualitative agreement between the measured and computed data is shown for the aft rotor than for the forward rotor. This result had been expected since the forward rotor operates in the downwash of the aft rotor.

The measured and computed time histories of the air loads for eight radial stations are shown in Figures 10, 18 and 26 for advance ratios of 0.08, 0.14 and 0.24, respectively, for the aft rotor and in each succeeding figure for the forward rotor.

At μ = 0.08, good qualitative agreement between the computed and measured time histories is shown for the aft rotor. The measured data, however, show a considerably larger content of higher harmonics than the computed results, particularly inboard of approximately the 80-percent blade radius. On the forward rotor, higher harmonic content is evident in the measured time histories throughout the blade, while the computed results show this trend only outboard of about the 80-percent blade radius. It could be expected that the outboard section of the blades of the forward rotor would exhibit this trend in the computed results, since the skewed wake from the blades of the aft rotor is swept down much closer to these blade sections. The distortions in the actual wake probably account for some of the higher harmonic content shown in the measured data. The measured results also indicate that the blade responses in the first torsion mode at the fifth and sixth harmonics were significant for one flight test case. These data were believed to be typical and, thus, could account for the higher harmonic content in the air load which was shown in the measured results but would not be evident in the computed results because of the lack of torsional deflection data. The effect of the tip vortex from the blade of the aft rotor on the computed time histories of the air loads of the forward rotor is quite obvious and is most pronounced at r/R = 0.90 as shown in Figure 11. Its effects are also noted at the other nearby radii and results in poor agreement in the magnitude of the measured and computed time histories of the air loads.

At $\mu = 0.14$ and $\mu = 0.24$, the computed time histories of the air loads on the forward rotor compare favorably with the measured data and the peak air loads are much smaller in absolute magnitude than those on the aft rotor. On the outboard sections of the blades, the computed peak air loads are advanced in time with respect to the measured data on the advancing side of the disk and retarded in time on the retreating side. This characteristic was also evident in the results for a single rotor reported in Reference 2. The computed results indicate that the x-components of the induced velocities, which were neglected in positioning the wake, are indeed small - at least on the outboard sections of the blade - and would not be expected to significantly change the wake transport velocities in the x direction as had been conjectured in Reference 2. It was noted in the cited work that the radial position of the tip vortex could also effect a pronounced influence on the phasing in the time histories of the air loads, but no computations were made to determine the effect of this parameter in the tandem-rotor case. The obvious conclusion which can be drawn from these efforts is that the wake configuration is significant in predicting the aerodynamic loads and dynamic response experienced by the blades of single- and tandem-rotor helicopters.

On the aft rotor at $\mu = 0.14$, two distinct peaks in the time histories of the air loads are noted outboard of the 80-percent blade radius both experimentally and in the computed data. Inboard of the 80-percent blade radius, the absolute magnitude of the peak air load drops sharply. At $\mu = 0.24$ on the aft rotor, the measured data show a more gradual decrease in the absolute magnitude of the peak air load from the tip inboard, but higher harmonic content is more prevalent throughout the blade than at $\mu = 0.14$ both in the measured and in the computed data. At all advance ratios, the tip-path plane of the aft rotor is oriented such that its thrust vector acts aftward. This factor, coupled with the reduced value of the momentum induced velocity at $\mu = 0.24$, retains the wake in the vicinity of the blades and leads to the larger indicated effect of the wake-induced velocity on the azimuthal distribution of the air loads.

In Reference 5, comparisons were made of the harmonic content of the azimuthal air load distribution of a blade of the forward rotor at a gross weight of 26,000 pounds and that of a blade of the aft rotor at a gross weight of 33,000 pounds for a high advance ratio. Both blades showed extensive sixth-harmonic variations in the air load distribution which appeared to be related to a negative lift region on the advancing side of the disk in each case. It was suggested that this phenomenon resulted from a corresponding excitation of the first torsion mode of the blade whose frequency lies near the sixth harmonic of the rotor speed. Although the torsional motions were not included in the computed results, fair correlation is still shown between the measured and computed azimuthal variations of the air loads at $\mu = 0.24$ for the aft rotor. At $\mu = 0.14$, fair correlation is also shown for the forward rotor, but the harmonic content is considerably reduced from that at $\mu = 0.24$. The extensive sixth-harmonic content in the air load and the

corresponding excitation of the blade torsional mode were apparently noted only at high advance ratios, so that the effect of gross weight on the azimuthal air load distribution could not be assessed from the computed data.

Comparison of Measured and Computed Bending Moments

The measured and computed radial distributions of the steady and the first three harmonic components of the flapwise bending moments are shown in Figures 12, 20 and 28 for the aft rotor for advance ratios of 0.08, 0.14, and 0.24, respectively, and in each succeeding figure for the forward rotor.

The fair correlation between the measured and computed results for the steady component of the bending moments outboard of the 50-percent blade radius is surprising in view of the poor correlation of the steady air loads outboard of the 85-percent radius. It is also seen that correlation between the measured and computed results is better for the forward rotor in contrast to the results obtained for the air loads. Inboard of the 50-percent blade radius, the agreement between the measured and computed results is very poor for both rotors. Since the measured frequencies of the third and fourth flapwise bending modes were not in good agreement with the computed values and since the computed frequencies were used in the analyses, it could be expected that substantial differences could be present in the response of the blades in these modes which would be directly reflected in the bending moment distributions. The improvement in the theoretical prediction of the steady air loads with advance ratio was not reflected in the steady bending moment distribution.

The poor correlation between the measured and computed steady components of the bending moments inboard of the 50-percent blade radius is not always reflected similarly in the first-harmonic components. At $\mu = 0.08$, the radial distributions of the measured and computed first-harmonic components of the bending moments for both rotors compare quite favorably with the measured data. At $\mu = 0.14$, only the first-harmonic sine components show a favorable comparison for both rotors, while the first-harmonic cosine components are poorly predicted for both rotors. At $\mu = 0.24$, the computed first-harmonic sine components of the bending moments also compare favorably with the measured data, while the first-harmonic cosine components are overpredicted for both rotors.

In general, the correlation between measured and computed results worsens as harmonic order increases for all advance ratios. This result is not surprising, firstly, in view of the merely fair correlation shown for the first-harmonic components of the bending moments and, secondly, since the harmonics of the air loads above the first are not generally well predicted. Since the response of the blades is significantly affected by the proximity of the natural frequencies

of the blade to the harmonics of the rotor speed, it is evident that the natural frequencies need to be accurately predicted to have confidence in the computed results for the higher harmonics.

The dynamic response of the second pinned-free bending mode is reflected in the radial distributions of the steady components of the blade bending moments. This mode is near resonance with the fifth harmonic of the rotor speed and is evidently the dominating mode with regard to the computed bending moments. Although not illustrated, a comparison was made of the measured and computed radial distributions of the fifth-harmonic components of the bending moments. At $\mu = 0.24$, the computed results agreed quite well with the experimental values, while at $\mu = 0.08$, poor correlation was obtained. It is believed that the change in rotational speed from 231 r.p.m. at $\mu = 0.24$ to 202 r.p.m. at $\mu = 0.08$ effected a pronounced change in the computed response of the fifth-harmonic components in this mode. In Reference 2, it was found that small changes in the natural frequencies of a blade could produce large changes in the response of the blade, particularly when the modes were near resonance with a harmonic of the rotor speed. The computed natural frequency of the second pinned-free bending mode, in particular, was apparently sufficiently different from its true value at the indicated rotational speed to produce the large changes in the computed dynamic response at the fifth harmonic.

The measured and computed time histories of the flapwise bending moments for eight radial stations are shown in Figures 14, 22 and 30 for advance ratios of 0.08, 0.14 and 0.24, respectively, for the aft rotor, and in each succeeding figure for the forward rotor.

At $\mu = 0.08$, the peak magnitudes of the computed histories of the flapwise bending moments are generally much lower than the measured values throughout the blade radius on the aft rotor. On the forward rotor, the measured and computed values of the azimuthal variation of the bending moments are of the same order of magnitude, with poor correlation shown in the phasing. At $\mu = 0.14$ and 0.24, the computed results generally show better agreement with the measured results both in absolute magnitude and in phasing. In general, both the measured and the computed data show that the magnitude of the dynamic response and, hence, the absolute magnitude of the bending moments are more critical on the aft rotor at the higher advance ratios, while at lower advance ratios they are about the same order of magnitude on the two rotors.

General Evaluation of the Method

The method described herein for predicting the aerodynamic loads and dynamic response of three-bladed, tandem-rotor helicopters is an adaptation of that described in References 1 and 2 for single-rotor helicopters. In view of the additional complexity inherent in representing the wakes of tandem-rotor configurations, it should be expected

that somewhat less confidence could be placed in the computed results presented herein in comparison to those of the cited references. Because of the geometry of the CH 47A helicopter, it could be expected that the effects of the wake of the forward rotor on the air load distribution and dynamic response of the blades of the aft rotor should be much less significant than the converse or the effects of the wake of either rotor on itself. Although no computations were carried out to determine these effects separately, it is believed that the effects of the forward rotor on the aft rotor are small and, hence, the differences between the measured and computed results for the aft rotor should be generally comparable to those of a single-rotor helicopter. This expectation was borne out as evidenced by the better correlation which was obtained between the measured and computed results for the aft rotor than for the forward rotor.

The measured air-load distribution of the forward rotor was, apparently, significantly affected by the wake from the blades of the aft rotor and significant differences were shown between the air-load distributions of the forward and aft rotors. The inboard section of the forward rotor blade was shown to carry a substantially greater portion of the total lift than that of a corresponding blade on the aft rotor. This phenomenon was evident to a lesser extent in the computed results. It was felt that the lack of accurate trim and live twist data led to poorer correlation between measured and computed results than had been anticipated. Consequently, computational efforts to isolate other parameters which could affect the measured differences in the air-load distributions between the forward and aft rotors were not deemed warranted.

The bending moments, as previously described, are computed from the blade response in each flapwise bending mode and the bending moment distribution in that mode. This procedure yields the steady blade displacements to sufficient accuracy for the aerodynamic aspects of the problem, since the blade section angle of attack depends only on the slope of the blade deflection shape. However, the bending moments depend on the blade curvature and, hence, cannot be as accurately defined. Further, as also discussed previously, the uncoupled flapwise bending moment distributions were used in the calculations, and these distributions can be expected to differ somewhat from the normal flapwise-edgewise modes, particularly for the higher modes. The computed frequencies used in the analyses of the uncoupled flapwise bending modes were nearly identical to the computed coupled flapwise bending-torsion modes as reported in Reference 3, but the measured dynamic response of the nonrotating blades indicated that the frequencies of the third and fourth flapwise bending modes were about 10 percent higher than predicted. The effects of these differences in frequency were not investigated.

The obvious shortcomings of the method are (1) the assumed fixed-wake configuration and (2) its dependency on accurate measured data as input. The measured data as reported in Reference 5 are generally statistical in nature; i.e., typical measured data are presented from samplings of data from similar flight conditions. Although this process eliminated many of the inconsistencies which were noted for individual data test points and placed confidence in the measured results, comparisons were made herein for individual test points and such comparisons probably should have been avoided. The sensitivity of the theoretical results to some of the input parameters also was not investigated; hence, the computed results do not necessarily reflect the "typical" results which were presented in Reference 5. The dependency on accurate measured data as input could be alleviated to a large extent by incorporating the torsion and the inplane degrees of freedom of the blades into the blade equations of motion and by imposing the rotor-fuselage trim constraints (as is concurrently being done for a single-rotor helicopter (Reference 6)). Although it is known that the assumed fixed-wake configuration needs improvement in its representation, it is felt that improvement in the dynamical representation of the blade and the imposition of the rotor-fuselage trim constraints are essential to better prediction of the problems associated with tandem-rotor configurations.

CONCLUSIONS AND RECOMMENDATIONS

The results of this effort have demonstrated the feasibility of implementing a method for predicting the aerodynamic loads and dynamic response experienced by the blades of a tandem-rotor helicopter.

In view of the limited comparisons made of measured and computed results, and the relatively few computations which have been performed. the method is considered to be satisfactory for the limited use in tandem-rotor design analysis for which it is intended. Single test-point comparisons were made of computed and measured results, whereas the measured results were generally presented as typical from a statistical sampling of data. The method which has been presented herein should thus be evaluated in the light of this circumstance.

Specifically, the following conclusions have been reached on the basis of the work which has been performed:

1. The radial distribution of the steady component of the air load for both rotors was overpredicted outboard of the 80-percent blade radius in all cases investigated. Inboard of the 80-percent blade radius, the steady components of the air loads were reasonably well predicted for both rotors. The total lift computed from the theoretical lift distributions overpredicted the run gross weight in all cases investigated, but the correlation improved with increasing advance ratio.

2. The marked reduction in the peak air loads on the outboard sections of the blades of the forward rotor and the higher loading on the inboard sections which was shown experimentally were only qualitatively evident in the computed results. The exact parameters which effected these phenomena were not confirmed by the theoretical or measured results.

3. The radial distribution of the harmonic components of the air loads was fairly well predicted for the blades of both rotors. At a low advance ratio ($\mu = 0.08$), the air load distribution of a blade of the forward rotor was markedly affected by a tip vortex from a blade of the aft rotor.

4. The measured azimuthal variations of the air loads were generally well predicted by the computed results. The notable exception was for the condition noted in Conclusion 3.

5. The steady components of the computed flapwise blade bending moments were fairly well predicted outboard of the 50-percent blade radius, and poorly predicted inboard. It is felt that the bending moment distributions obtained from the coupled flapwise-edgewise modes could significantly improve the correlation between measured and computed results on the inboard sections of the blade. Similar improvement was obtained for the blades of a single-rotor helicopter in a concurrent program conducted at CAL.

6. The measured radial distribution of the harmonic components of the flapwise bending moments was well predicted by the computed results.

7. The measured azimuthal variation of the flapwise bending moments was well predicted by the computed results. Correlation generally improved with increasing advance ratio.

In order to evaluate the method described herein for predicting the aerodynamic loads and blade response constructively and for expanding its application, it is recommended that:

1. Computations be performed to establish the extent of the influence of the wake of the aft rotor on the blade loads and dynamic response of the forward rotor, and conversely.

2. Computations be performed for other tandem-rotor configurations, particularly for those for which more rigorously controlled experimental data are available as, for example, in Reference 7.

3. Investigations be conducted to determine the influence of wake configuration parameters on the computed results, particularly to determine what factors influence the air loads to shift inboard on the forward rotor.

4. The rotor-fuselage trim constraints be imposed in the method for predicting the aerodynamic loads and dynamic response of tandem-rotor configuration as has been applied to a single-rotor configuration in Reference 6.

5. The combined flapwise-edgewise bending, the torsional degrees of freedom, and the coupling between all degrees of freedom be incorporated in the computational procedure to improve the representation of the dynamic characteristics of the blade.

REFERENCES

1. Piziali, R. A., and DuWaldt, F. A., A METHOD FOR COMPUTING ROTARY WING AIRLOAD DISTRIBUTION IN FORWARD FLIGHT, Cornell Aeronautical Laboratory, Inc.; TRECOM Technical Report 62-44, U. S. Army Transportation Research Command, Fort Eustis, Virginia, November 1962.

2. Piziali, R. A., A METHOD FOR PREDICTING THE AERODYNAMIC LOADS AND DYNAMIC RESPONSE OF ROTOR BLADES, Cornell Aeronautical Laboratory, Inc.; USAAVLABS Technical Report 65-74, U. S. Army Aviation Materiel Laboratories, Fort Eustis, Virginia, January 1966.

3. Pruyn, R. R., PRELIMINARY DATA REPORT OF DYNAMIC AIRLOADS FLIGHT TEST RESULTS AS PREPARED FOR CORNELL AERONAUTICAL LABORATORIES CORRELATION STUDIES, Boeing Company, Vertol Division Report D8-0408, Morton, Pennsylvania, June 1966.

4. Peck, W. B., SUPPLEMENTARY TANDEM-ROTOR DATA, Private communication from Boeing Company, Vertol Division, Morton, Pennsylvania, 17 January 1967.

5. Pruyn, R. R., IN-FLIGHT MEASUREMENT OF ROTOR BLADE AIRLOADS, BENDING MOMENTS, AND MOTIONS, TOGETHER WITH ROTOR SHAFT LOADS AND FUSELAGE VIBRATION, ON A TANDEM ROTOR HELICOPTER, Boeing Company, Vertol Division Report D8-0382-4, Morton, Pennsylvania, To be issued.

6. Chang, T. T., A METHOD FOR PREDICTING THE TRIM CONSTANTS OF A SINGLE-ROTOR HELICOPTER AND THE ROTOR-BLADE LOADINGS AND RESPONSES, Cornell Aeronautical Laboratory, Inc.; U. S. Army Aviation Materiel Laboratories, Fort Eustis, Virginia, To be issued.

7. Huston, R. J., WIND-TUNNEL MEASUREMENTS OF PERFORMANCE, BLADE MOTIONS, AND BLADE AIR LOADS FOR TANDEM-ROTOR CONFIGURATIONS WITH AND WITHOUT OVERLAP, NASA TN D-1971, National Aeronautics and Space Administration, Langley Field, Virginia, October 1963.

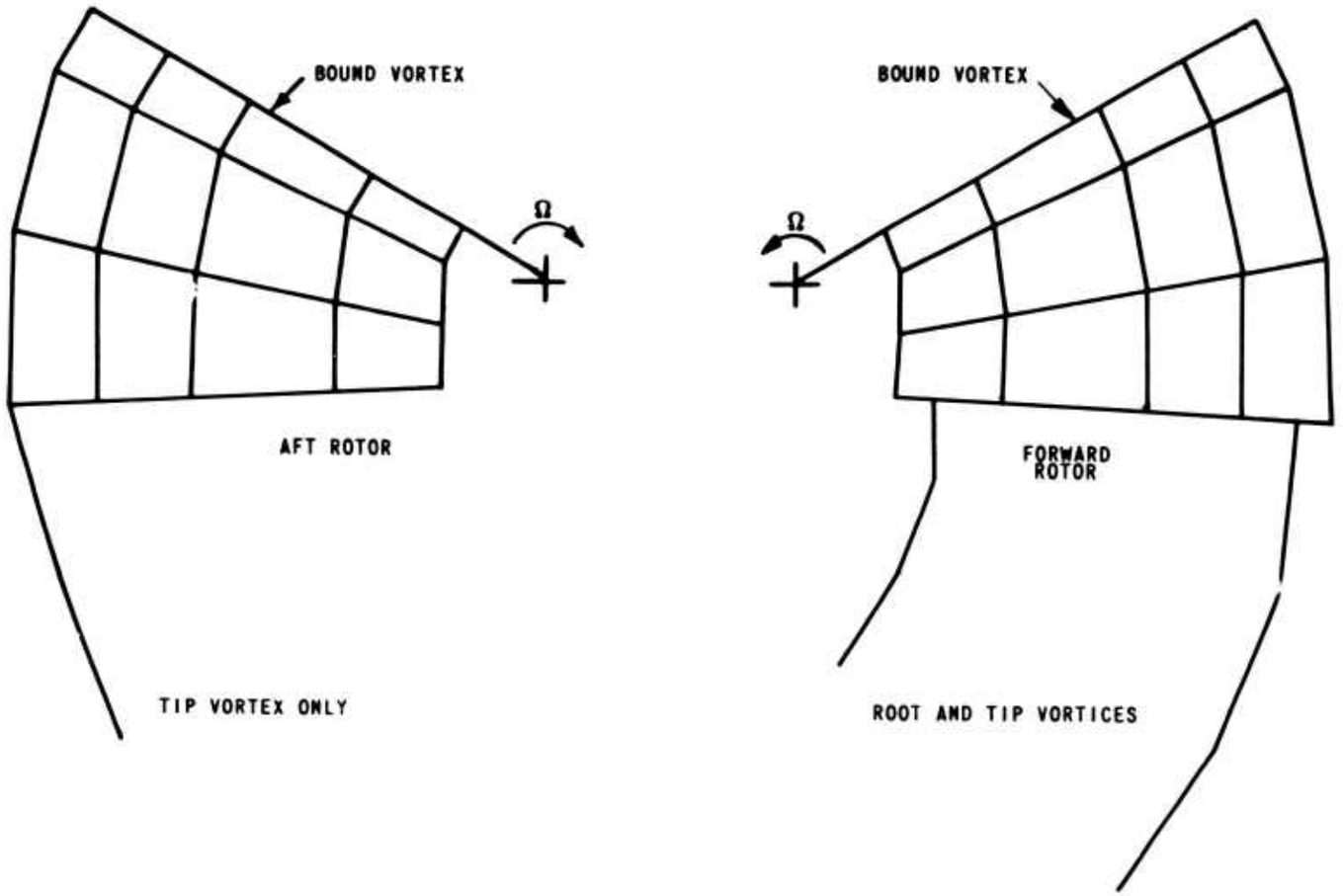

Figure 1. EXAMPLES OF WAKE CONFIGURATIONS

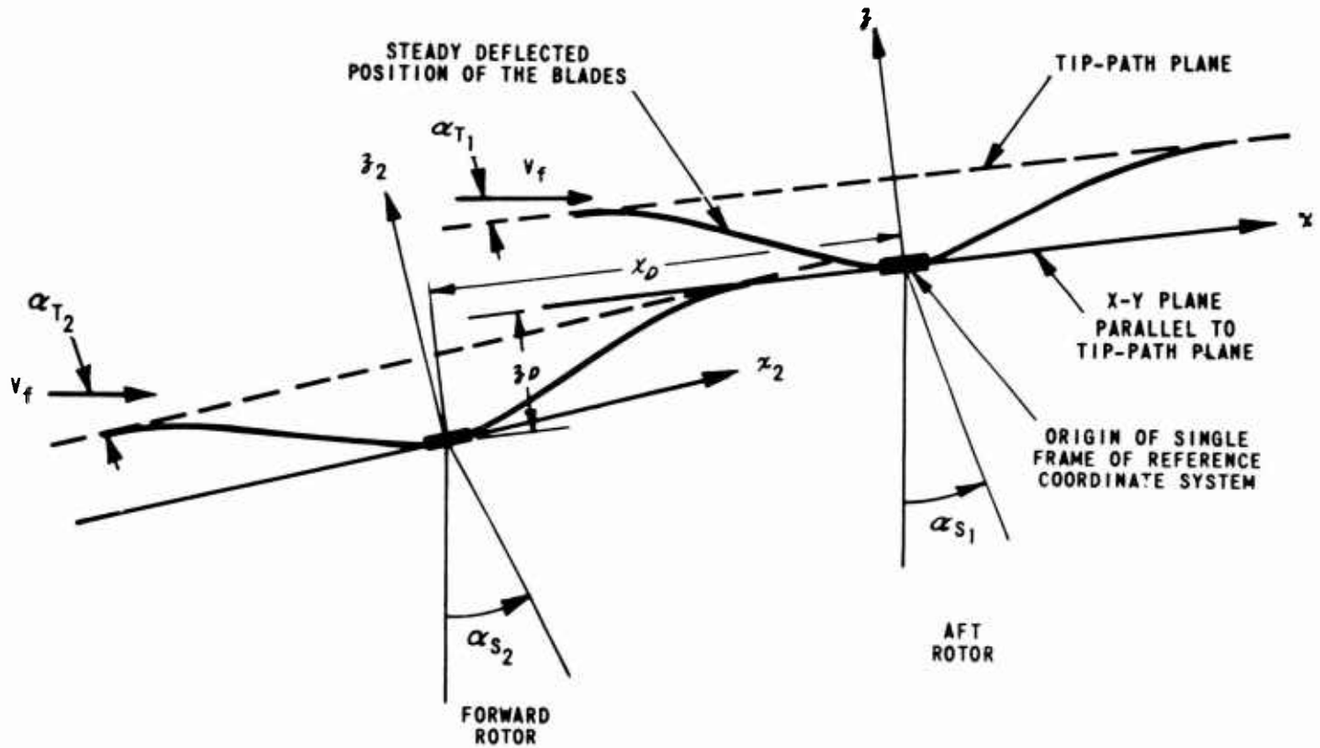

Figure 2. THE TIP-PATH-PLANE-ORIENTED COORDINATE SYSTEM (USED FOR COMPUTING THE INDUCED VELOCITIES)

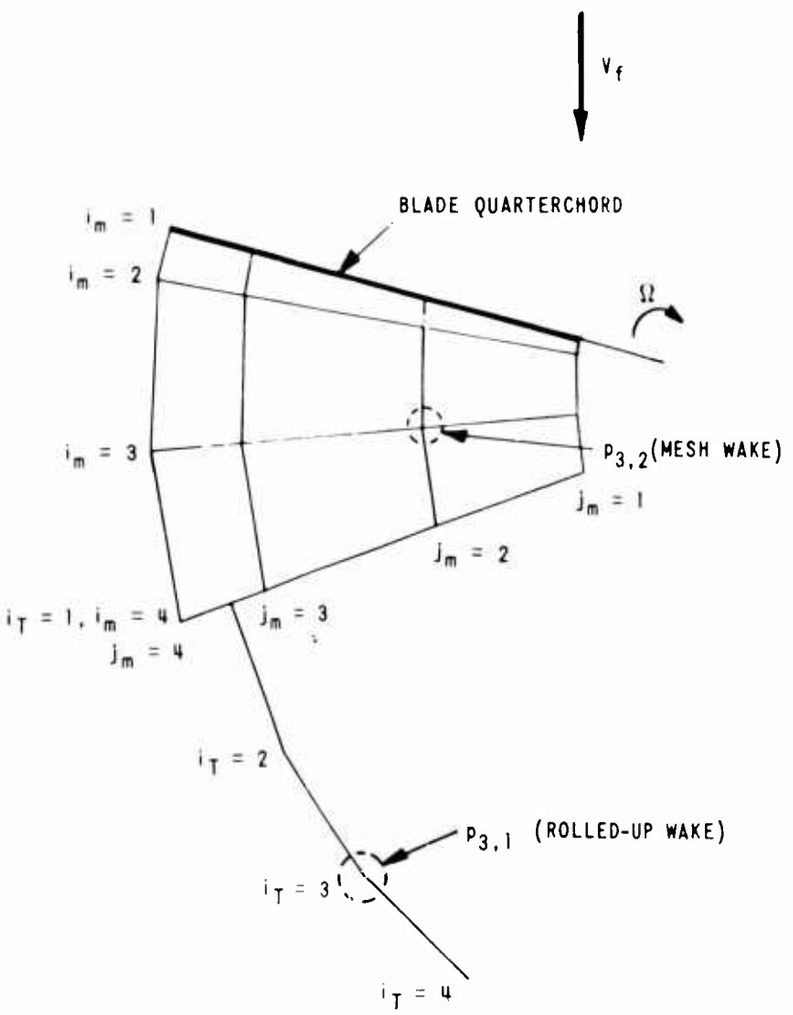

Figure 3. NOTATION USED FOR DESCRIBING THE POSITION OF THE ENDPOINTS OF THE WAKE ELEMENTS

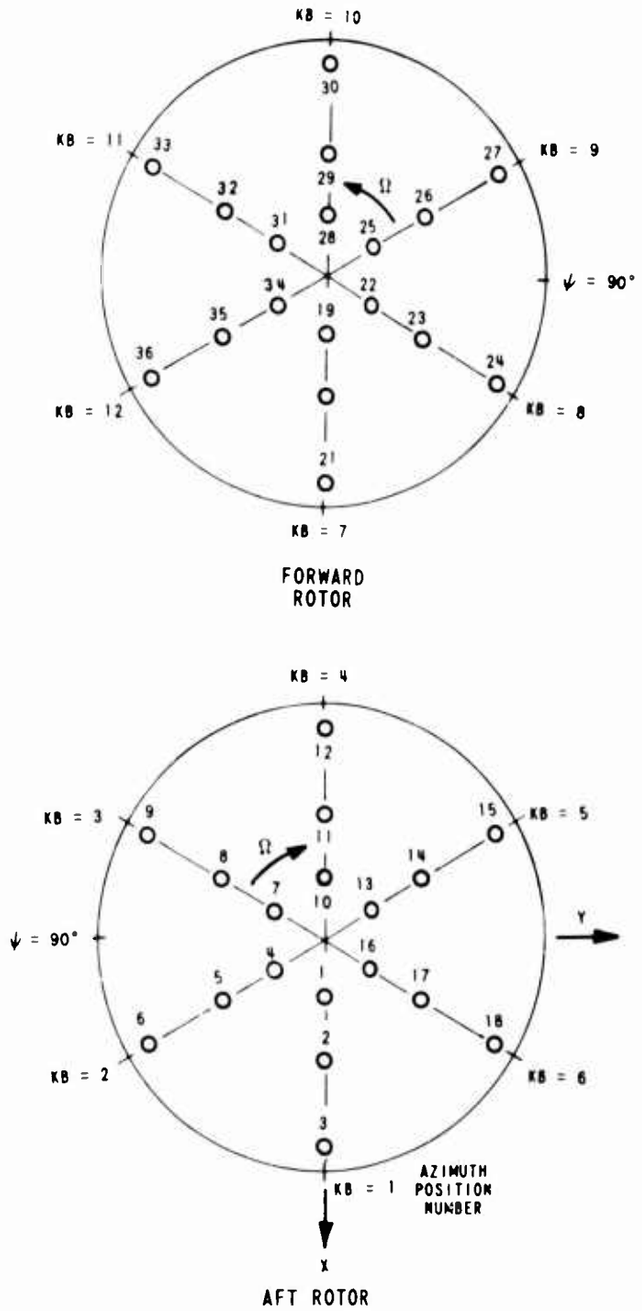

Figure 4. EXAMPLE OF THE NOTATION USED TO DEFINE THE POINTS AT WHICH AIR LOADS ARE COMPUTED IN THE DISKS OF THE ROTORS, NR = 3; NA = 6

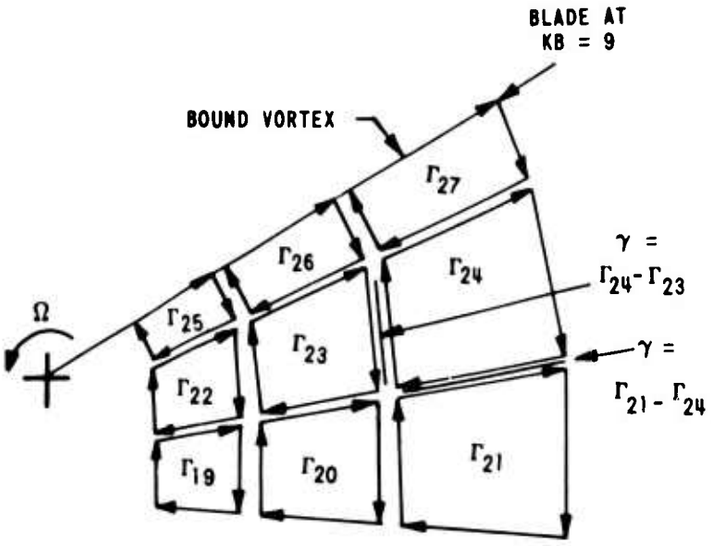

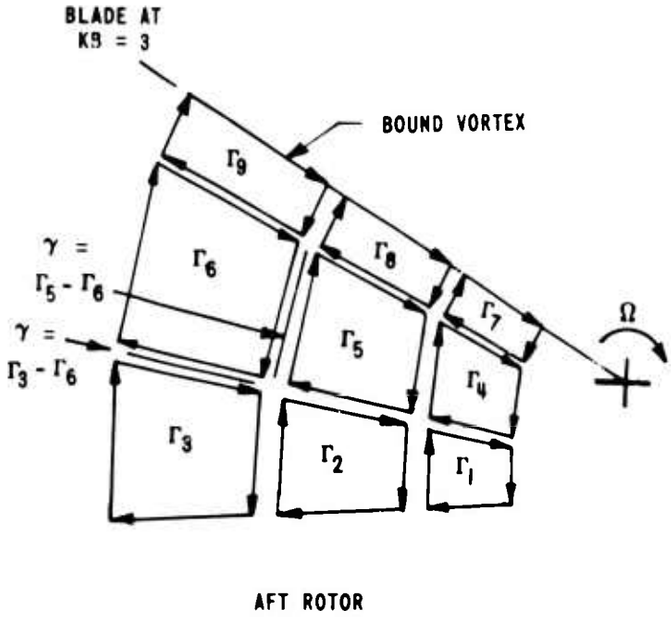

Figure 5. RELATION BETWEEN THE STRENGTHS OF THE WAKE VORTICES AND THE NRA2 BOUND VORTEX STRENGTHS, NR = 3, NA = 6

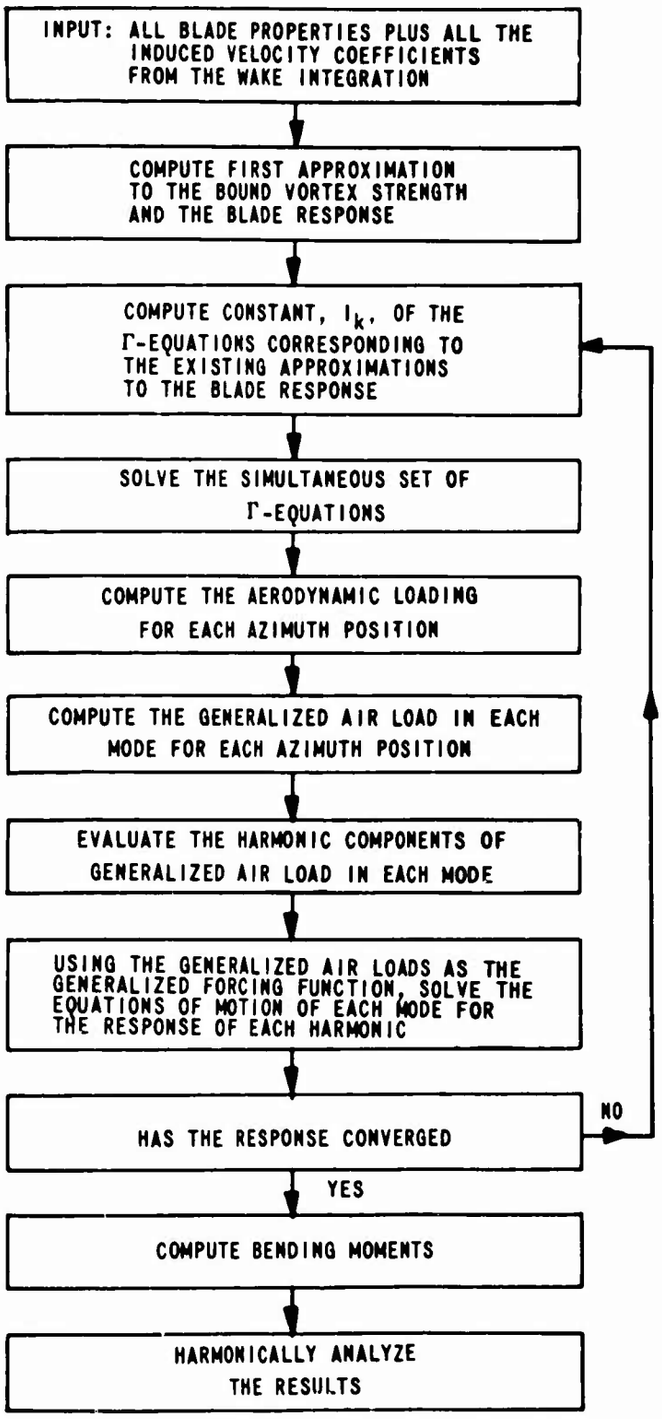

Figure 6. MAJOR STEPS IN THE ITERATIVE PROCEDURE OF SOLVING THE EQUATIONS

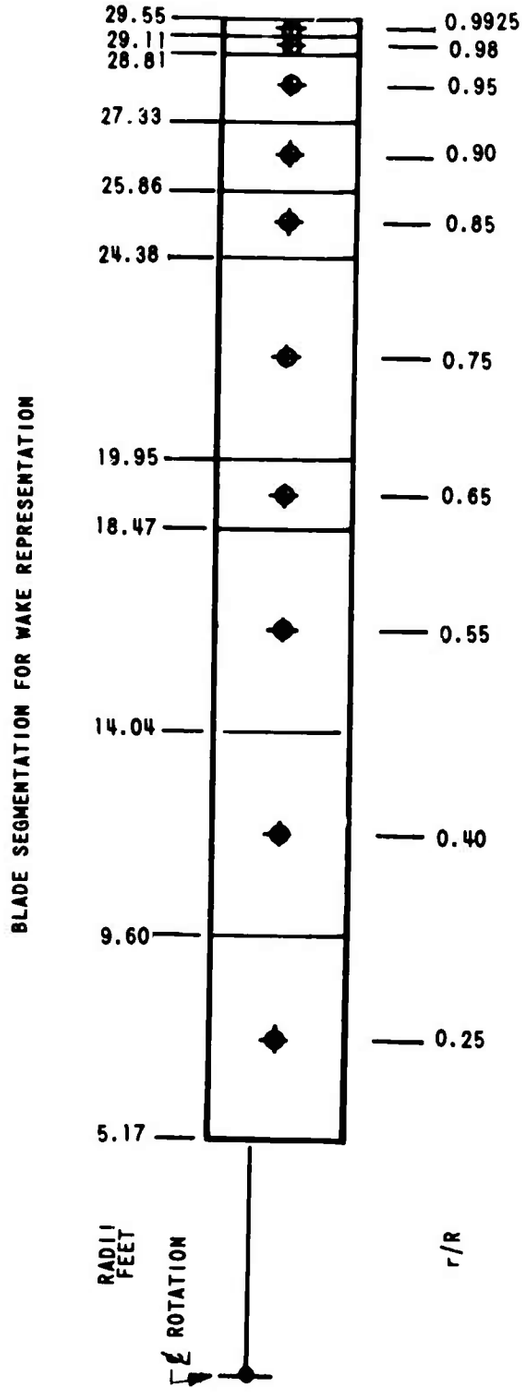

Figure 7. SEGMENTATION OF THE ROTOR BLADES FOR COMPUTATIONS

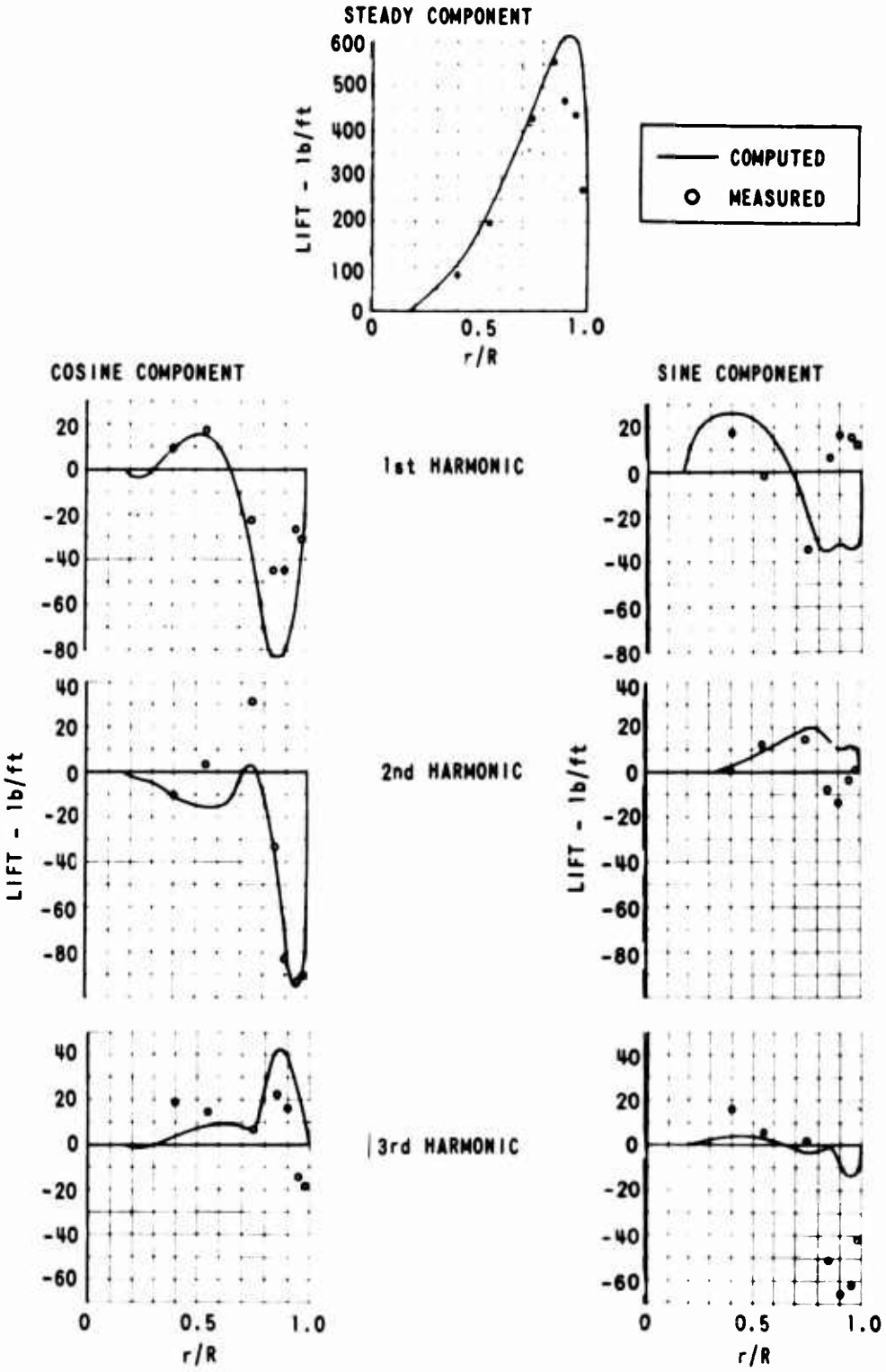

Figure 8. COMPARISON OF THE RADIAL VARIATION OF MEASURED AND COMPUTED LIFT, μ = 0.08, AFT ROTOR

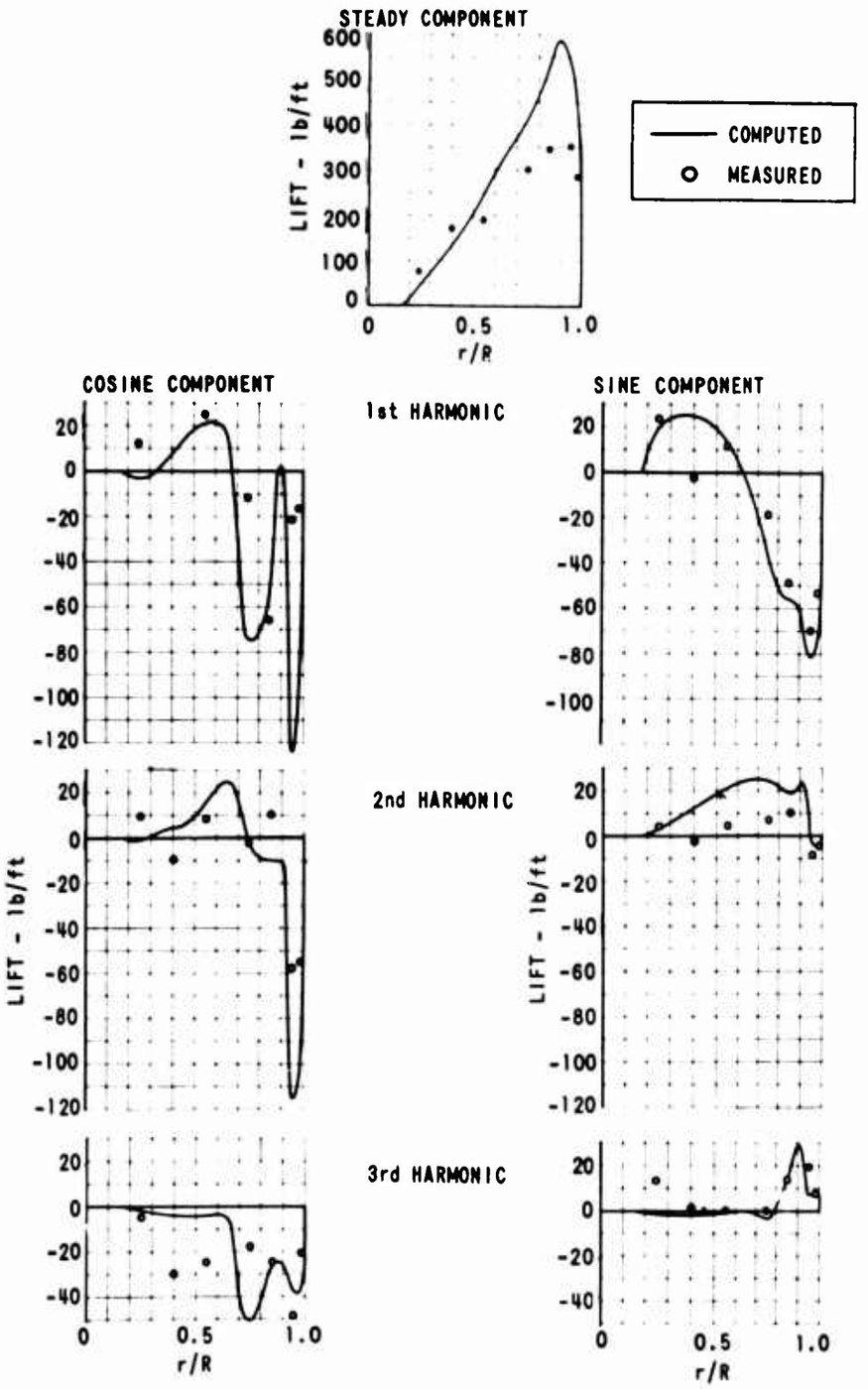

Figure 9. COMPARISON OF THE RADIAL VARIATION OF MEASURED AND COMPUTED LIFT, μ = 0.08, FORWARD ROTOR

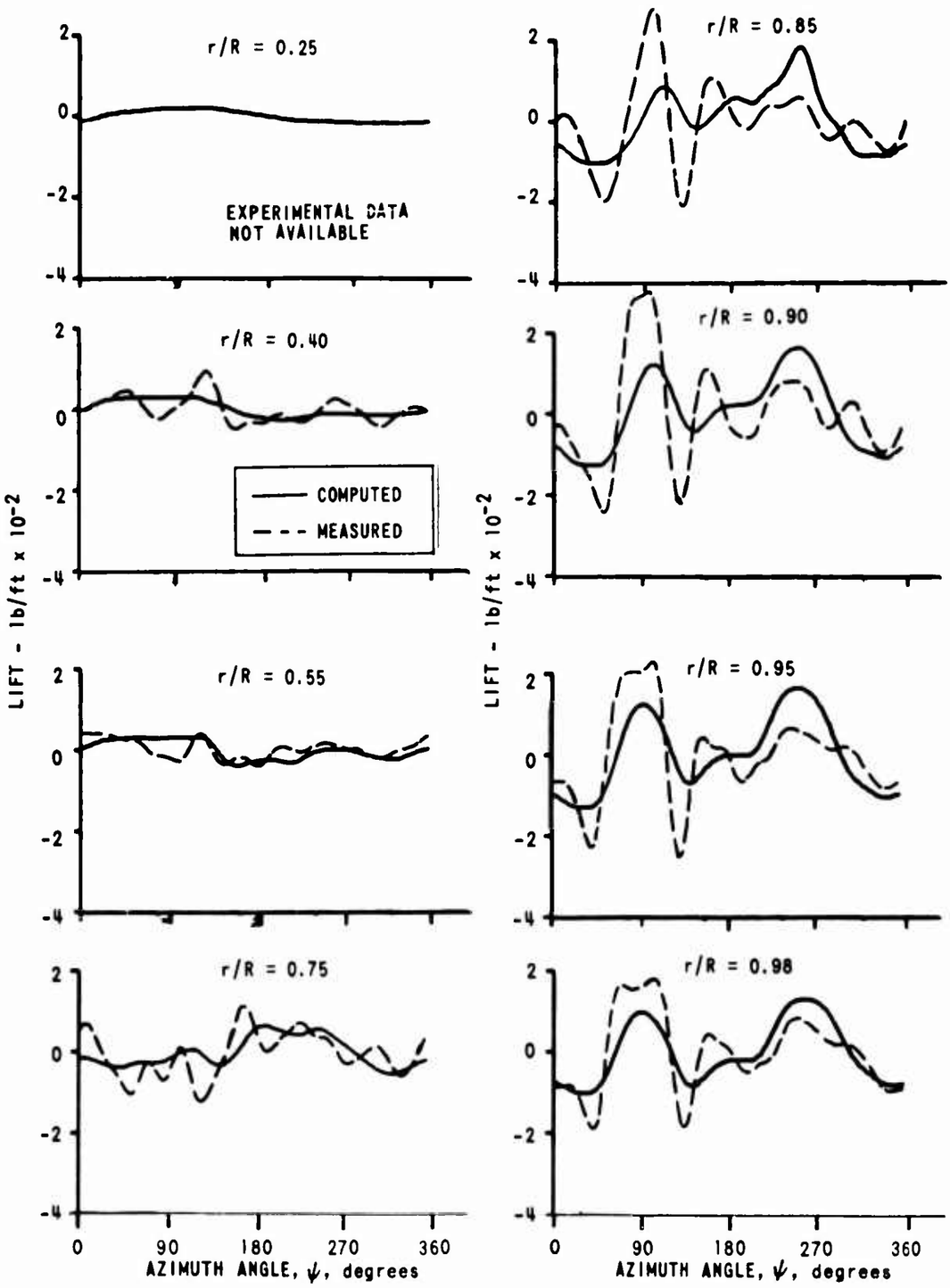

Figure 10. COMPARISON OF THE AZIMUTHAL VARIATION OF MEASURED AND COMPUTED LIFT, μ = 0.08, AFT ROTOR

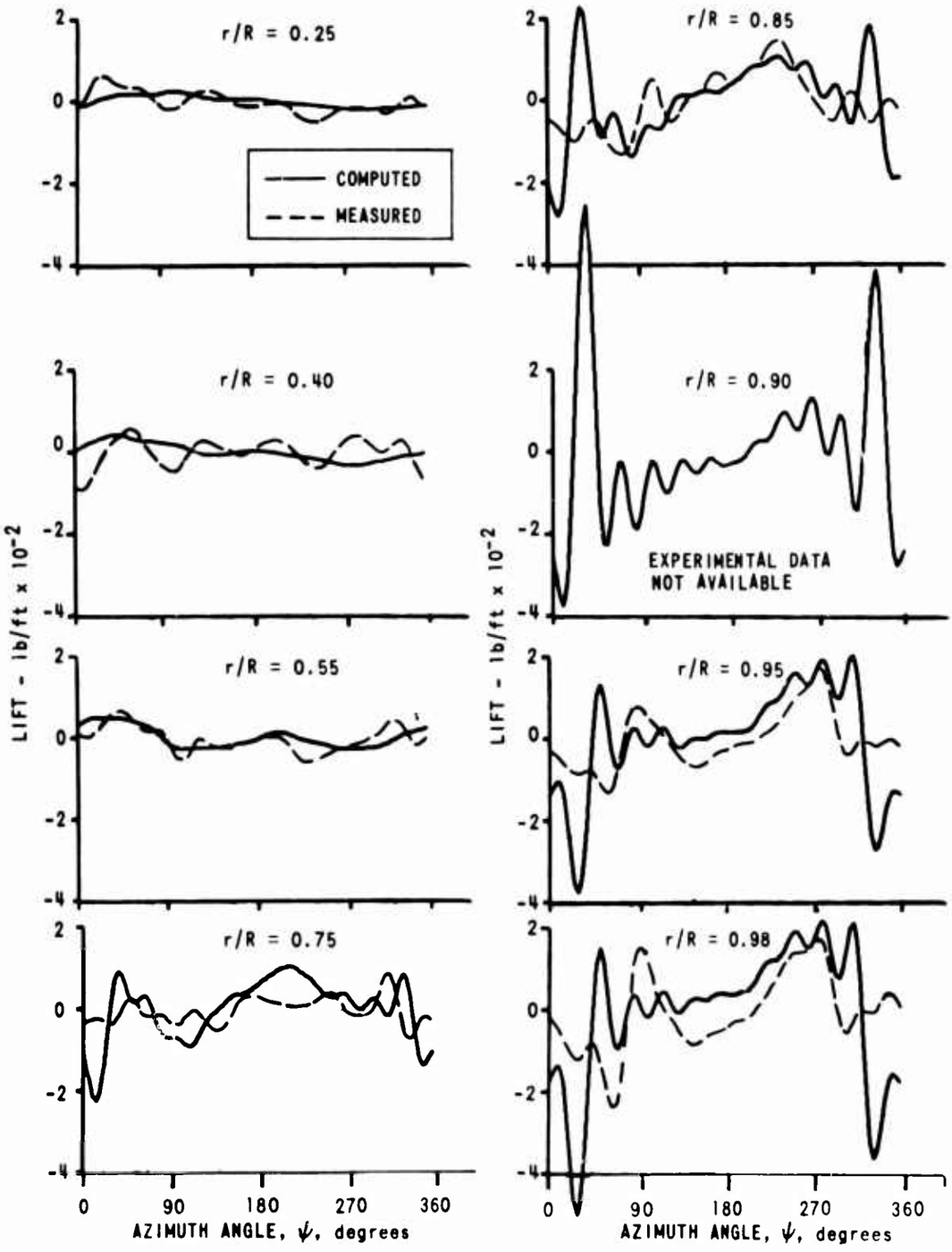

Figure 11. COMPARISON OF THE AZIMUTHAL VARIATION OF MEASURED AND COMPUTED LIFT, μ = 0.08, FORWARD ROTOR

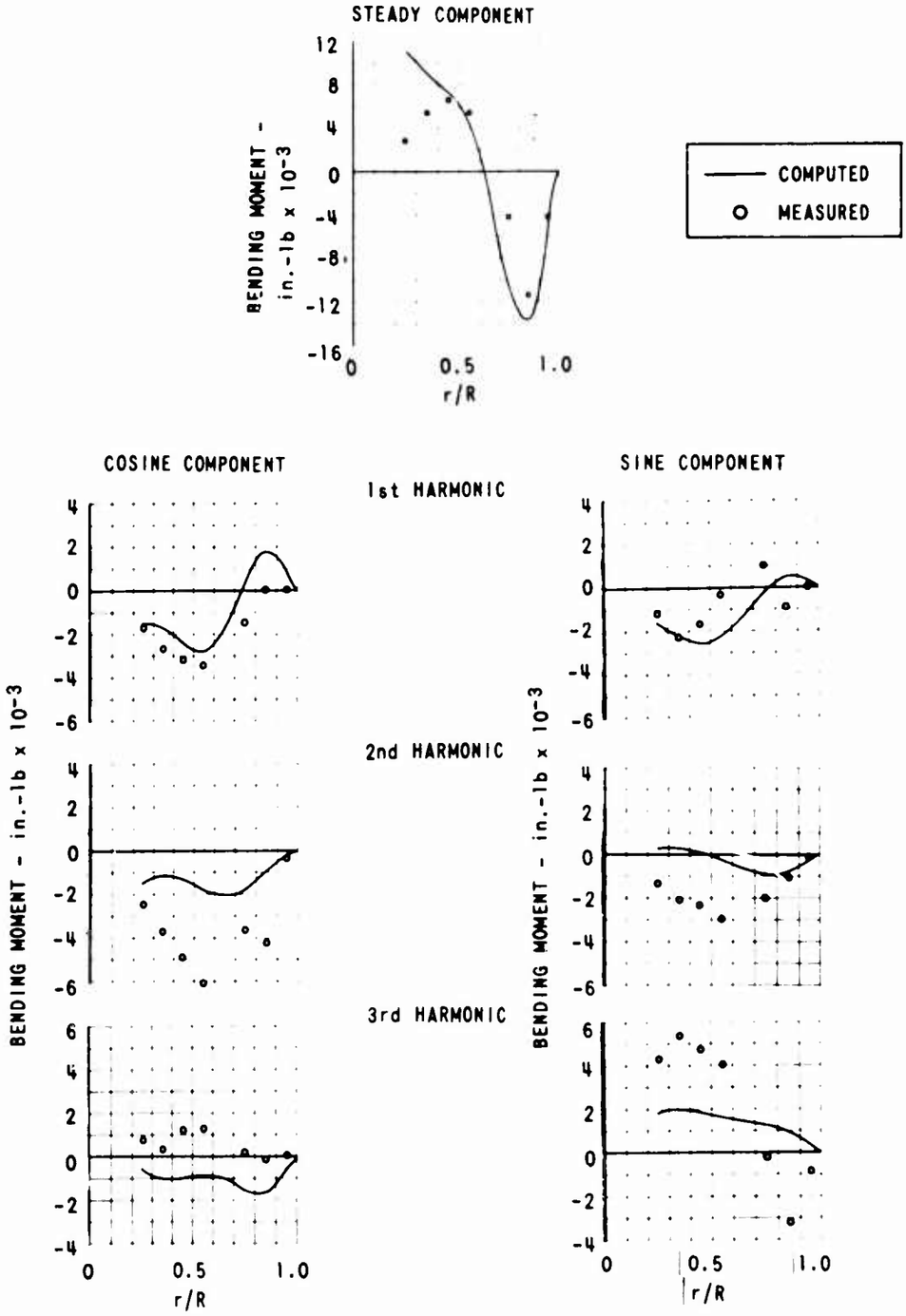

Figure 12. COMPARISON OF THE RADIAL VARIATION OF MEASURED AND COMPUTED FLAPWISE BENDING MOMENT, μ = 0.08, AFT ROTOR

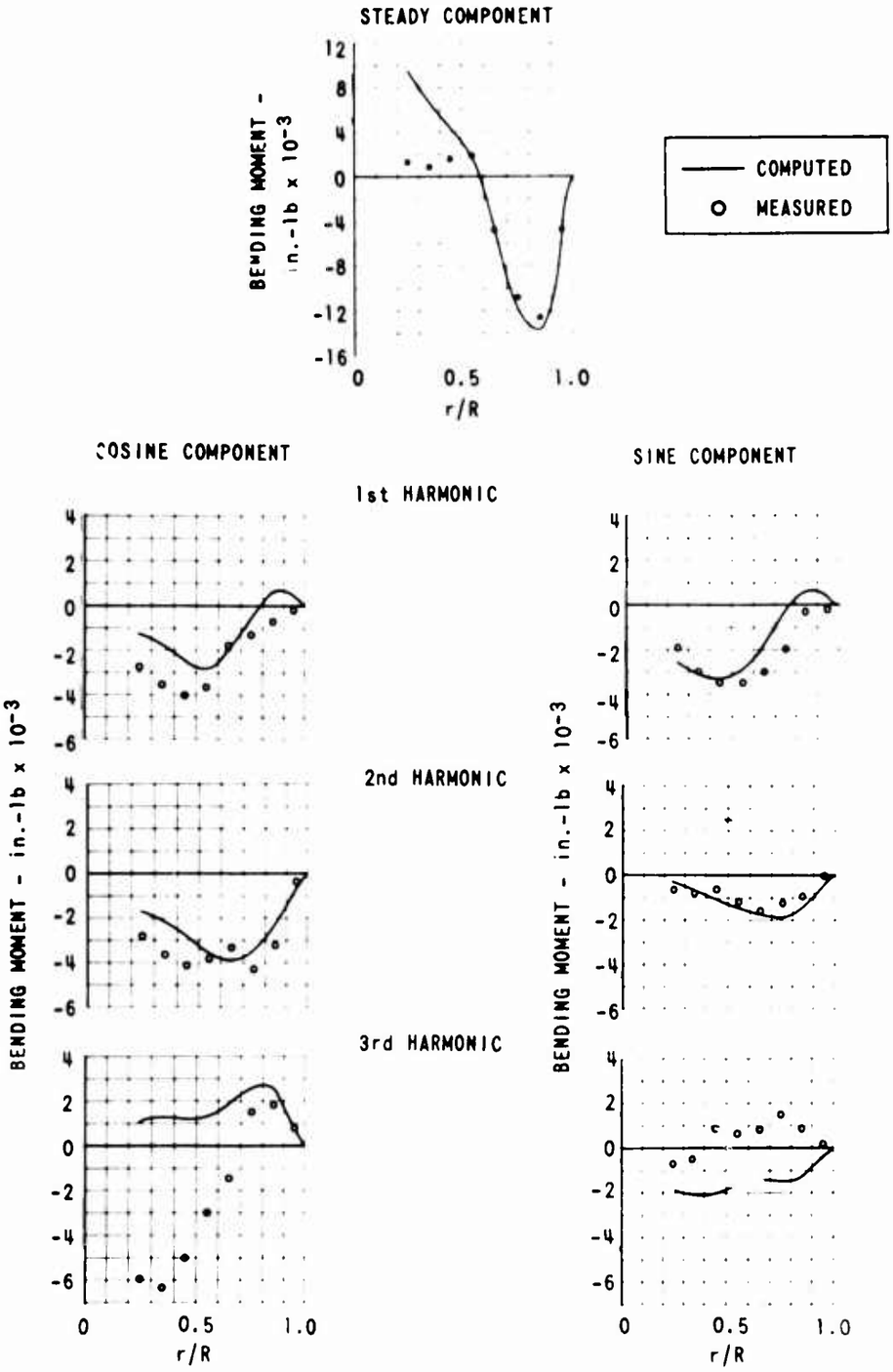

Figure 13. COMPARISON OF THE RADIAL VARIATION OF MEASURED AND COMPUTED FLAPWISE BENDING MOMENT, μ = 0.08, FORWARD ROTOR

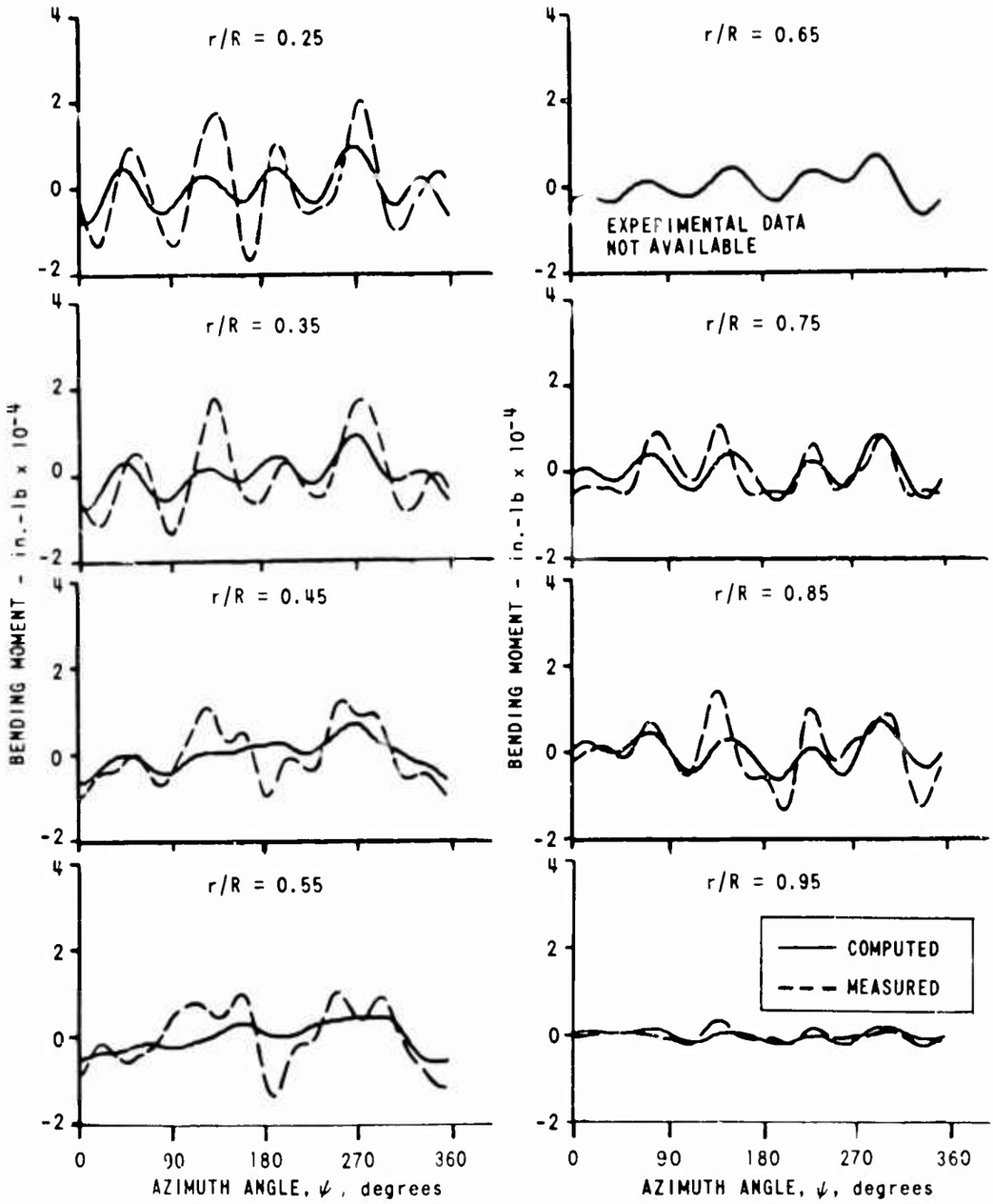

Figure 14. COMPARISON OF THE AZIMUTHAL VARIATION OF MEASURED AND COMPUTED FLAPWISE BENDING MOMENT, μ = 0.08, AFT ROTOR

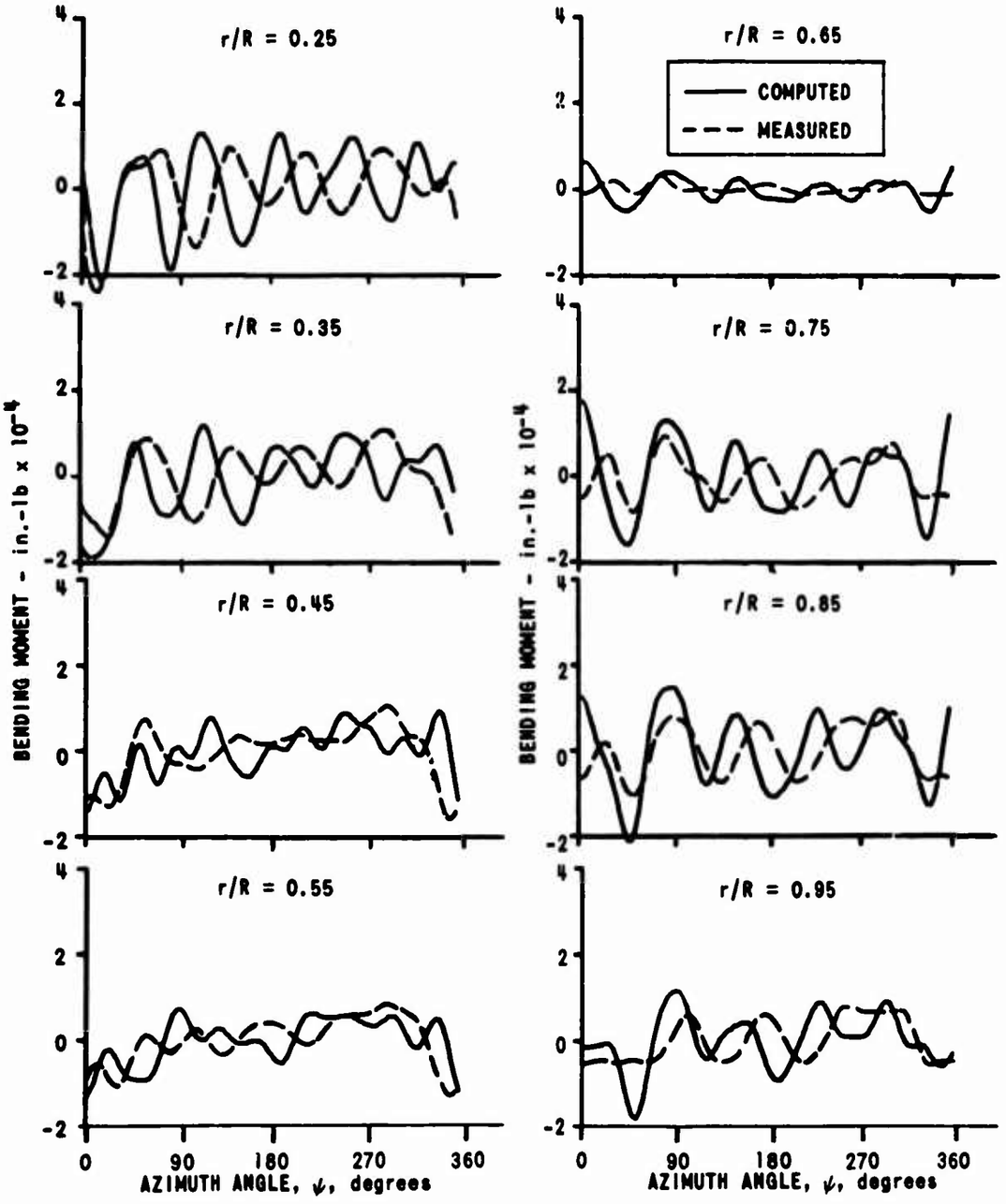

Figure 15. COMPARISON OF THE AZIMUTHAL VARIATION OF MEASURED AND COMPUTED FLAPWISE BENDING MOMENT, μ = 0.08, FORWARD ROTOR

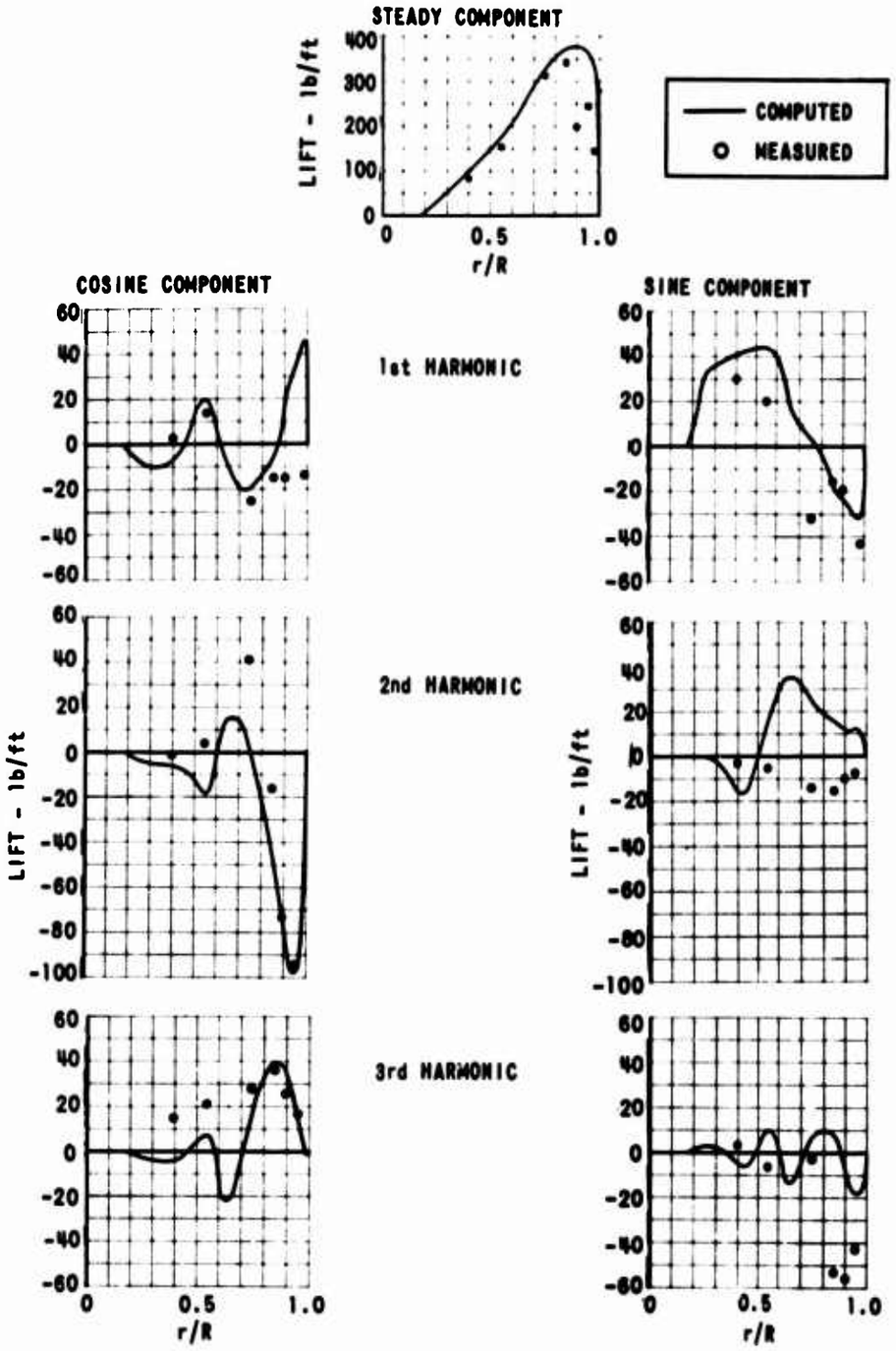

Figure 16. COMPARISON OF THE RADIAL VARIATION OF MEASURED AND COMPUTED LIFT, μ = 0.14, AFT ROTOR

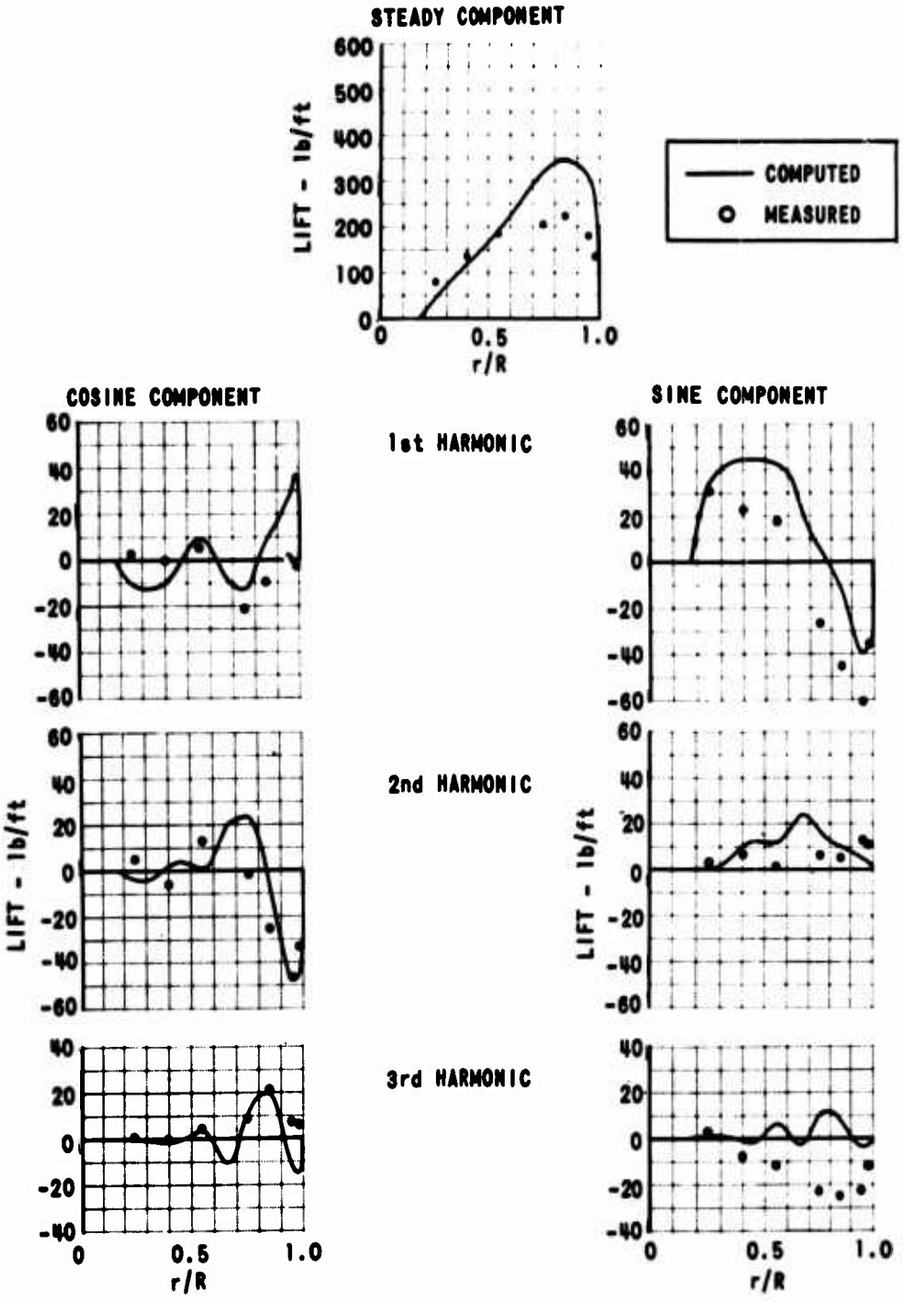

Figure 17. COMPARISON OF THE RADIAL VARIATION OF MEASURED AND COMPUTED LIFT, μ = 0.14, FORWARD ROTOR

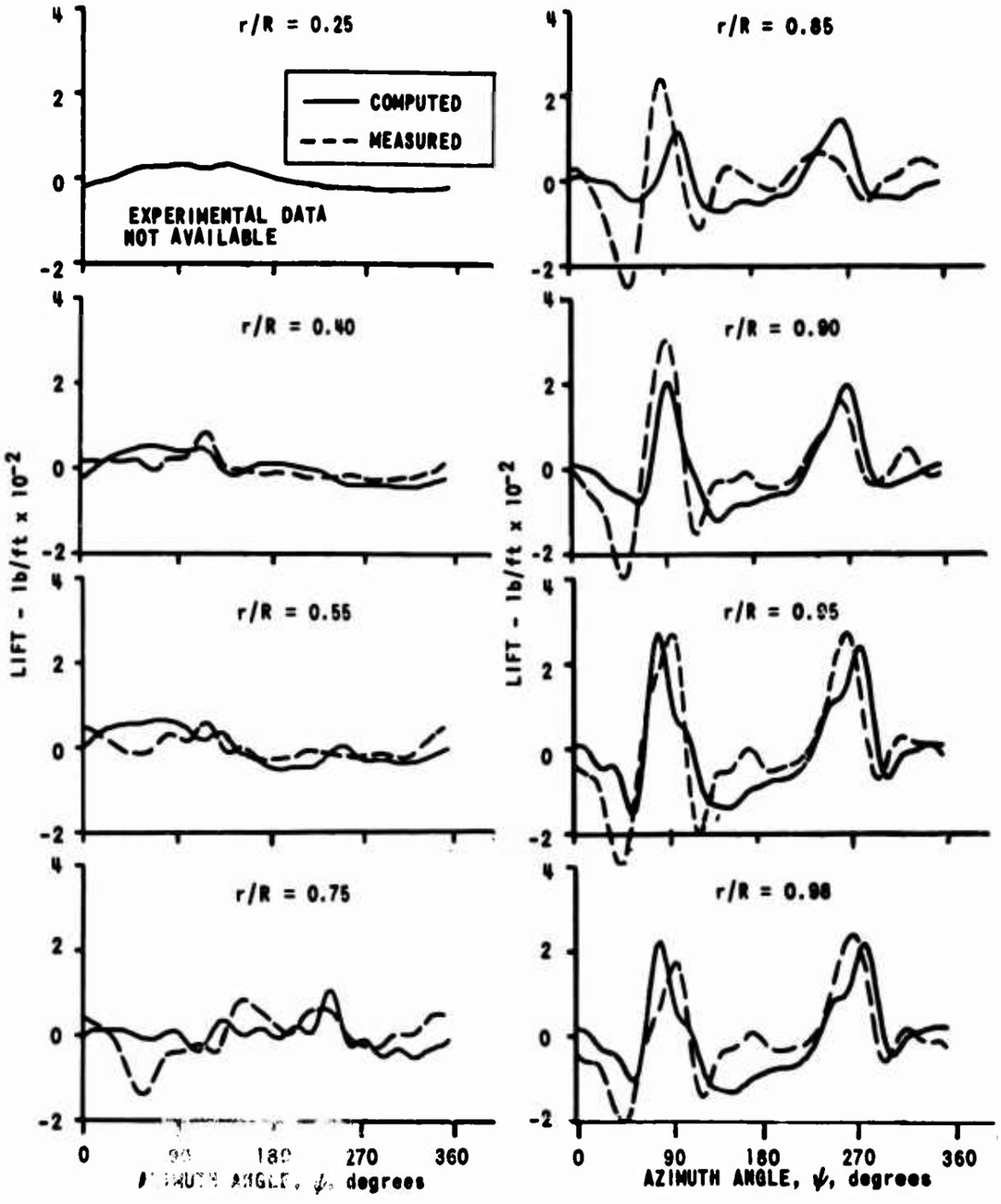

Figure 18. COMPARISON OF THE AZIMUTHAL VARIATION OF MEASURED AND COMPUTED LIFT, $\mu = 0.14$, AFT ROTOR

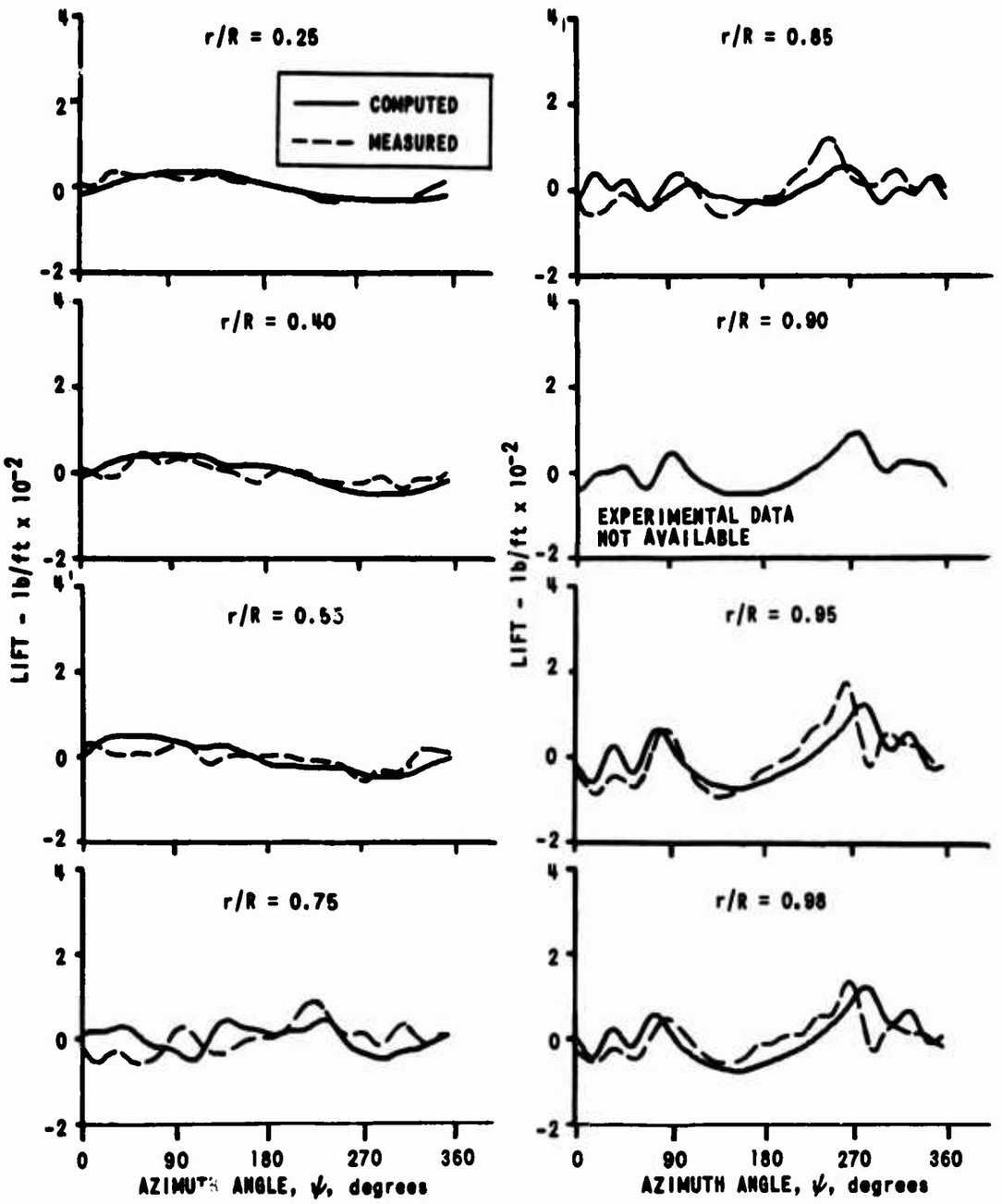

Figure 19. COMPARISON OF THE AZIMUTHAL VARIATION OF MEASURED AND COMPUTED LIFT, $\mu = 0.14$, FORWARD ROTOR

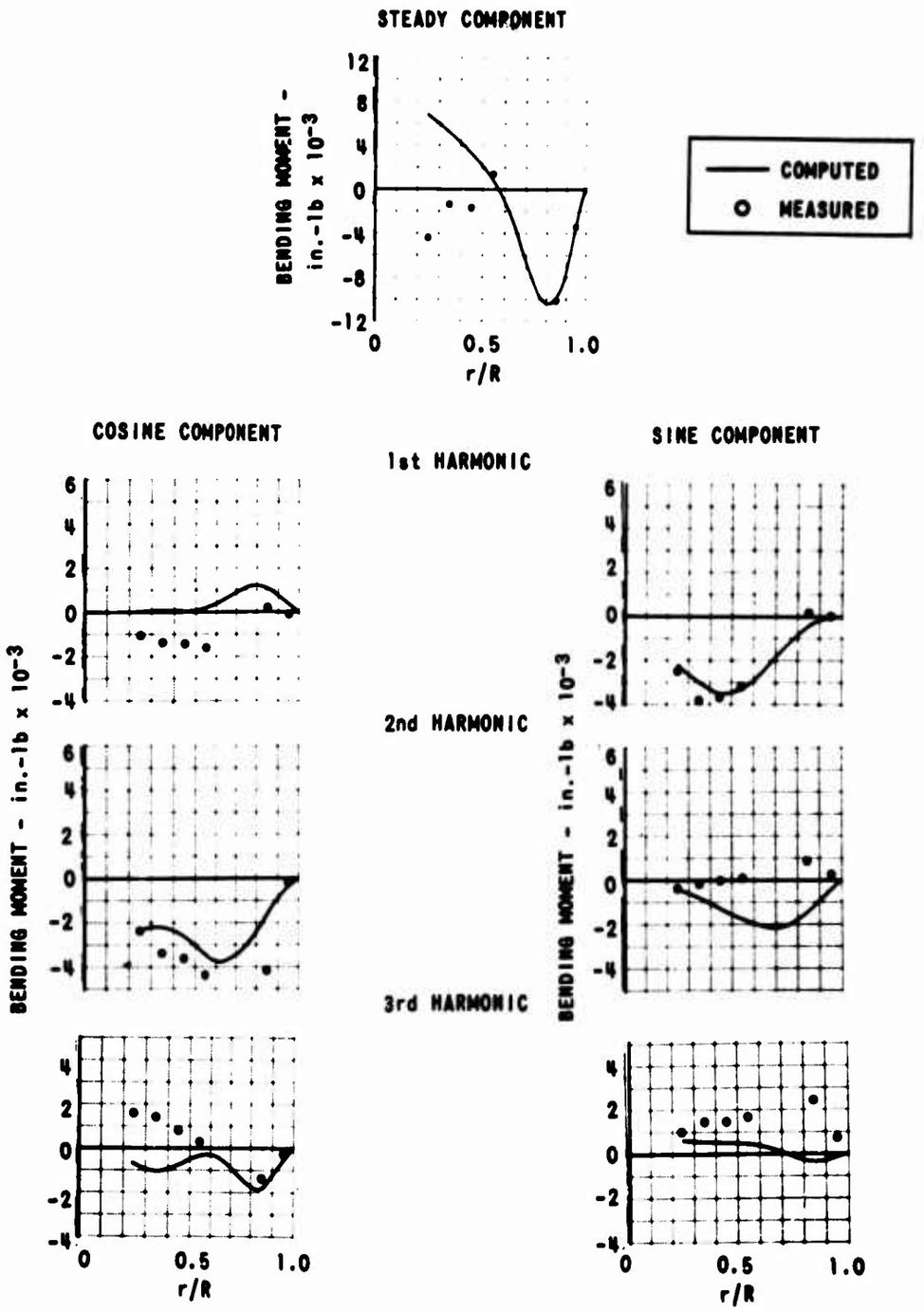

Figure 20. COMPARISON OF THE RADIAL VARIATION OF MEASURED AND COMPUTED FLAPWISE BENDING MOMENT, μ = 0.14, AFT ROTOR

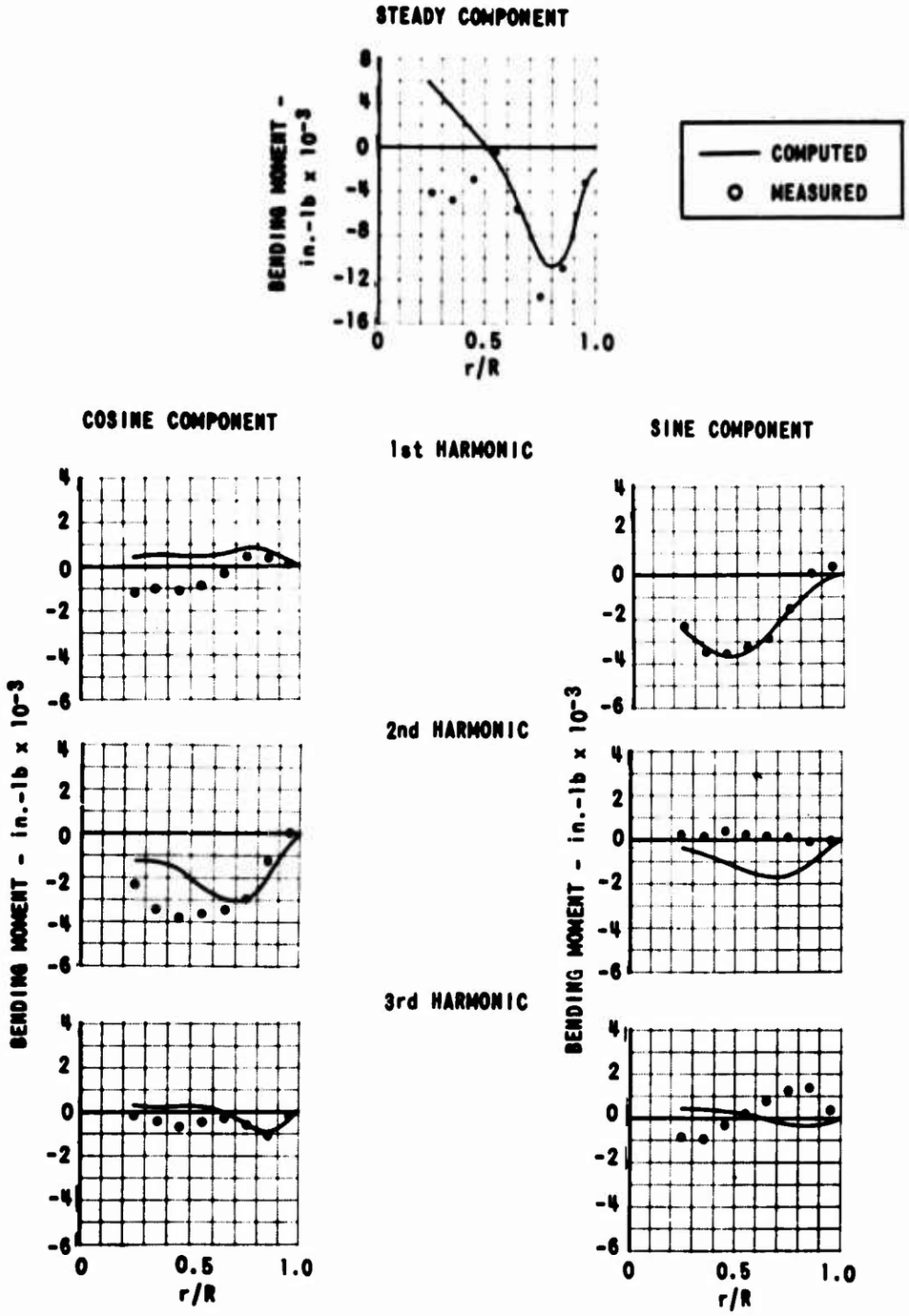

Figure 21. COMPARISON OF THE RADIAL VARIATION OF MEASURED AND COMPUTED FLAPWISE BENDING MOMENT, μ = 0.14, FORWARD ROTOR

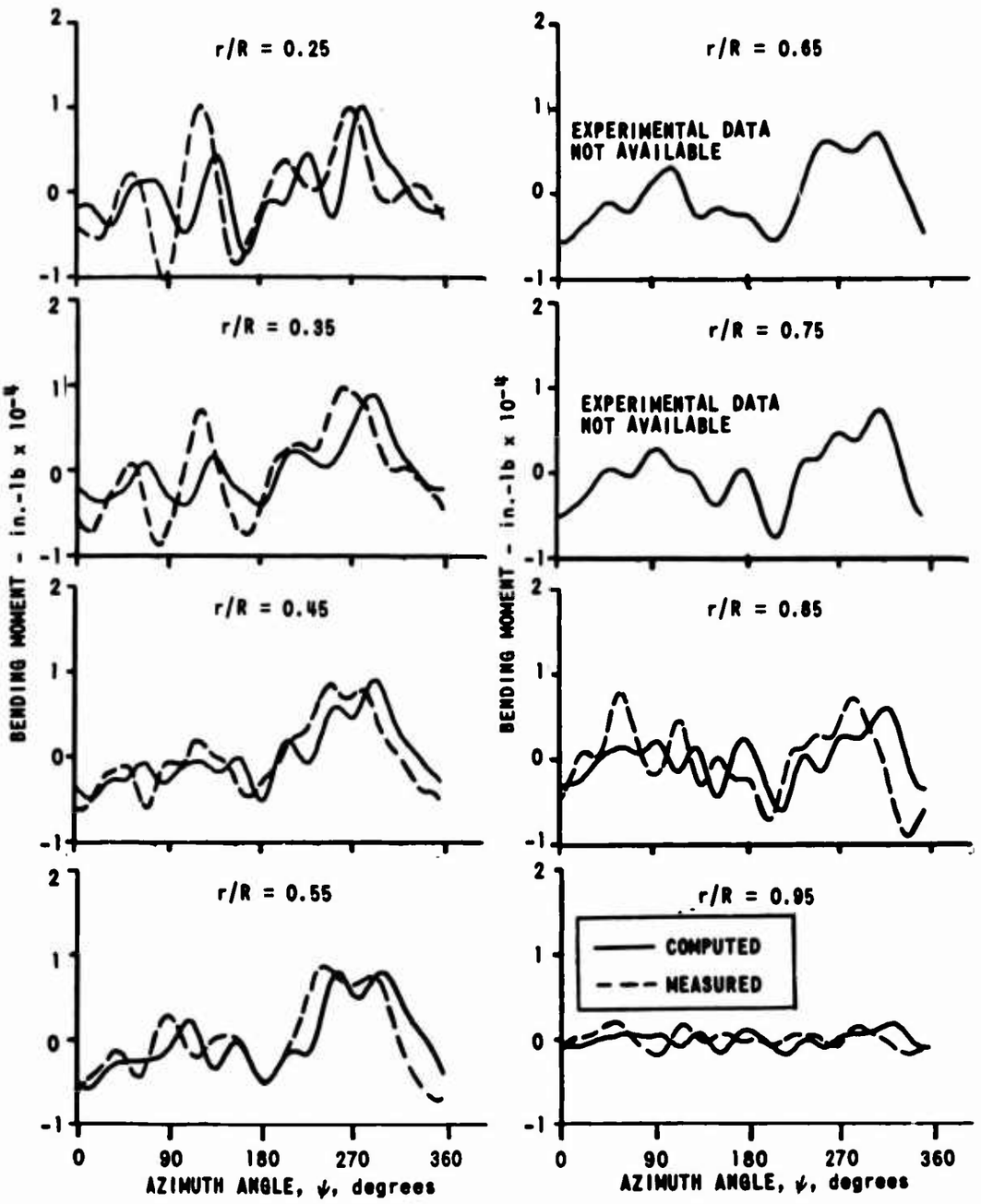

Figure 22. COMPARISON OF THE AZIMUTHAL VARIATION OF MEASURED AND COMPUTED FLAPWISE BENDING MOMENT, $\mu = 0.14$, AFT ROTOR

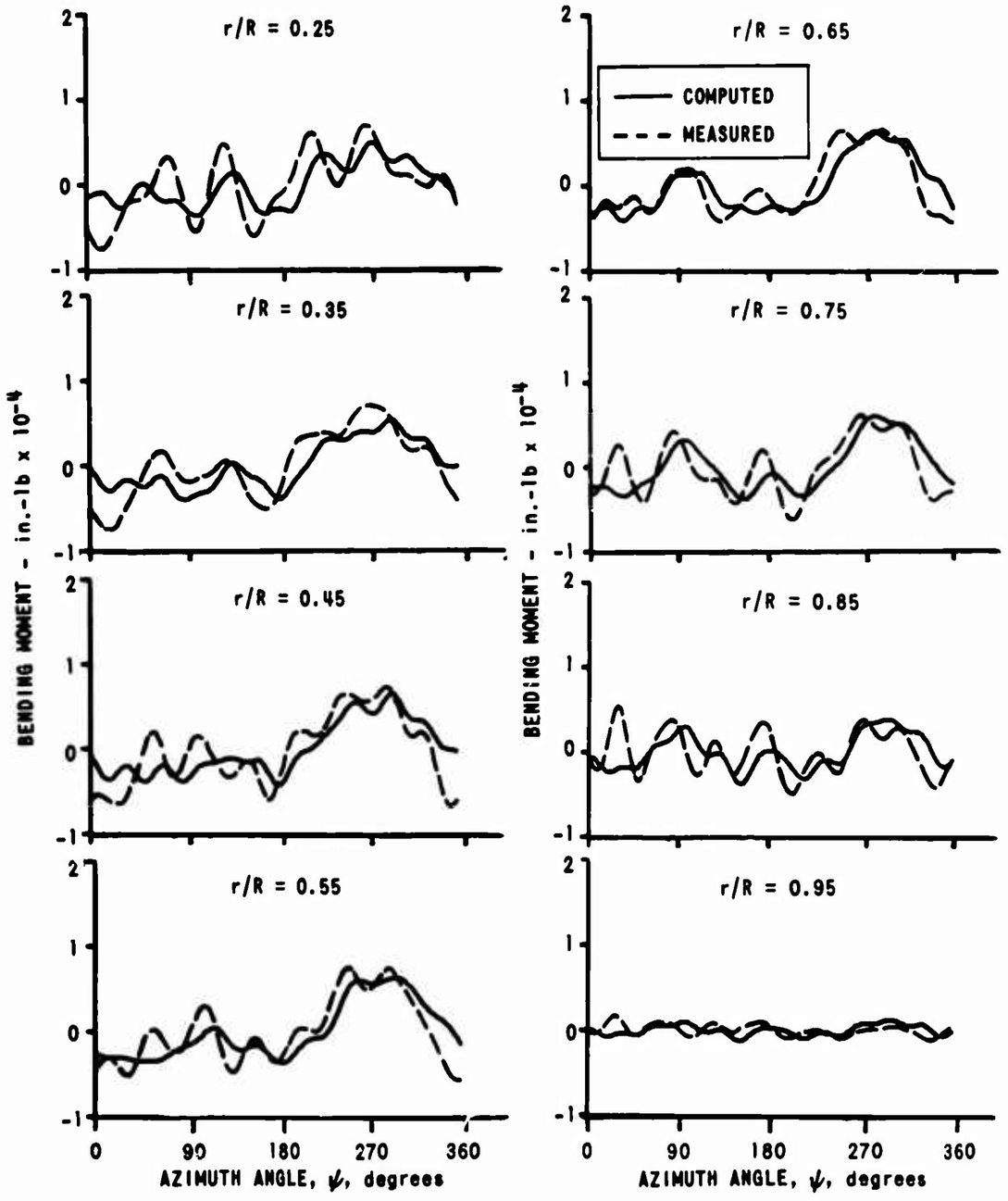

Figure 23. COMPARISON OF THE AZIMUTHAL VARIATION OF MEASURED AND COMPUTED FLAPWISE BENDING MOMENT, $\mu = 0.14$, FORWARD ROTOR

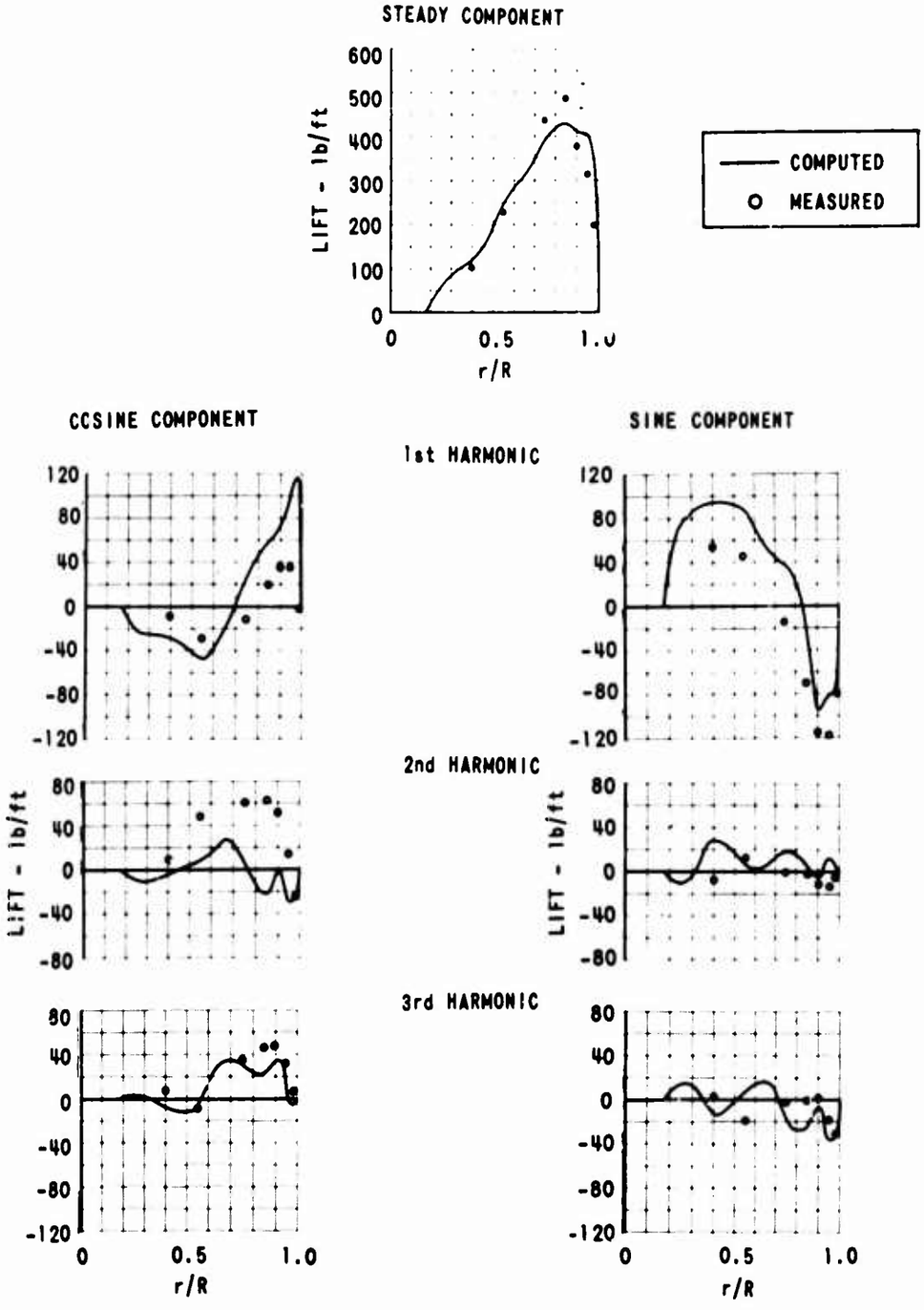

Figure 24. COMPARISON OF THE RADIAL VARIATION OF MEASURED AND COMPUTED LIFT, μ = 0.24, AFT ROTOR

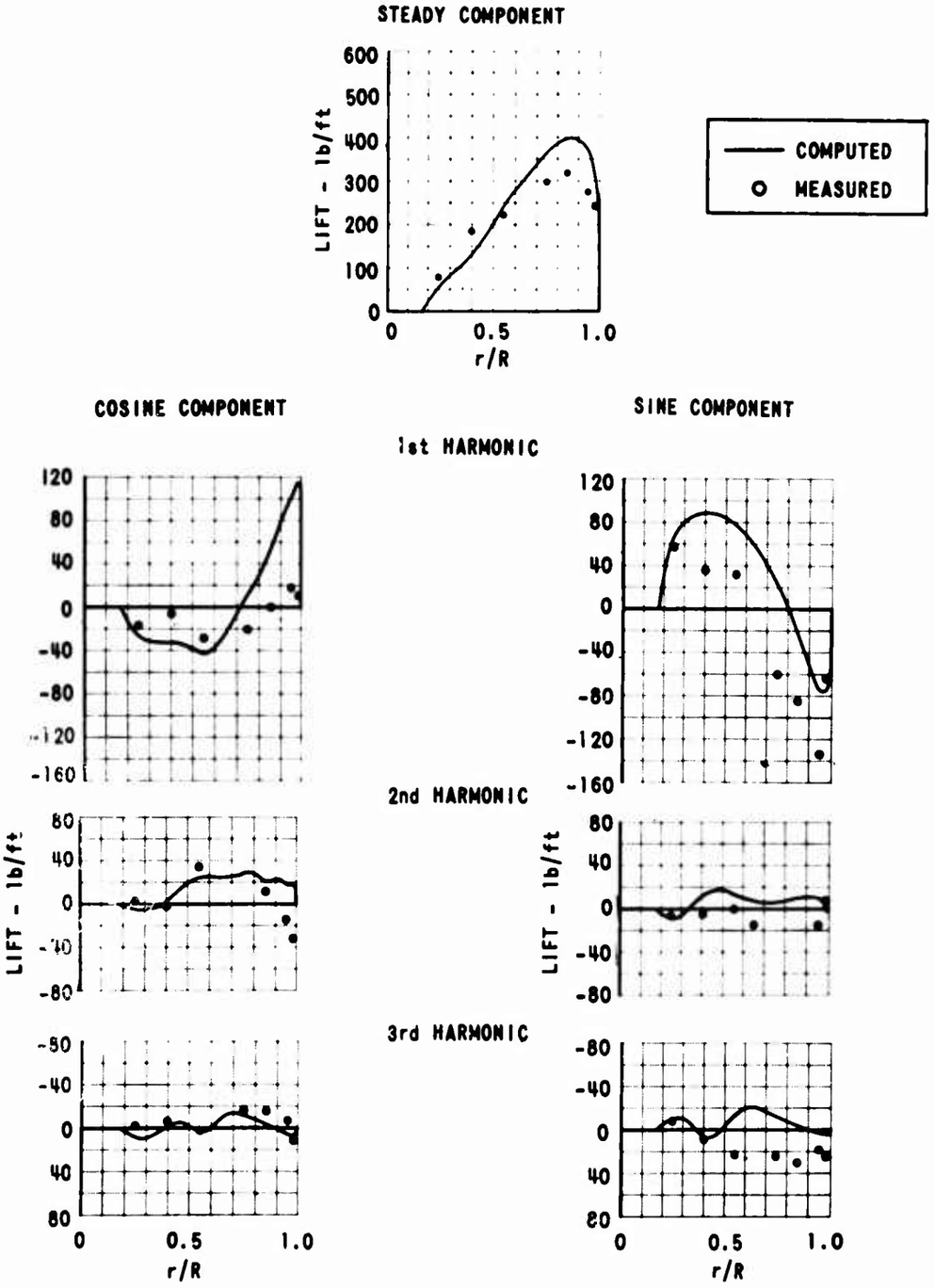

Figure 25. COMPARISON OF THE RADIAL VARIATION OF MEASURED AND COMPUTED LIFT, $\mu = 0.24$, FORWARD ROTOR

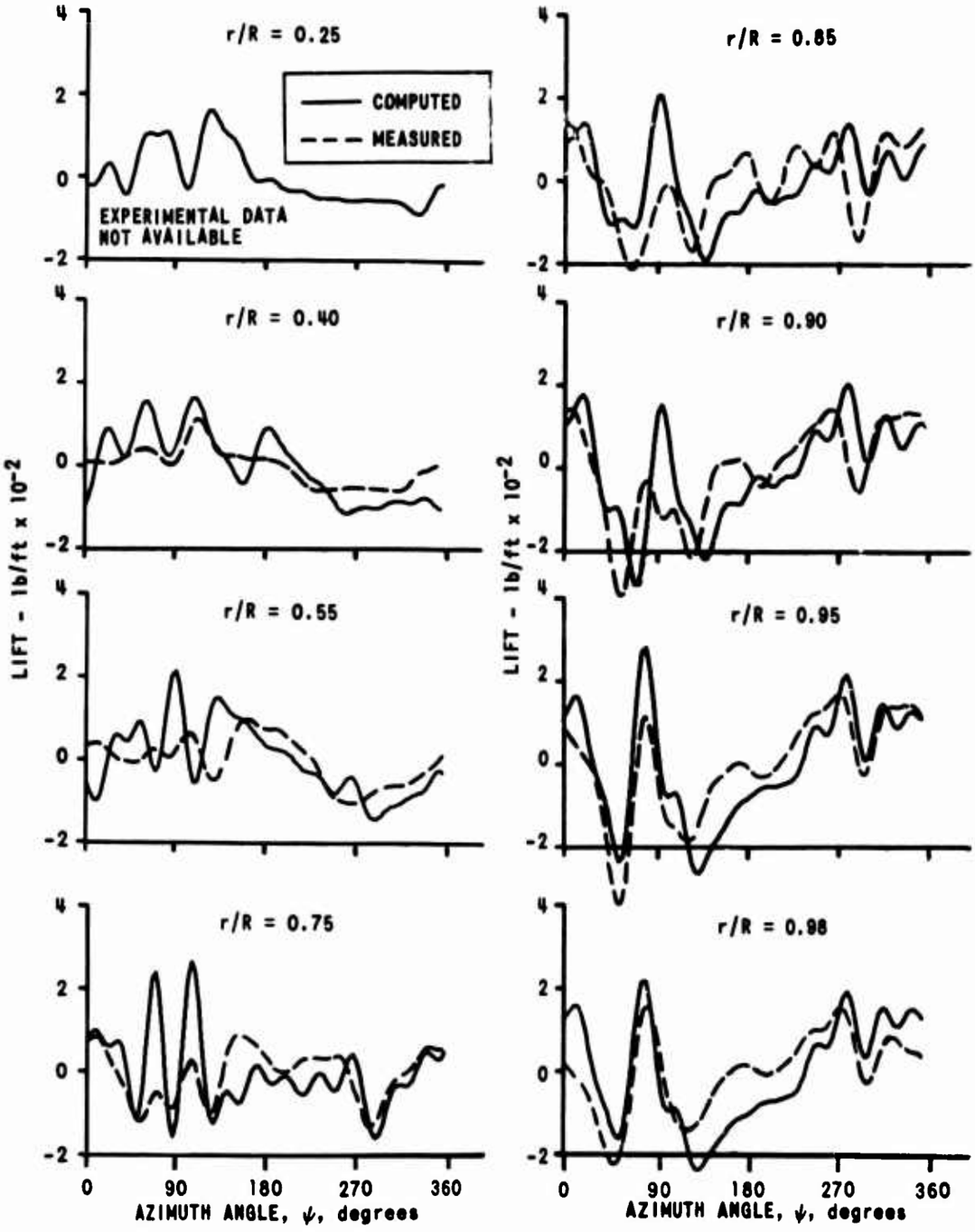

Figure 26. COMPARISON OF THE AZIMUTHAL VARIATION OF MEASURED AND COMPUTED LIFT, $\mu = 0.24$, AFT ROTOR

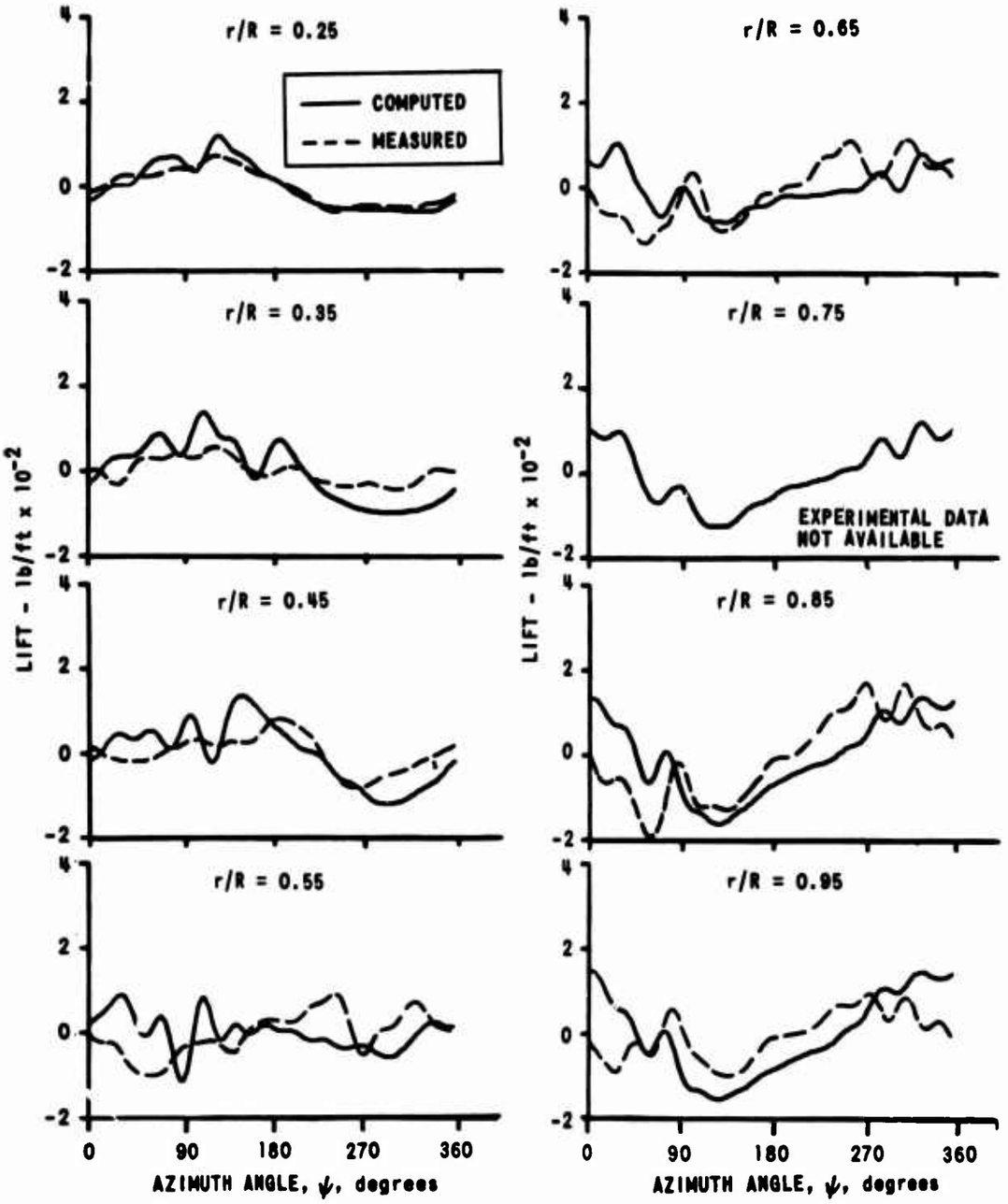

Figure 27. COMPARISON OF THE AZIMUTHAL VARIATION OF MEASURED AND COMPUTED LIFT, $\mu = 0.24$, FORWARD ROTOR

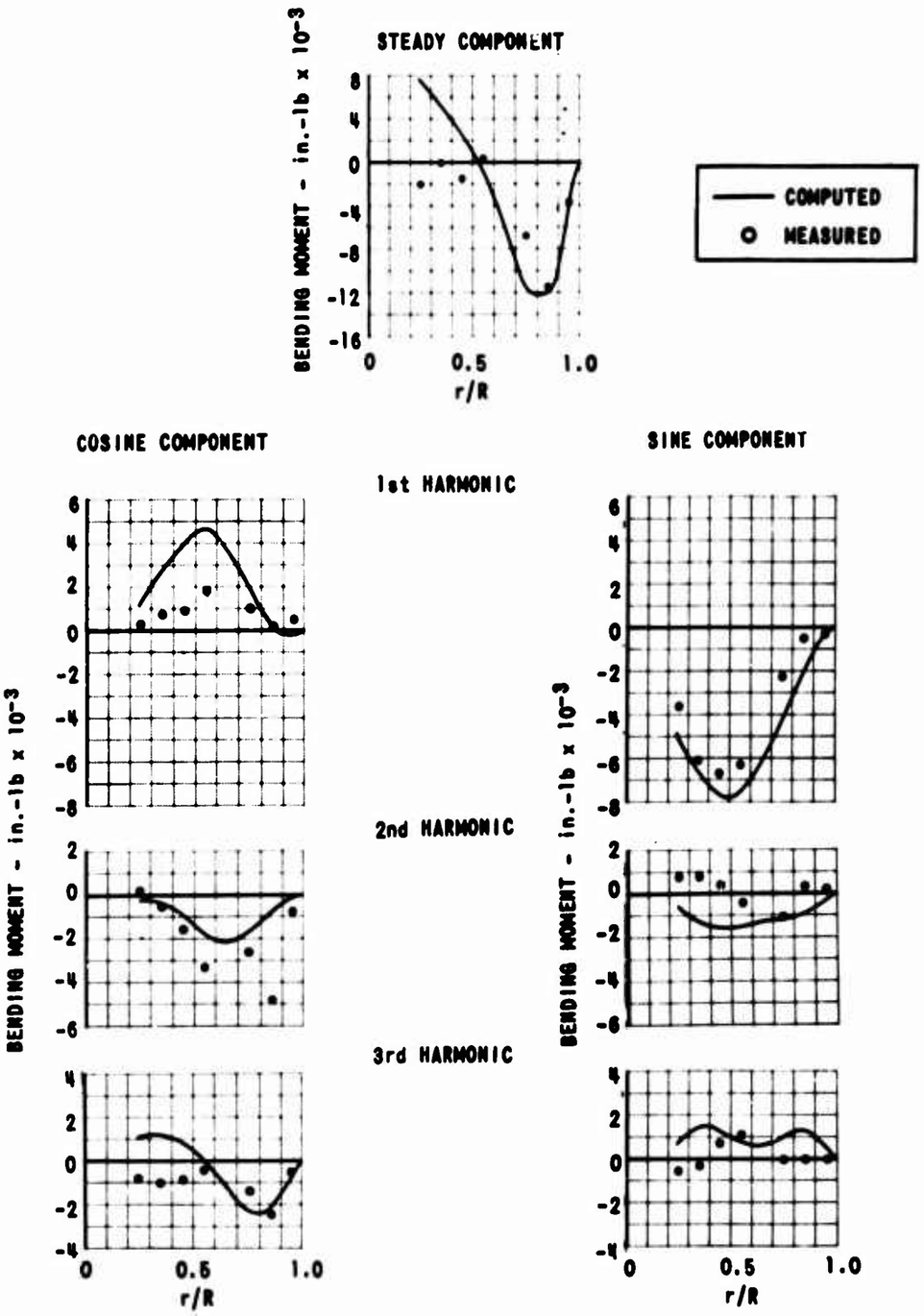

Figure 28. COMPARISON OF THE RADIAL VARIATION OF MEASURED AND COMPUTED FLAPWISE BENDING MOMENT, $\mu = 0.24$, AFT-ROTOR

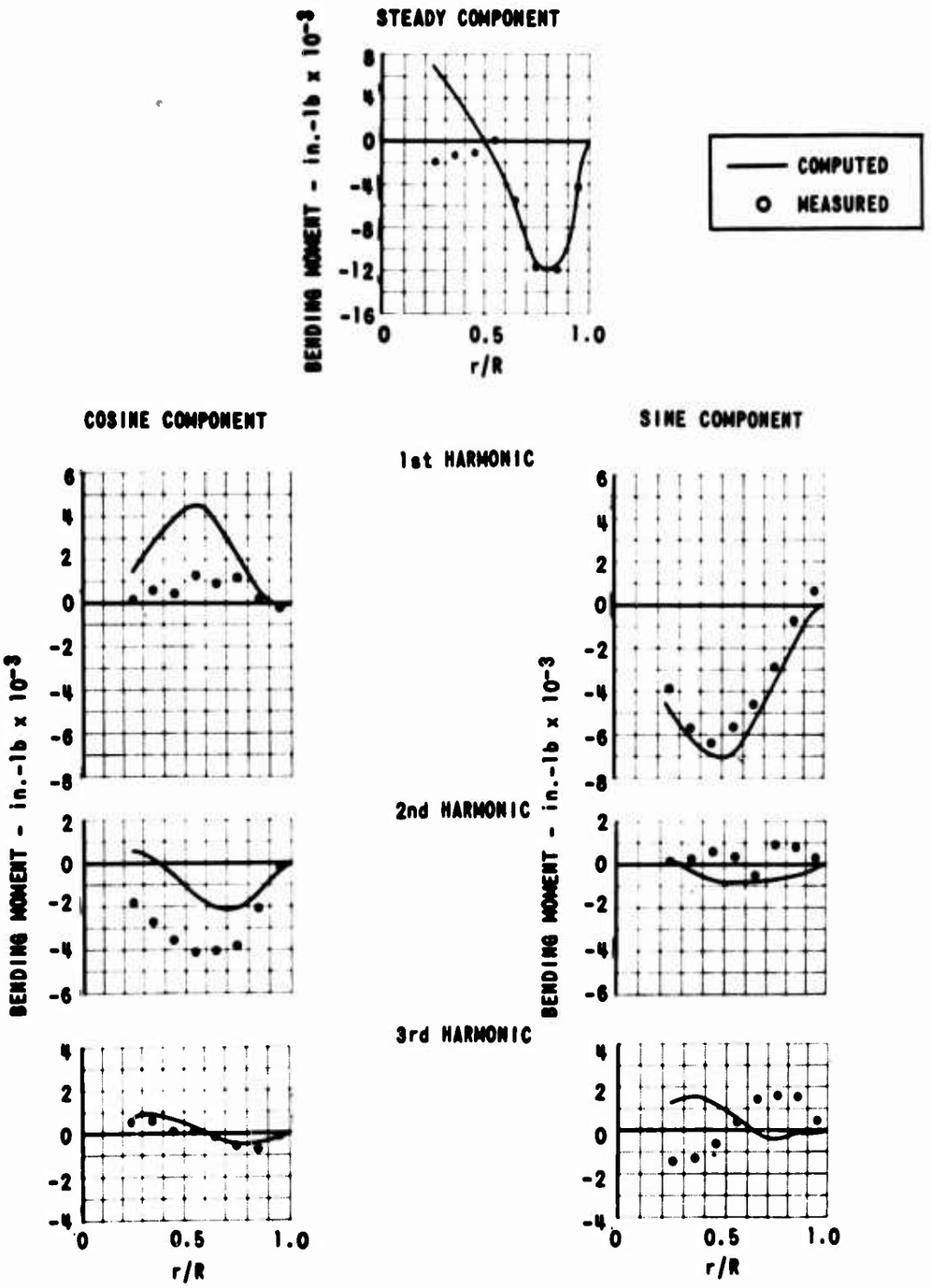

Figure 29. COMPARISON OF THE RADIAL VARIATION OF MEASURED AND COMPUTED FLAPWISE BENDING MOMENT, $\mu = 0.24$, FORWARD ROTOR

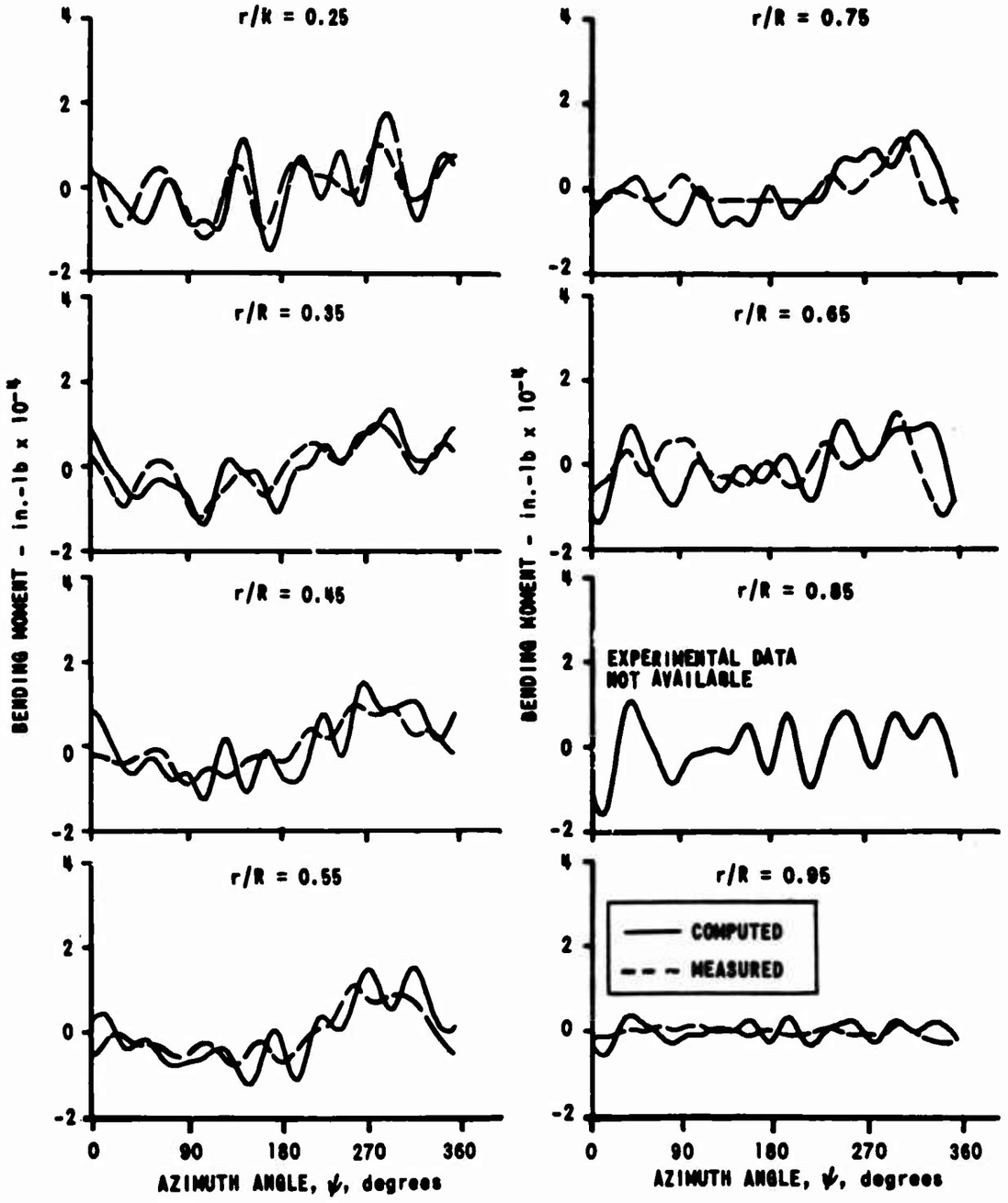

Figure 30. COMPARISON OF THE AZIMUTHAL VARIATION OF MEASURED AND COMPUTED FLAPWISE BENDING MOMENT, $\mu = 0.24$, AFT ROTOR

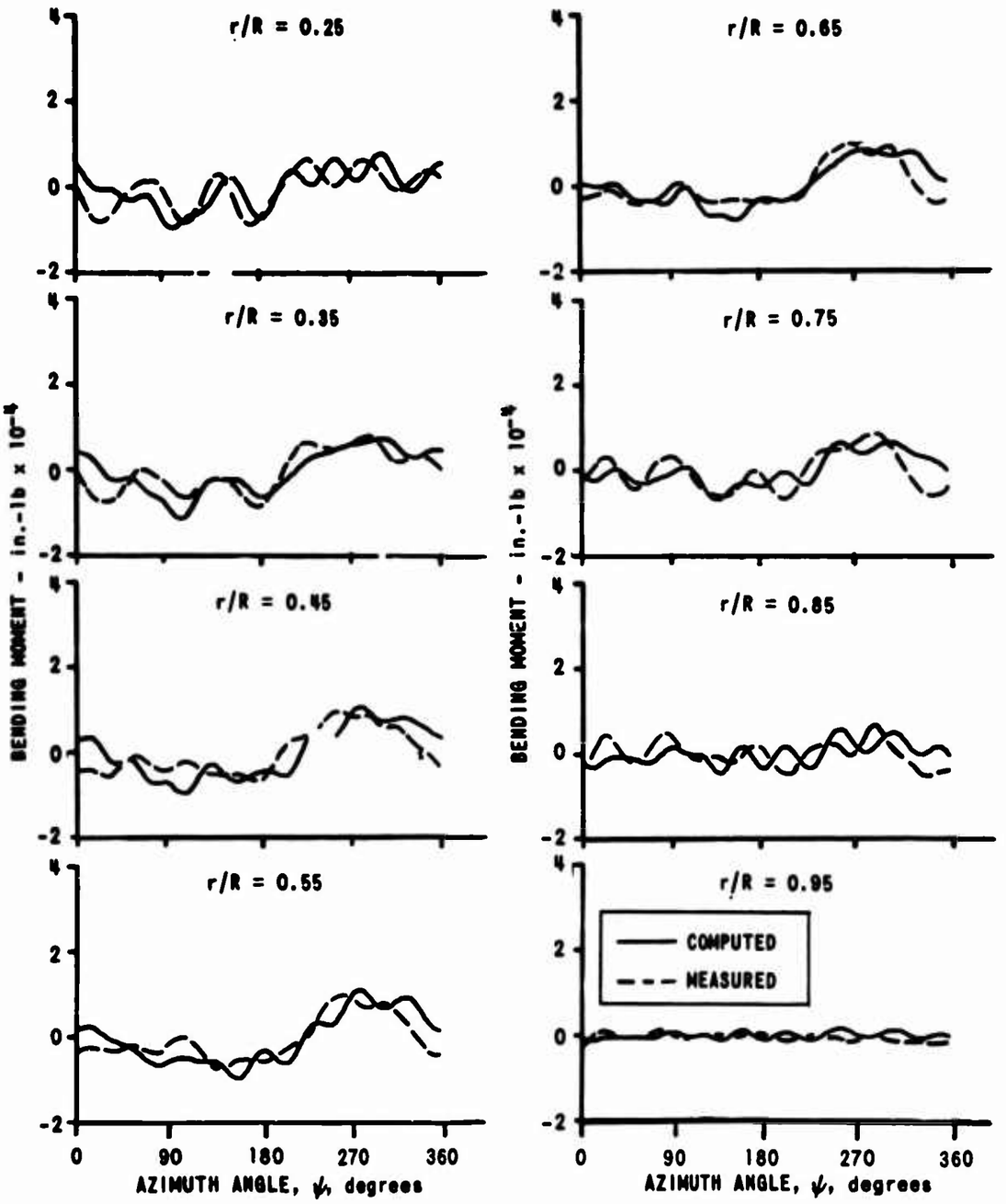

Figure 31. COMPARISON OF THE AZIMUTHAL VARIATION OF MEASURED AND COMPUTED FLAPWISE BENDING MOMENT, $\mu = 0.24$, FORWARD ROTOR

BLANK PAGE

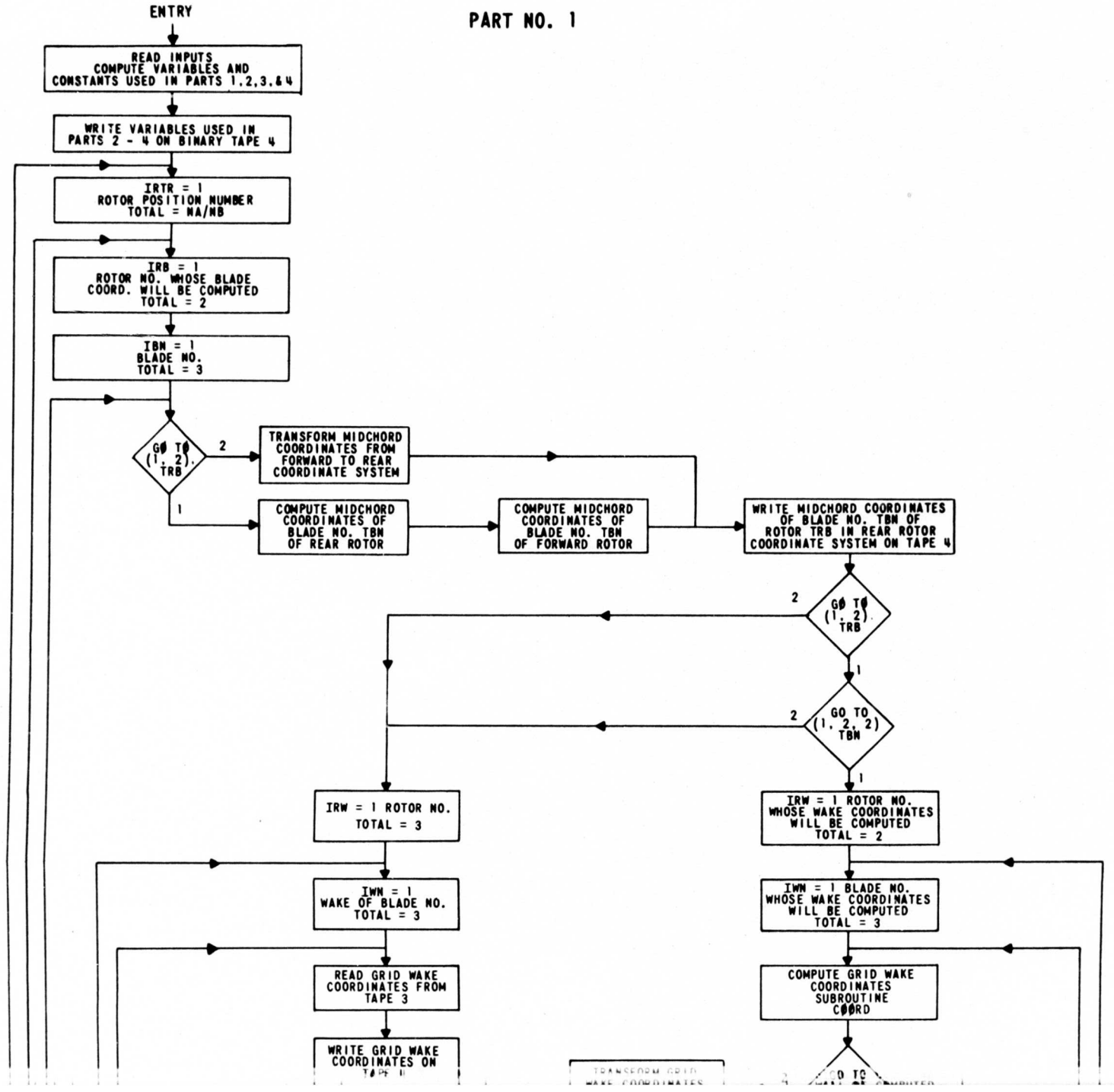

Figure 32. FLOW DIAGRAMS FOR COMPUTER PROGRAM

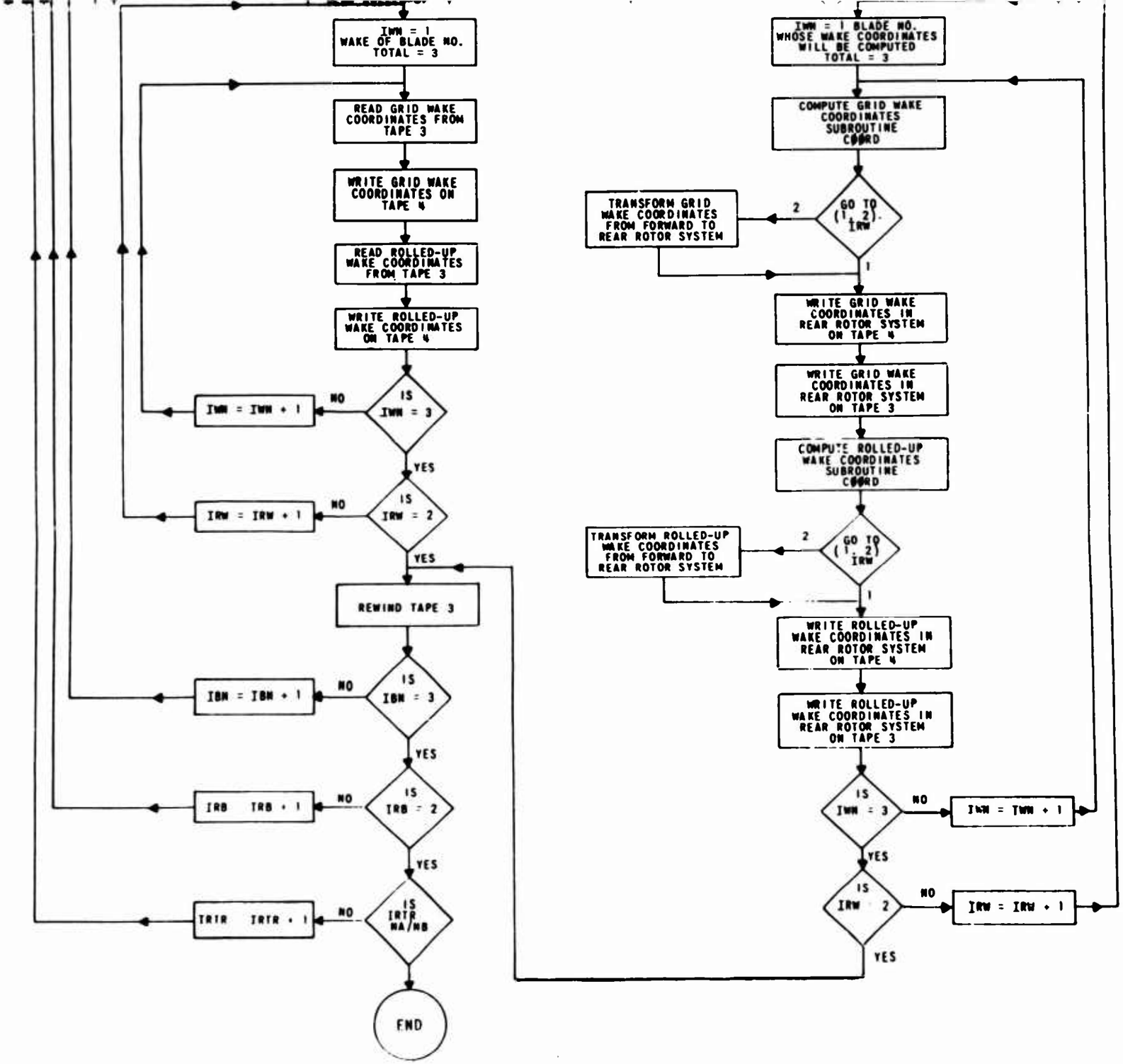
IWW = 1
WAKE OF BLADE NO.
TOTAL = 3
READ GRID WAKE COORDINATES FROM TAPE 3
WRITE GRID WAKE COORDINATES ON TAPE 4
READ ROLLED-UP WAKE COORDINATES FROM TAPE 3
WRITE ROLLED-UP WAKE COORDINATES ON TAPE 4
IS IWW = 3
NO
IWW = IWW + 1
YES
IS IRW = 2
NO
IRW = IRW + 1
YES
REWIND TAPE 3
IS IBW = 3
NO
IBW = IBW + 1
YES
IS IRB = 2
NO
IRB = IRB + 1
YES
IS IRTR = NA/NB
NO
IRTR = IRTR + 1
END
IWW = 1 BLADE NO. WHOSE WAKE COORDINATES WILL BE COMPUTED TOTAL = 3
COMPUTE GRID WAKE COORDINATES SUBROUTINE COORD
GO TO (1, 2), IRW
2
TRANSFORM GRID WAKE COORDINATES FROM FORWARD TO REAR ROTOR SYSTEM
1
WRITE GRID WAKE COORDINATES IN REAR ROTOR SYSTEM ON TAPE 4
WRITE GRID WAKE COORDINATES IN REAR ROTOR SYSTEM ON TAPE 3
COMPUTE ROLLED-UP WAKE COORDINATES SUBROUTINE COORD
GO TO (1, 2), IRW
2
TRANSFORM ROLLED-UP WAKE COORDINATES FROM FORWARD TO REAR ROTOR SYSTEM
1
WRITE ROLLED-UP WAKE COORDINATES IN REAR ROTOR SYSTEM ON TAPE 4
WRITE ROLLED-UP WAKE COORDINATES IN REAR ROTOR SYSTEM ON TAPE 3
IS IWW = 3
NO
IWW = IWW + 1
YES
IS IRW = 2
NO
IRW = IRW + 1
YES

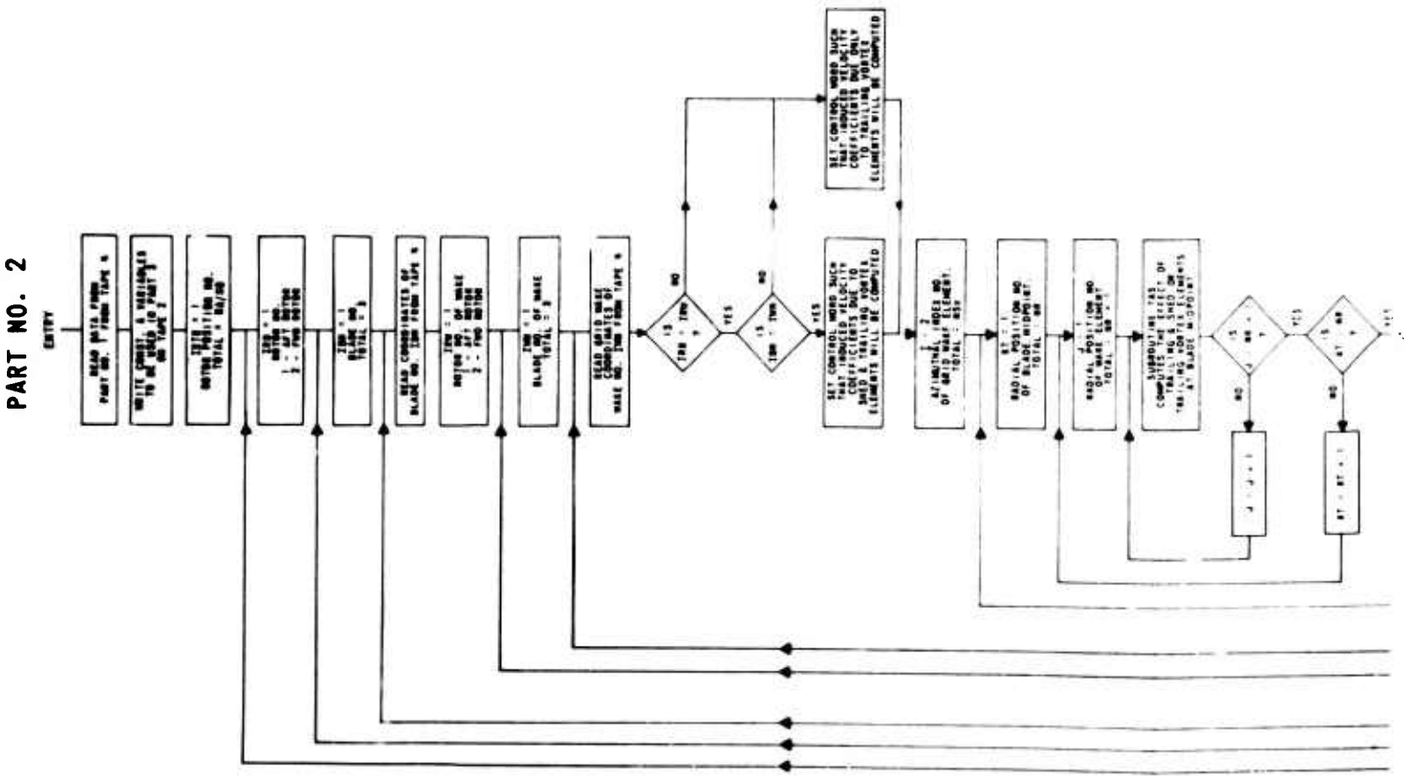

Figure 32 (Cont.)

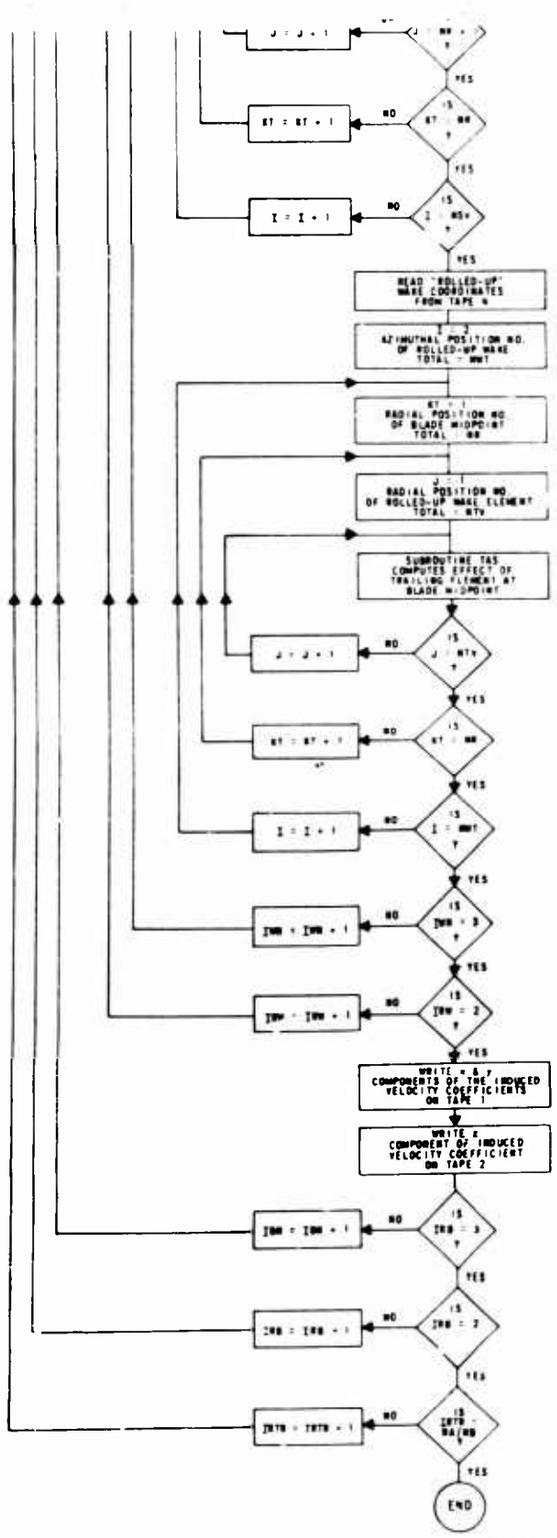
J = J + 1
NO
IS J = NBW + 1 ?
YES
KT = KT + 1
NO
IS KT = NR ?
YES
I = I + 1
NO
IS I = NSW + 1 ?
YES
READ 'ROLLED-UP' WAKE COORDINATES FROM TAPE 4
I = 2
AZIMUTHAL POSITION NO. OF ROLLED-UP WAKE TOTAL = NWT
KT = 1
RADIAL POSITION NO OF BLADE MIDPOINT TOTAL = NR
J = 1
RADIAL POSITION NO OF ROLLED-UP WAKE ELEMENT TOTAL = NTV
SUBROUTINE TAS COMPUTES EFFECT OF TRAILING ELEMENT AT BLADE MIDPOINT
J = J + 1
NO
IS J = NTV + 1 ?
YES
KT = KT + 1
NO
IS KT = NR ?
YES
I = I + 1
NO
IS I = NWT ?
YES
IWB = IWB + 1
NO
IS IWB = 3 ?
YES
IRW = IRW + 1
NO
IS IRW = 2 ?
YES
WRITE A & F COMPONENTS OF THE INDUCED VELOCITY COEFFICIENTS ON TAPE 1
WRITE E COMPONENT OF INDUCED VELOCITY COEFFICIENT ON TAPE 2
IBW = IBW + 1
NO
IS IBW = 3 ?
YES
IRB = IRB + 1
NO
IS IRB = 2 ?
YES
IRTR = IRTR + 1
NO
IS IRTR = NR/NB ?
YES
END

SUBROUTINE TAS

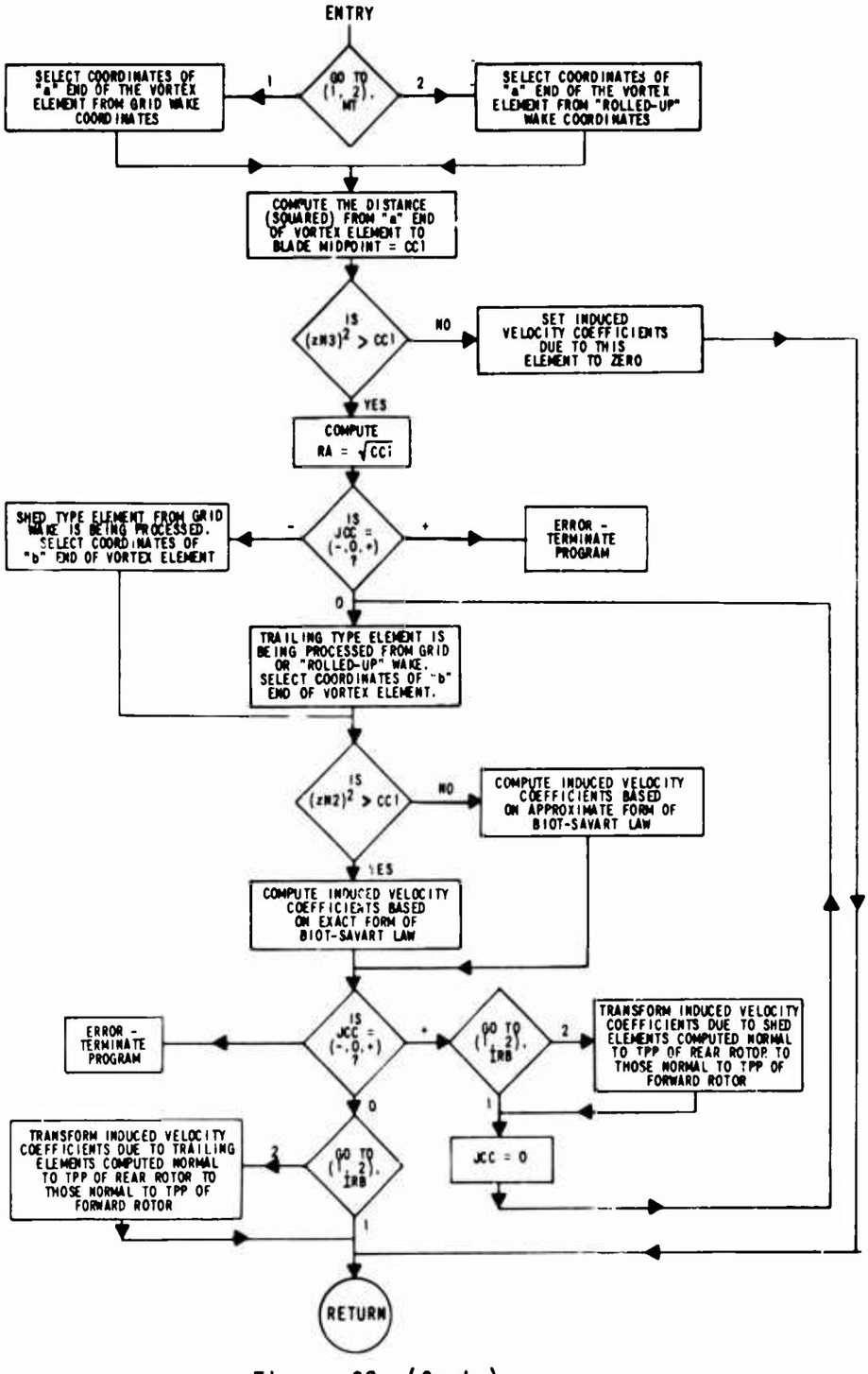

Figure 32. (Cont.)

PART NO. 3

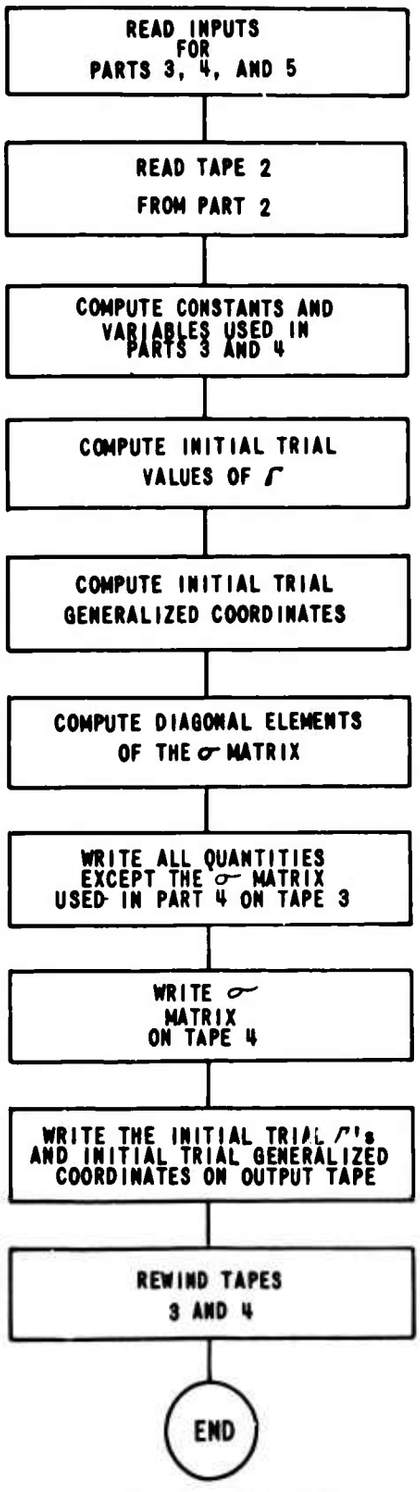

Figure 32. (Cont.)

PART NO. 4

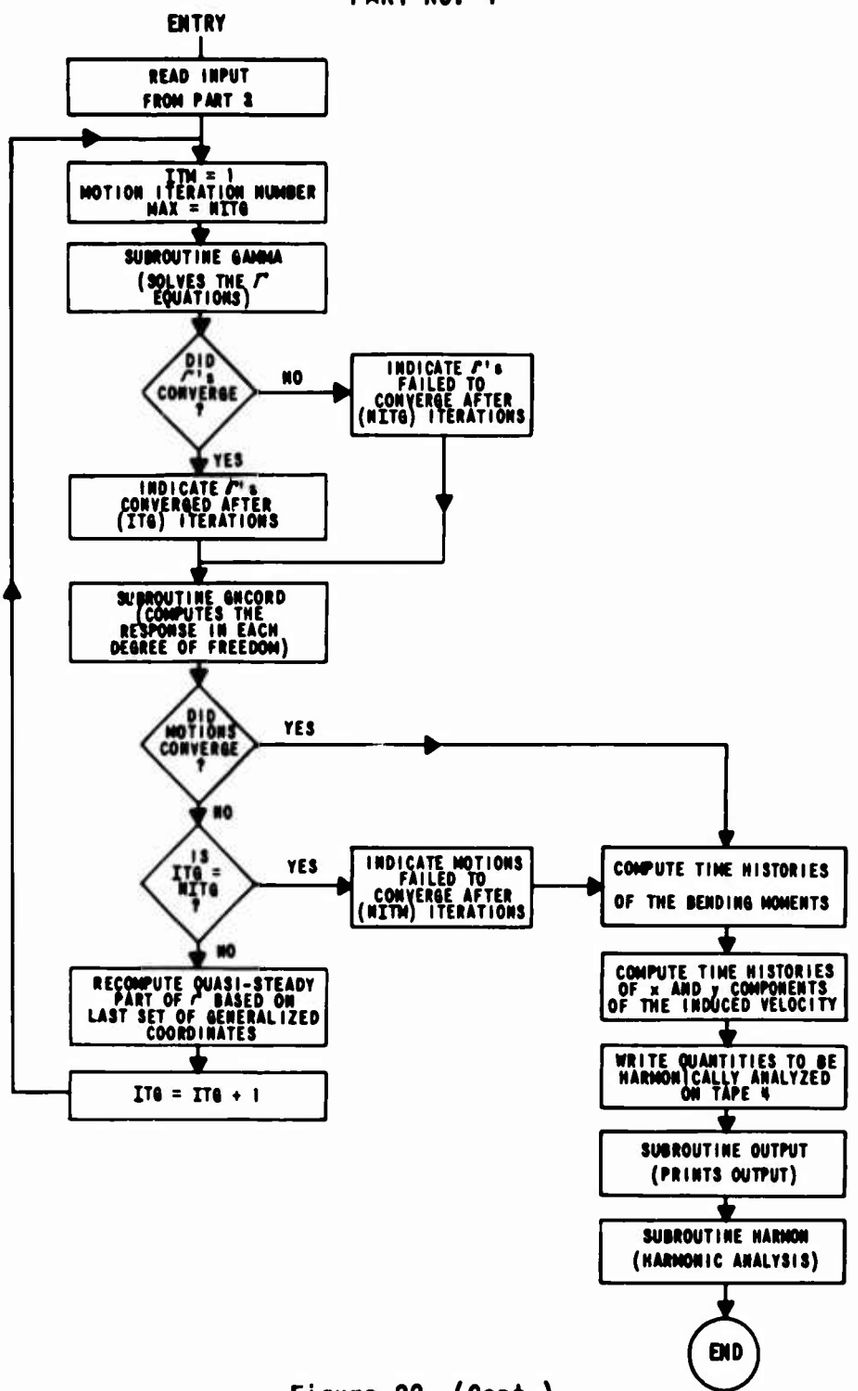

Figure 32. (Cont.)

BLANK PAGE

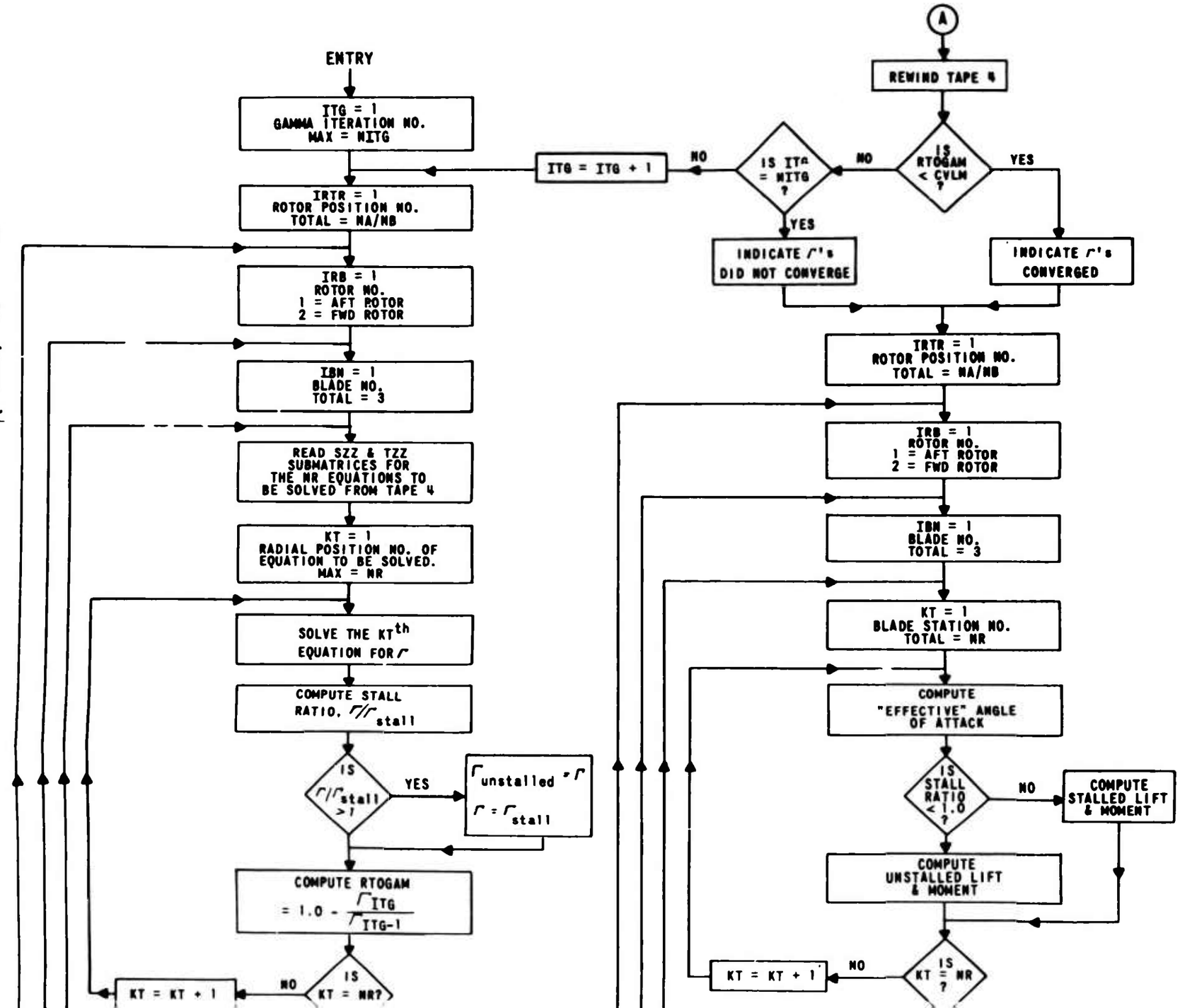

Figure 32 (Cont.)

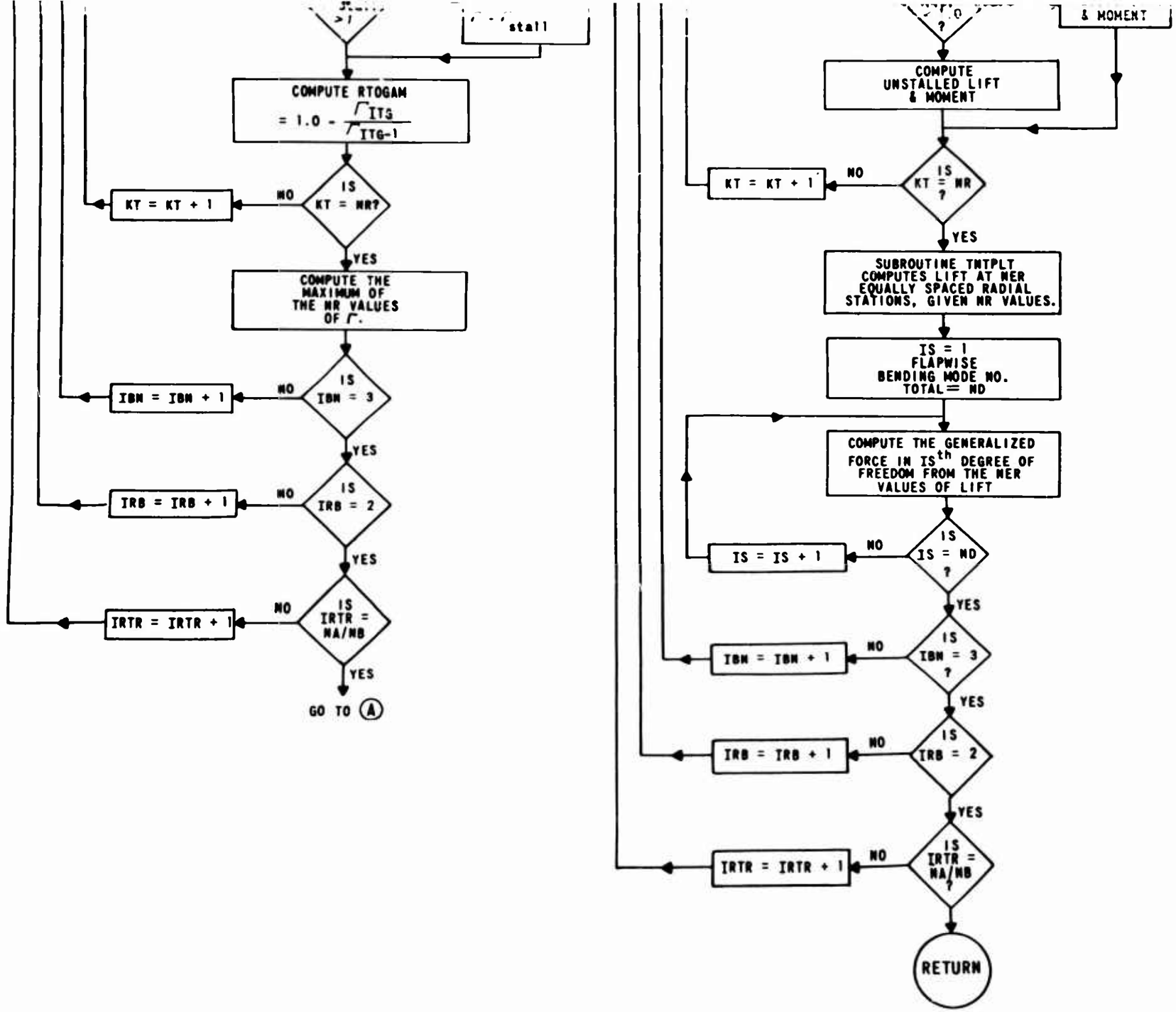
stall
COMPUTE RTOGAM
= 1.0 - ΓITS / ΓITG-1
IS KT = NR?
NO
KT = KT + 1
YES
COMPUTE THE MAXIMUM OF THE NR VALUES OF Γ.
IS IBN = 3
NO
IBN = IBN + 1
YES
IS IRB = 2
NO
IRB = IRB + 1
YES
IS IRTR = NA/NB
NO
IRTR = IRTR + 1
YES
GO TO (A)
& MOMENT
COMPUTE UNSTALLED LIFT & MOMENT
IS KT = NR ?
NO
KT = KT + 1
YES
SUBROUTINE TNTPLT COMPUTES LIFT AT NER EQUALLY SPACED RADIAL STATIONS, GIVEN NR VALUES.
IS = 1 FLAPWISE BENDING MODE NO. TOTAL = ND
COMPUTE THE GENERALIZED FORCE IN IS th DEGREE OF FREEDOM FROM THE NER VALUES OF LIFT
IS IS = ND ?
NO
IS = IS + 1
YES
IS IBN = 3 ?
NO
IBN = IBN + 1
YES
IS IRB = 2
NO
IRB = IRB + 1
YES
IS IRTR = NA/NB ?
NO
IRTR = IRTR + 1
RETURN

SUBROUTINE GNCORD

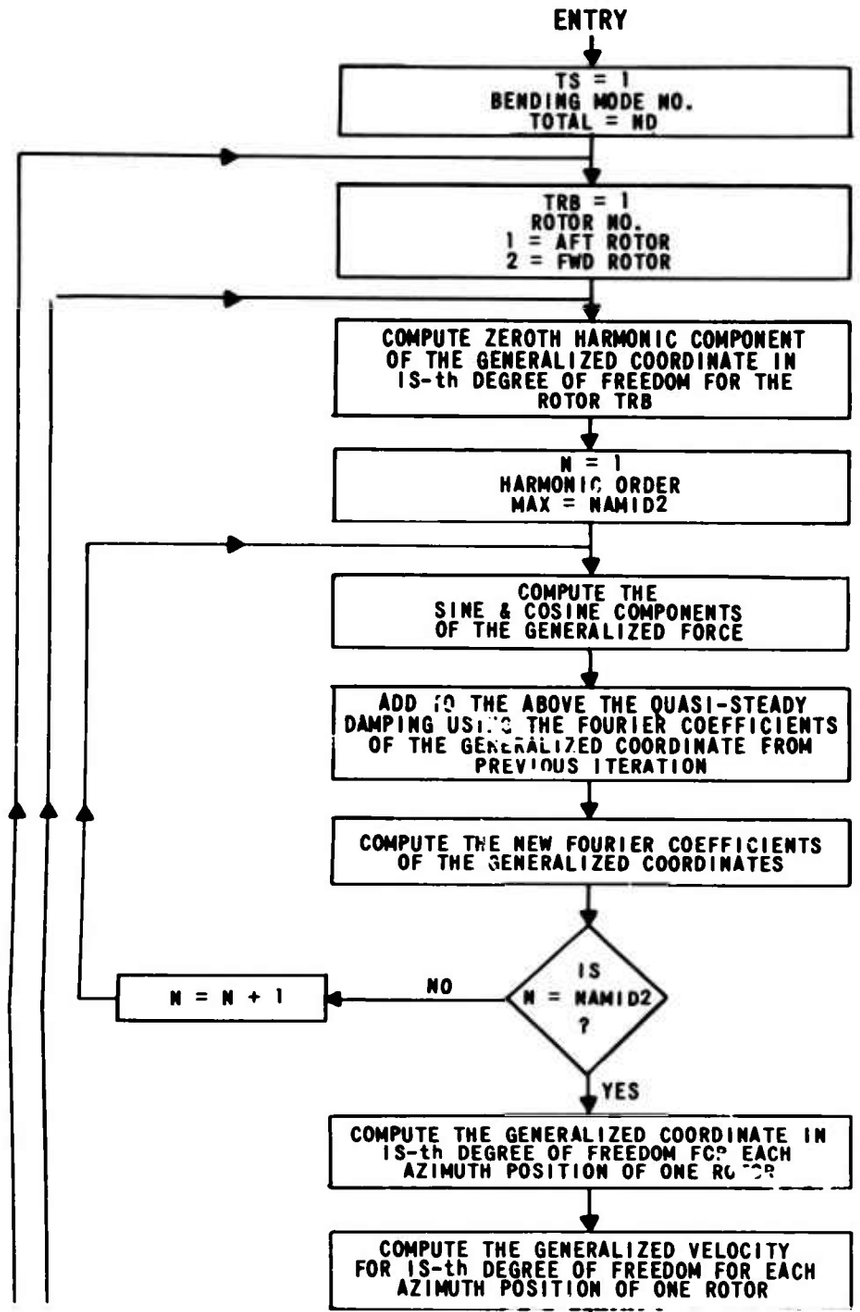

Figure 32 (Cont.)

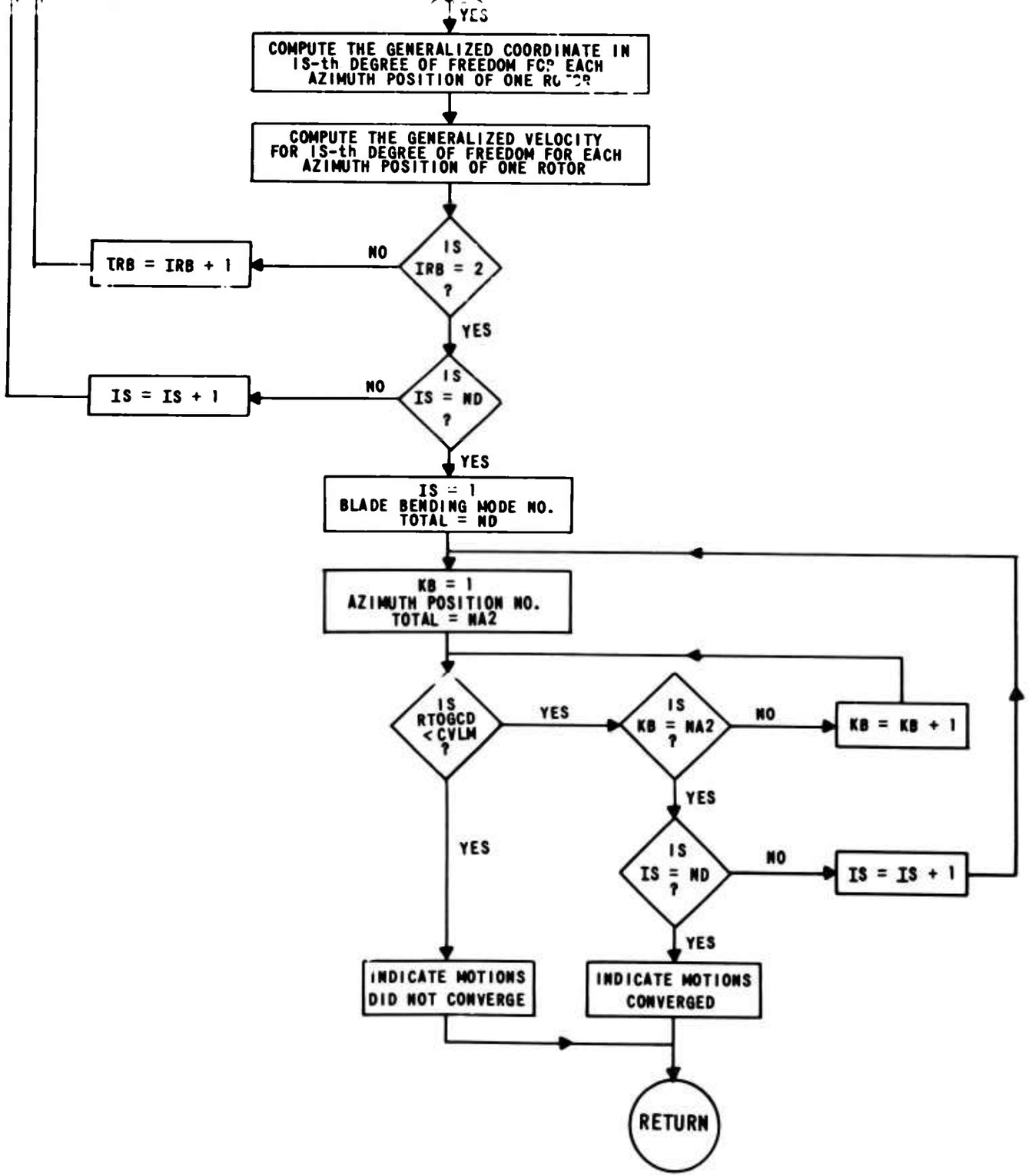
YES
COMPUTE THE GENERALIZED COORDINATE IN IS-th DEGREE OF FREEDOM FOR EACH AZIMUTH POSITION OF ONE ROTOR
COMPUTE THE GENERALIZED VELOCITY FOR IS-th DEGREE OF FREEDOM FOR EACH AZIMUTH POSITION OF ONE ROTOR
IS IRB = 2 ?
NO
IRB = IRB + 1
YES
IS IS = ND ?
NO
IS = IS + 1
YES
IS = 1
BLADE BENDING MODE NO. TOTAL = ND
KB = 1
AZIMUTH POSITION NO. TOTAL = NA2
IS RTOGCD < CVLM ?
YES
IS KB = NA2 ?
NO
KB = KB + 1
YES
IS IS = ND ?
NO
IS = IS + 1
YES
YES
INDICATE MOTIONS DID NOT CONVERGE
INDICATE MOTIONS CONVERGED
RETURN

APPENDIX I

TABLE V. COMPARISON OF SELECTED INPUT PARAMETERS AND RUNNING TIME FOR COMPUTED PROGRAM

μ	0.08	0.14	0.24
NR	10	10	10
NW (AFT)	6	3	2
NW (FWD)	9	5	3
NUMBER OF ITERATIONS PERFORMED FOR Γ'S TO CONVERGE IN EACH MOTION ITERATION	5-3-2-1-1-1	5-3-3-1-1	6-5-4-3-2-1
OPTIONAL OUTPUT*	(1), (3), (4),	(1), (3) (5), (6)	(1), (2), (3), (4), (5), (6),
ND	5	5	5
PLOTTING TAPE GENERATED	NO	YES	YES
RUNNING TIME (hrs)			
PARTS 1 AND 2	0.34	0.25	0.36
PARTS 3 AND 4	0.60	0.61	0.88

*OPTIONAL OUTPUT

(1) BLADE AND WAKE COORDINATES.

(2) ζ-COMPONENTS OF INDUCED VELOCITY COEFFICIENTS.

(3) COMPUTATIONAL DETAILS OF THE EFFECT OF A VORTEX ELEMENT ON THE INDUCED VELOCITY AT A POINT ON THE BLADE WHEN THE "a" END OF THE VORTEX ELEMENT IS LESS THAN DAMPRAD (4.9 FT, INPUT) FROM THE AERODYNAMIC STATION.

(4) THE "I's" OF THE Γ EQUATION FOR EACH MOTION ITERATION.

(5) THE Γ DISTRIBUTION FOR EACH ITERATION ON THE Γ.

(6) THE GENERALIZED COORDINATES FOR EACH MOTION ITERATION.

APPENDIX II

FLOW DIAGRAMS FOR THE COMPUTER PROGRAM

(Parts 1, 2, 3 and 4)

The flow diagrams presented in Figure 32 show sufficient details of the logic and subroutines of the program to provide a meaningful illustration of its general flow. Symbols which are used in these charts are defined below.

NA	Number of azimuth positions in each rotor.
NB	Number of blades in each rotor.
IRB	Index for specifying the rotor in which the blade used in the computation is located. If *IRB* = 1, the blade is in the aft rotor; if *IRB* = 2, the blade is in the forward rotor.
IRW	Index for specifying the rotor in which the wake of a blade used in the computation is located. If *IRW* = 1, the wake of the blade is in the aft rotor; if *IRW* = 2, the wake of the blade is in the forward rotor.
IBN	Blade number in each rotor. Initially, blade No. 1 is at $\psi = 0$ and the blades are numbered in the direction of rotation.
NSV	The azimuth position number of the last shed vortex wake element in the mesh wake.
NR	The number of radial stations on the blade at which the air loads are computed.
NW	The number of revolutions of wake used in the computations.
NWT	*NA* × *NW*.

NTV	The number of trailing vortices in the rolled-up representation of the wake. If NTV = 1, only a tip vortex is used ; if NTV = 2, tip and root vortices are used.
SZZ	Matrix of z-component of induced velocity coefficients due to vortex elements in the grid wake.
TZZ	Matrix of z-component of induced velocity coefficients due to vortex elements in the rolled-up wake.
NAMIO2	(NA - 1)/2.
NA2	NA × 2.

Unclassified

Security Classification

DOCUMENT CONTROL DATA - R&D

(Security classification of title, body of abstract and indexing annotation must be entered when the overall report is classified)

1 ORIGINATING ACTIVITY (Corporate author) Cornell Aeronautical Laboratory, Inc. Buffalo, New York	2a REPORT SECURITY CLASSIFICATION Unclassified 2b GROUP

3 REPORT TITLE

A Method for Predicting the Aerodynamic Loads and Dynamic Response of the Rotor Blades of a Tandem-Rotor Helicopter

4 DESCRIPTIVE NOTES (Type of report and inclusive dates)

5 AUTHOR(S) (Last name, first name, initial)

Balcerak, John C.

6 REPORT DATE	7a TOTAL NO. OF PAGES	7b NO. OF REFS
June 1967	92	7

8a CONTRACT OR GRANT NO.	9a ORIGINATOR'S REPORT NUMBER(S)
DA 44-177-AMC-207(T) b. PROJECT NO. Task 1F125901A14604 c d	USAAVLABS Technical Report 67-38 9b OTHER REPORT NO(S) (Any other numbers that may be assigned this report) BB 1960-S-1

10 AVAILABILITY/LIMITATION NOTICES

Distribution of this document is unlimited.

11 SUPPLEMENTARY NOTES	12 SPONSORING MILITARY ACTIVITY
	U.S. Army Aviation Materiel Laboratories Fort Eustis, Virginia

13 ABSTRACT

In recent efforts, refined methods have been developed for predicting the aerodynamic loads and dynamic response of the blades of a single-rotor helicopter. The method described herein adopts similar procedures and applies them to the tandem-rotor helicopter.

The blades of each rotor are represented by segmented lifting lines located at the quarterchord positions of the blades and the vortex strength is assumed to be constant over each segment of the blade at each of an arbitrary number of azimuth positions. The wake is represented by a mesh of shed and trailing vortex filaments up to an arbitrary finite distance behind each blade, and beyond this point the wake is represented by a segmented, tip-trailing vortex or by segmented, tip- and root-trailing vortices.

The aerodynamic loadings and the flapwise structural bending moments were computed for the CH 47A tandem-rotor helicopter for advance ratios of 0.08, 0.14 and 0.24. Comparisons of these results with measured results for individual test points are presented as radial distributions of the first three harmonic components and as time histories which include eleven harmonics. The measured data were generally presented in the form of typical results from a statistical sampling of measured data from similar test conditions.

DD FORM 1 JAN 64 1473

Unclassified

Security Classification

Unclassified
Security Classification

14 KEY WORDS	LINK A		LINK B		LINK C	
	ROLE	WT	ROLE	WT	ROLE	WT
Helicopter Rotor Blades Aerodynamic Loads Dynamic Tandem						

INSTRUCTIONS

1. ORIGINATING ACTIVITY: Enter the name and address of the contractor, subcontractor, grantee, Department of Defense activity or other organization *(corporate author)* issuing the report.

2a. REPORT SECURITY CLASSIFICATION: Enter the overall security classification of the report. Indicate whether "Restricted Data" is included. Marking is to be in accordance with appropriate security regulations.

2b. GROUP: Automatic downgrading is specified in DoD Directive 5200.10 and Armed Forces Industrial Manual. Enter the group number. Also, when applicable, show that optional markings have been used for Group 3 and Group 4 as authorized.

3. REPORT TITLE: Enter the complete report title in all capital letters. Titles in all cases should be unclassified. If a meaningful title cannot be selected without classification, show title classification in all capitals in parenthesis immediately following the title.

4. DESCRIPTIVE NOTES: If appropriate, enter the type of report, e.g., interim, progress, summary, annual, or final. Give the inclusive dates when a specific reporting period is covered.

5. AUTHOR(S): Enter the name(s) of author(s) as shown on or in the report. Enter last name, first name, middle initial. If military, show rank and branch of service. The name of the principal author is an absolute minimum requirement.

6. REPORT DATE: Enter the date of the report as day, month, year, or month, year. If more than one date appears on the report, use date of publication.

7a. TOTAL NUMBER OF PAGES: The total page count should follow normal pagination procedures, i.e., enter the number of pages containing information.

7b. NUMBER OF REFERENCES: Enter the total number of references cited in the report.

8a. CONTRACT OR GRANT NUMBER: If appropriate, enter the applicable number of the contract or grant under which the report was written.

8b, 8c, & 8d. PROJECT NUMBER: Enter the appropriate military department identification, such as project number, subproject number, system numbers, task number, etc.

9a. ORIGINATOR'S REPORT NUMBER(S): Enter the official report number by which the document will be identified and controlled by the originating activity. This number must be unique to this report.

9b. OTHER REPORT NUMBER(S): If the report has been assigned any other report numbers *(either by the originator or by the sponsor)*, also enter this number(s).

10. AVAILABILITY/LIMITATION NOTICES: Enter any limitations on further dissemination of the report, other than those imposed by security classification, using standard statements such as:

(1) "Qualified requesters may obtain copies of this report from DDC."

(2) "Foreign announcement and dissemination of this report by DDC is not authorized."

(3) "U. S. Government agencies may obtain copies of this report directly from DDC. Other qualified DDC users shall request through

_____."

(4) "U. S. military agencies may obtain copies of this report directly from DDC. Other qualified users shall request through

_____."

(5) "All distribution of this report is controlled. Qualified DDC users shall request through

_____."

If the report has been furnished to the Office of Technical Services, Department of Commerce, for sale to the public, indicate this fact and enter the price, if known.

11. SUPPLEMENTARY NOTES: Use for additional explanatory notes.

12. SPONSORING MILITARY ACTIVITY: Enter the name of the departmental project office or laboratory sponsoring *(paying for)* the research and development. Include address.

13 ABSTRACT: Enter an abstract giving a brief and factual summary of the document indicative of the report, even though it may also appear elsewhere in the body of the technical report. If additional space is required, a continuation sheet shall be attached.

It is highly desirable that the abstract of classified reports be unclassified. Each paragraph of the abstract shall end with an indication of the military security classification of the information in the paragraph, represented as *(TS)*, *(S)*, *(C)*, or *(U)*.

There is no limitation on the length of the abstract. However, the suggested length is from 150 to 225 words.

14 KEY WORDS: Key words are technically meaningful terms or short phrases that characterize a report and may be used as index entries for cataloging the report. Key words must be selected so that no security classification is required. Identifiers, such as equipment model designation, trade name, military project code name, geographic location, may be used as key words but will be followed by an indication of technical context. The assignment of links, rules, and weights is optional.

Unclassified
Security Classification

4846-67